2016

Space-Time Processing Methods to Enhance GNSS Signal Robustness under Electronic Interference

Marathe, Thyagaraja

UNIVERSITY OF CALGARY

Space-Time Processing Methods to Enhance GNSS Signal Robustness under Electronic Interference

by

Thyagaraja Marathe

A THESIS

SUBMITTED TO THE FACULTY OF GRADUATE STUDIES

IN PARTIAL FULFILMENT OF THE REQUIREMENTS FOR THE DEGREE OF

DOCTOR OF PHILOSOPHY

GRADUATE PROGRAM IN GEOMATICS ENGINEERING

CALGARY, ALBERTA

APRIL, 2016

Abstract

Open access GNSS signals have enabled the development of receivers that find their use spanning multitude of user segments. Owing to the long distance travel from the satellite to the user, the received signal level is very weak on or near earth. This is due to the free-space loss and, to a small extent, atmospheric losses. The signals arriving at the RF front-end can be affected by the presence of signals from other communication systems. Since GNSS has to coexist with other such systems, it is not abnormal to expect that even in normal operations, receivers experience interference. Additionally, undesirable signals can appear in the GNSS frequency band due to other man-made high power signal transmissions. The levels of these disturbing signals will determine the impact that they may have on the performance metrics of the receiver.

Antenna array processing techniques are studied in GNSS as effective tools to mitigate interference in spatial and spatiotemporal domains. Analyzing the performance of array based mitigation methods involves many challenges, such as prohibition to propagate test interference signals and the challenge involved with the design and execution of cost-effective experimental setups. To reduce this burden, a new approach is proposed and developed and tested herein. Without specific filter design considerations, the array **space-time processing (STP)** results in distortions. This research also focuses on characterizing these degradations for different controlled signal scenarios and for live data from an antenna array. The capability of antenna array STP to mitigate the interference from near zone pseudolites and provide subsequent enhancements is studied in the latter part of the thesis.

An array simulator is developed during the research and is effectively used for assessing STP measurement distortions. The characterization results show that distortions due to STP are significant and can lead to erroneous pseudorange measurements. From the simulation results, it is concluded that the antenna array STP methods are beneficial for interference mitigation in GPS-pseudolite combined signal environments.

Preface

Some parts of this thesis contain materials from one journal paper and three previously published peer reviewed conference papers. These papers are referenced below.

Marathe, T., S. Daneshmand, and G. Lachapelle (2016) “Assessment of measurement distortions in GNSS antenna array space-time processing," in *International Journal of Antennas and Propagation*, January 2016, Article ID 2154763, 17 pages.

Marathe, T., S. Daneshmand, and G. Lachapelle (2016) "A High Fidelity Multi Antenna Software Simulator for Array Processing in GNSS", in *Proceedings of ION International Technical Meeting (ITM) 2016*, 25-28 January, Monterey, California, The Institute of Navigation, 11 pages.

Marathe, T., S. Daneshmand, and G. Lachapelle (2015) "Pseudolite Interference Mitigation and Signal Enhancements Using an Antenna Array," in *Proceedings of the International Conference on Indoor Positioning and Indoor Navigation (IPIN)*, 13-16 October, Banff, Alberta, IEEE, pp. 1-9.

Marathe, T., S. Daneshmand, and G. Lachapelle (2015) "Characterizing Signal Distortion Due to Space-time Processing of Interference Impacted GNSS Signals," in *Proceedings of the ION GNSS+ 2015*, 14-18 September, Tampa, Florida, The Institute of Navigation, pp. 3084-3093.

Acknowledgements

I would like to express my sincere gratitude to my supervisor Professor Gérard Lachapelle for his support, guidance and encouragement throughout my studies. I feel honoured to have been his student and I convey my heartfelt thanks to him for keeping me motivated throughout my research work.

I would like to thank my adviser Dr. Saeed Daneshmand for his guidance. In addition to providing original inspiration for the project, his continued encouragement, attention to detail and in-depth mathematical perspective on this work have been invaluable for my research.

The PLAN researchers and students who contributed directly or indirectly in the success of my studies are kindly acknowledged.

I acknowledge the efforts of my previous supervisors at Accord Software & Systems Pvt. Ltd, Bengaluru, India, for leading me through the first steps in GNSS and introducing to me the research opportunities at the PLAN Group of the University of Calgary.

The wonderful environment created by Vijay, Suvarna, Sujay, Naveen, Ashwitha, Ranjeeth, Kavya, Niranjan, Shruthi, Vimal, Aruna, Sajan, Jyothi, Ahmad, Nahal, Anup, Rakesh, Srinivasa B, Srinivas Tantry, and Sashidharan made my stay in Calgary enjoyable. Thank you all.

Finally and no least, I would like to thank my parents, my wife Pavana, my brother Gurudutt and my in-laws. This study would not have been possible without their unconditional love, encouragement, patience and continued support. Heartfelt thank you.

Dedication

To my parents- B. Vittal Marathe and
Nalini V. Marathe

ಸಂದೇಹವೀ ಕೃತಿಯೊಳಿನ್ನಿಲ್ಲವೆಂದಲ್ಲ ।
ಇಂದು ನಂಬಿಹುದೆ ಮುಂದೆಂದುಮೆಂದಲ್ಲ ॥
ಕುಂದು ತೋರ್ದಂದದನು ತಿದ್ದಿಕೊಳೆ ಮನಸುಂಟು ।
ಇಂದಿಗೀ ಮತವುಚಿತ - ಮಂಕುತಿಮ್ಮ ॥

"It is not that after reading this book, there will be no more doubts.
It is not that what we believe today will hold up forever.
If someone points at some shortcomings, I have an open mind to correct.
But for now, I believe this is right." - Mankutimma

[*Verse #939 in 'Mankutimmana Kagga' by Dr. D.V. Gundappa*]

Table of Contents

List of Tables

List of Figures and Illustrations

List of Abbreviations

Abbreviation	Expansion
ADC	Analog to digital converter
AGC	Automatic gain control
AoA	Angle of arrival
C/A	Coarse-Acquisition
CAF	Cross Ambiguity Function
CCF	Cross Correlation Function
C-DL	Cascade Distortionless
CDMA	Code Division Multiple Access
C/N_0	carrier-to-noise-density ratio
CRPA	Controlled Radiation Pattern Antenna
CW	Continuous Wave
CWI	Continuous Wave Interference
DFT	Discrete Fourier Transform
DM	Distortion Metric
DME	Distance Measuring Equipment
DoF	Degrees of Freedom
DOP	Dilution of Precision
DSSS	Direct Sequence Spread Spectrum
DSP	Digital Signal Processing
ECEF	Earth Centred Earth Fixed
EIRP	Effective Isotropically Radiated Power
E-L	Early-Late
E-MPDR	Extended MPDR
ENU	East North Up
EVD	Eigen Value Decomposition
FCC	Federal Communications Commission
FFT	Fast Fourier Transform
FIR	Finite Impulse Response
FM	Frequency modulation
FRPA	Fixed Radiation Pattern Antenna
GATE	Galileo Test and Development Environment
GLONASS	Globalnaya Navigazionnaya Sputnikovaya Sistema
GNSS	Global Navigation Satellite System
GPS	Global Positioning System
ICU	Interference Combiner Unit
IF	Intermediate Frequency
IFFT	Inverse FFT
IIR	Infinite Impulse Response

JNR	Jamming to Noise power ratio
J/S	Jamming to Signal ratio
LMS	LMS
LNA	Low Noise Amplifier
MatLab	Matrix Laboratory
MMSE	Minimum Mean Squared Error
MPDR	Minimum Power Distortion less Response
MSNWF	Multi Stage Nested Wiener Filter
MVDR	Minimum Variance Distortion less Response
NLMS	Normalized Least Mean Squares
PED	Personal Electronic Devices
PCB	Printed Circuit Board
PLAN	Position, Location and Navigation
PM	Power Minimization
PRN	Pseudo Random Number
PSD	Power Spectral Density
PVT	Position, Velocity and Time
RADAR	Radio detection and ranging
R&S	Rohde and Schwarz
RF	Radio Frequency
RFI	RF Interference
RLS	Recursive Least Square
RMS	Root mean square
RTCM	Radio Technical Commission for Maritime Services
RTCM (SC)	RTCM Special Committee
SDR	Software Defined Radio
SFAP	Space Frequency Adaptive Processing
SIC	Successive Interference Cancellation
SINR	Signal to Interference plus Noise Ratio
SMI	Simple Matrix Inversion
SNR	Signal to Noise Ratio
SPM	Simple Power Minimization
ST	Space-Time
STP	Space Time Processing
STAP	Space Time Adaptive Processing
SV	Satellite Vehicle
SVD	Singular Value Decomposition
TDL	Tapped Delay Line
TOA	Time Of Arrival
UAV	Unmanned Aerial Vehicles

UHF	Ultra-High Frequency
VHF	Very High Frequency
WB	Wideband

List of Symbols

Symbol	Definition
t	Time variable
$\underset{N\times 1}{\mathbf{x}}$	Received baseband signal vector at an antenna array
x_n	Received signal at the n^{th} antenna element
N	Number of isotropic antenna elements
M	Number of taps in the temporal filter
P	Number of satellites
L	Number of interference sources
K	Number of pseudolites
s_p	Signal waveform of p^{th} signal
$\mathbf{a}_p$	Steering vector of p^{th} signal
i_l	Signal waveform of l^{th} interference
$\mathbf{b}_l$	Steering vector of l^{th} interference
v_k	Signal waveform of k^{th} pseudolite
$\mathbf{c}_k$	Steering vector of k^{th} pseudolite
$\underset{N\times 1}{\boldsymbol{\eta}}$	White Gaussian noise vector
$\vec{\mathbf{r}}$	Received signal vector for the antenna array
$x_{M,N}$	the m^{th} delayed sample at the n^{th} antenna element
$(\ )^T$	Transpose operator
$(\ )^H$	Hermitian transpose operator
$E\{\ \}$	Mathematical expectation operator
$\mathbf{R}_{\vec{\mathbf{r}}}$	Space time correlation matrix
$\mathbf{P}$	Projection matrix
$\mathbf{U}_{Int}$	Eigen vector matrix of interference subspace
$\mathbf{U}_{Null}$	Eigen vector matrix of interference-free signal subspace
$\mathbf{\Lambda}_{Int}$	Eigen value matrix of interference subspace
$\mathbf{\Lambda}_{Null}$	Eigen value matrix of interference-free signal subspace
$\mathbf{w}$	Space-time filter weights
$\mathbf{g}$	Gain selection vector
$\mathbf{q}$	Constraint vector
$\hat{\mathbf{e}}_p$	Vector pointing in the direction of the desired signal
λ_c	Carrier wavelength
$\mathbf{d}_j^{ant}$	Antenna coordinates vector

θ_{El}^{i}	Elevation angle of the p^{th} signal direction
ϕ_{Az}^{p}	Azimuth angle of the p^{th} signal direction
AG	Antenna array gain
$\mathbf{h}(f)$	Frequency response vector
A_p	Amplitude of the generated signal
$d_p(t)$	Navigation data
$c_p(t)$	C/A code (Spreading code)
τ_p	Code offset
f_p^{RF}	Carrier frequency
f_p^d	Carrier Doppler frequency
φ_p	Carrier phase
$\Delta\rho^p$	Measurement bias
$\Delta\rho_F^p$	Fixed part of $\Delta\rho^p$
$\Delta\rho_V^p$	Variable part of $\Delta\rho^p$
ρ_{MPDR}^p	Pseudorange measurement corresponding to array processing
ρ_c^p	Pseudorange measurement for a single RF signal
τ_n	Time delay between the reference antenna element and the n^{th} array element
B_s	Maximum envelope bandwidth
$\Delta T_{\max}$	Maximum time required for the signal to traverse the array
$R(\tau)$	Correlation function of the signal
$P(f)$	Power spectrum of the signal
$H(f)$	Frequency response of the filter
$\mathbf{c}_{NM\times 1}$	Constraint vector for MPDR
T_s	Delay due to one tap
C	Speed of light
$\left(\frac{C}{N_0}\right)_{eff}$	Effective C/N_0
C_s	Received power of the desired signal
$G_s(f)$	Normalized power spectral density (PSD) of the desired signal
N_0	Thermal noise power density

C_j	Interference power
$G_j(f)$	Normalized PSD of the interference signal
β_r	Receiver front-end bandwidth
$\left(\frac{C}{N_0}\right)_{eff}^{Array}$	Effective C/N_0 for array processing
A_{BF}	Beamforming gain
A_{NS}	Loss due to null steering
β_I	Interference bandwidth

CHAPTER 1: INTRODUCTION

Global Navigation Satellite System (GNSS) based position, velocity and time (PVT) solutions in standalone mode still find limited applicability in critical applications due to increased operational risks. Critical applications like first responders, law enforcement, autonomous vehicle navigation, infrastructure, maritime, aviation, etc, often integrate the data obtained from GNSS receivers with other sensors to improve reliability. A major GNSS risk is susceptibility to non-intentional and intentional interference, the latter being electronic spoofing and jamming. Interference results in signal ill-conditioning. As a consequence, all processing phases in a receiver namely acquisition, tracking and positioning are affected, leading to degraded GNSS receiver outputs.

Several countermeasures are proposed in the literature for different types of interference based on either spatial, temporal, or spectral characteristics or using a combination of these. Mitigation techniques based on antenna arrays that can employ processing in acquisition and tracking phases are found to be more effective in detection and suppression. Array processing techniques can also cater to a wide variety of interference. However, 100% recovery of a clean signal is not guaranteed by any of these methods. Spatial domain processing can be combined with temporal or frequency domains to achieve Space Time Adaptive Processing (STAP) and Space Frequency Adaptive Processing (SFAP), respectively. A simple form of a space-time filter is shown in Figure 1-1. In spatial only processing, data available from antenna elements is used; however, in space-time processing, additional temporal processing is added to spatial processing. The SFAP approach is an alternative to STAP where the time domain signals received by antenna elements are transformed to the frequency domain using Discrete Fourier

Transform (DFT). STAP and SFAP are equivalent if the inter-tap spacing within the temporal filter is equal to the sampling interval (Godara 1995). The space-time methods are explored in the course of this investigation.

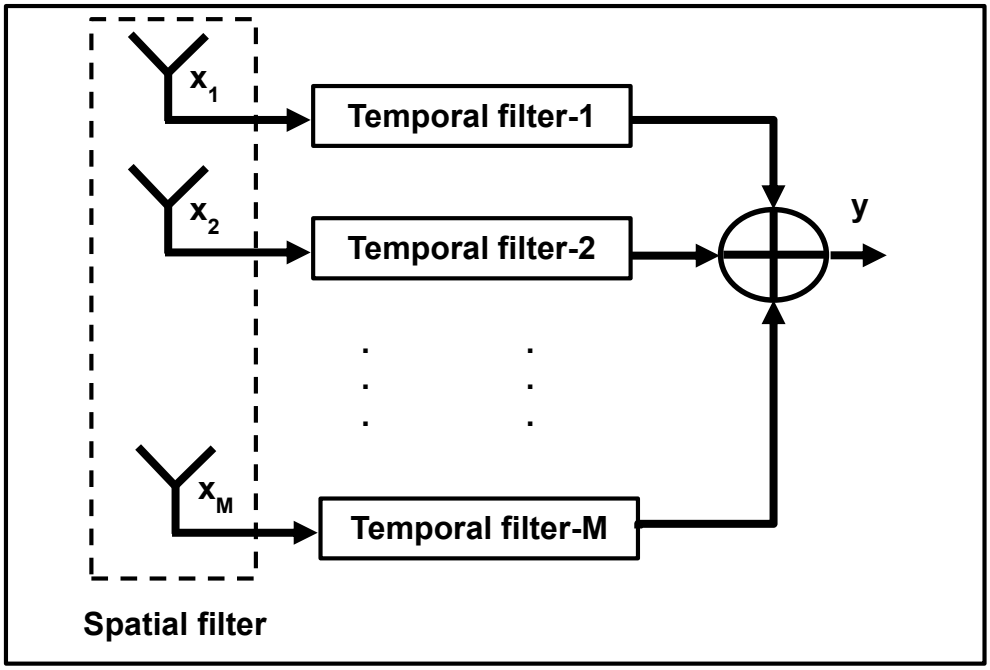

Figure 1-1: Simple form of a space-time filter

A brief summary of work done by other researchers in the space-time processing domain is given in the sequel. Subsequently, the objectives and contributions of this thesis are summarized. The chapter concludes by presenting the outline of the thesis.

1.1 Background and motivation

The Effective Isotropically Radiated Power (EIRP) at the satellite vehicle (SV) (i.e. the satellite) is 28.3 dBW. However, due to the free space loss, the signal strength at the receiver's antenna is very weak. At a received signal power of approximately -158.5 dBW (in case of Global Positioning System (GPS) L1), the signal is sensitive to the presence

of other undesirable signals. The direct sequence spread spectrum (DSSS) modulation used in the GNSS signals provides some degree of protection against narrowband interfering signals. Any interfering signal having a magnitude greater than this margin (based on the cross correlation properties and the difference in first peak and the next subsequent peak, it is 23.94dB in GPS L1) will contribute adversely to the normal receiver operation (Kaplan & Hegarty 2006).

The undesirable signals can be intentional or unintentional. The intentional interference could be due to a transmission of a continuous wave high power signal in the GNSS bandwidth or by smart transmitting devices like spoofers emitting a signal resembling GNSS signals. Unintentional interference can occur due to receiver hardware components that operate in a non-linear region, thereby generating harmonics and inter-modulation components. Based on the bandwidth of frequencies affected, interference can be categorized as either narrowband or wideband interference. The narrowband interferers occupy only a small portion of the GNSS signal bandwidth and the wideband jammers occupy a significant part of the band of interest. A high level of interference can fully stop a GNSS receiver from acquiring the signals, whereas a low level of interference can adversely affect the tracking and accuracies of position estimates.

With present-day advancements in design technologies, unintentional signals due to harmonics and inter-modulation components are reduced. However, the systems that reuse the GNSS spectrum still act like interference sources and this provides a motivation and impetus for performing further research on GNSS interference and investigate new and effective countermeasures. In addition, the intentional jamming produced using compact, portable low cost jammers degrades receiver performance if this is not properly

addressed. The concern of industry regarding interference is seen when reviewing recent meetings organized by the Federal Communications Commission (FCC) on this topic (e.g. Divis 2014). The meeting agenda was to have a comprehensive path forward to protect GPS operations from harmful interference due to neighboring transmitters and to discuss design mandates for certification and standards for receivers.

Several interference mitigation techniques have been proposed and use of antenna arrays for GNSS interference mitigation is now a major research interest (Daneshmand 2013, Chang & Wu 2011, Zheng 2008, Church et al 2007, De Lorenzo et al 2005). Antenna electronics and design technologies are advancing rapidly and there is focus on achieving the best possible performance with a reduced antenna form factor. To the best of the author's knowledge, receivers for civilian usage with multiple antennas are not available at the time of this writing. However, designing hand held receivers with multiple antennas could be practicable in the near future. Especially with space-time processing, such receivers could be very effective for interference mitigation. Even with existing antenna designs, it is realistic and viable to use space-time processing for automotive and defense applications. This subject of space-time processing is explored further in this thesis.

Adaptive array processing methods have been explored in GNSS for many years (e.g. Lu et al 2006, Hatke 1998, Moelker et al 1996). They are the desirable beamformers for today's complex interference scenarios. These methods cater to real world scenarios like maneuvering platforms, moving interference sources and changing interference environments. Some advanced methods require some additional information like the reference signals (e.g. true signals in case of MMSE based approaches or angle of arrival

(AoA) details). Considering all complex interference scenarios that can be experienced, adaptive methods are conceptually very beneficial.

Array processing has been used in several fields for a few decades. However, compared to other fields where the array processing has been used, it requires special attention for use in GNSS. For GNSS use, extraction of ranges and Doppler estimates is critical. Any contribution from array processing on the above two estimates will lead to degradation of final position performance. On the contrary, these considerations are not important in other fields. During GNSS array processing, there are pseudorange errors added by spatial or space-time filters. Furthermore, if particular consideration is not given to these while adding the signals from different array elements, this leads to a deformed correlator function and poor signal-to-noise ratio (SNR). Also, when adaptive arrays are used to cater to changing signal environments, filter weights are updated continuously. These updates produce phase discontinuities of varying magnitudes. Larger phase continuities affect tracking performance and result in inferior carrier Doppler estimates (Kalyanaraman 2009). In GNSS, user velocities are derived from the Doppler estimates and hence velocities are also erroneous. If code tracking is aided with carrier tracking (as done in many receivers), carrier errors propagate to code and subsequently to position estimates. Hence, GNSS array processing is a field that requires additional attention from the GNSS community and that provides new research opportunities.

1.2 Simulation of multiple antenna GNSS signals

Due to the interaction with the atmosphere during propagation from the satellite to the user receiver on earth, GNSS signals experience different types of disturbances. The

user receiver should process these signals. In such cases, the estimated navigation solution includes contributions from atmospheric effects and equipment errors. However, the use of a simulation platform that models the real world scenarios would provide the user flexibility to control the environment and retain maximum signal fidelity. Subsequently, the receiver performance metrics under consideration can be quantified accurately with the simulation environment.

To undertake research involving GNSS signals impacted by interference from jammers and other transmitters, one should ideally have access to outdoor test facilities like the Galileo Test and Development Environment (GATE) (Cuntz et al 2011, Heinrichs et al 2010) or an anechoic chamber. GATE is an outdoor test environment primarily created for developing and testing Galileo in Southern Bavaria. It consists of pseudo satellites located on mountain tops. An alternative to the above two methods and followed by a majority of researchers is a two-step data collection approach, i.e. collect live or simulated data followed by the addition of interfering signals offline (using a simulation platform). When interference signals are generated from signal generators, they are physically combined with the live signals using wires; in this case, the data collection setup becomes complex with many combiners, cables and connectors. A simpler method employing software simulations is an alternative and provides full control of the simulation environment; in this case, desirable signals and interference can be generated concurrently.

Several methods have been proposed to achieve signal resilience in interference environments. In these methods, interference detection and mitigation are performed by analyzing the temporal, spectral and spatial properties of the incoming signals. Among

these, antenna array based approaches stand out with advantageous features. These spatial processing methods typically use the controlled radiation pattern antenna (CRPA). A CRPA can be realized using an antenna array where the antenna gain in a particular direction can be controlled by changing the beamformer weights appropriately. The process of data collection for performing research in this area requires substantial efforts. A multi-antenna hardware simulator is an option. But, this is challenging to implement and costly.

For GNSS applications, a single antenna GPS signal simulation platform was proposed by Dong (2003). Zhao et al (2006) discussed an approach to generate signals for space-time adaptive processing in GPS. A GPS array signal simulator obtains the positions and velocities of satellites from stored ephemeris or internet archives and the array configuration. Most GNSS software simulations have been performed using only carrier and coarse-acquisition (C/A) codes, without considering navigation data. A sample navigation data was added in a few simulations. All signal processing related results can be analyzed with these methods; however, to perform navigation domain evaluations, actual navigation data should be embedded.

Having a multiple antenna signal simulator testbed would accomplish the following objectives:

- enables signal generation in a controlled environment
- provides flexibility in maintaining signal and interference source parameters (e.g. number of sources / signal levels / directions)
- flexibility to extend to any number of antenna array elements
- flexibility to have any type of array configuration

- enables analysis in the navigation domain
- provides control on the signal bandwidth of the collected samples
- enables easy simulation of other GNSS (e.g. pseudolites).

1.3 Exploring space-time processing in GNSS

In antenna array processing, multiple antennas are arranged in different configurations (linear, planar, rectangular, circular, etc).The diversity obtained from the antennas is exploited in spatial processing. Attaching a tapped delay line (TDL) to each antenna facilitates temporal processing. The signal arriving at each of the array element along with the delayed versions from TDLs will be combined in spatio-temporal processing in such a way that the signal-to-interference plus noise ratio (SINR) increases and at the same time results in interference cancellation. The amplitude and phase array weights (complex weights) are computed based on different optimization criteria. The CRPA can be achieved using an antenna array, in which case the antenna gain in a particular direction can be controlled by changing weights appropriately. Thus, the array pattern can be controlled electronically without physically moving the antenna.

1.3.1 Space-time beamformers and applications

There have been several approaches proposed by researchers to explore spatial and temporal degrees of freedom. Following are the highlights of these methods.

Antenna array processing can be performed in the pre-correlation stage, post-correlation stage, or at both stages with different algorithms. Generally, when details about the desired signal are not available, a processing method is chosen for the pre-correlation

stage. If the desired signal characteristics are known or extracted (navigation data bits in case of GPS) one can use post-correlation processing (De Lorenzo et al 2005). When the direction of arrival information of either satellite or interference source is not known, a simple Power Minimization (PM) algorithm can be used (Fante et al 2004). A comparison of spatial domain Minimum Variance Distortionless Response (MVDR) and space-time MVDR was done by Puska et al (2005); it was concluded from the study that, when angular separation between the desired and undesirable signals is relatively low, space-time MVDR gives best performance compared against the space MVDR method. The MVDR beamformer provides a high SNR increase for the direct signal. In the process of adapting the weights, the algorithm minimizes the output power subject to a linear constraint, which preserves the desired direct signal and leaves it undisturbed.

Research undertaken by Lijun et al (2007) shows that the tracking performance obtained by multiple MVDR is better than a single MVDR optimized to maintain unity gain in all desired directions simultaneously.

The mathematical formulation of Eigen beamformers for use in GNSS applications is given in Fernández-Prades et al (2011). This only requires estimation of the noise power and the power and spatial signature of the signal of interest. This method can be used to obtain improved SINR performance even when the details of the reference signal are not known. This method is also known as Eigen vector beamforming, projection based beamforming or reduced covariance matrix beamforming.

Similar in approach to the Eigen beamformer method is the subspace orthogonal projection method (Hongwei et al 2011). Here, strong interference signals are suppressed by projecting the received signal on the interference-free subspace. After orthogonal

projection, the antenna array will bring about nulling effects in the direction of interference to suppress it.

Reduced rank STAP methods are powerful and effective with the advantage that they have faster convergence and better tracking performance than full rank. Additionally, large numbers of interference signals are rejected with less complexity. Multi Stage Nested Wiener Filter was also one such method proposed (Lu & Sun 2010). When antenna array processing is used in an interference free environment, increasing the number of antennas or the number of time taps yields higher carrier-to-noise-density ratio (C/N_0) values (Chang & Juang 2008). However, the introduction of antenna array processing leads to distortions such as cross correlation function (CCF) misshaping, attenuation and noise domination, and measurement biases. In GPS, it may be functionally easier to add time taps than adding antennas. As quoted in De Lorenzo et al (2005), even with two antennas, STAP will dramatically improve weak signal tracking performance. In the same work, it is shown that C/N_0 performance depends on the accuracy of the steering vectors. Methods that require prior knowledge about the desired signal (e.g. least mean squares (LMS), minimum mean squared error (MMSE) approach) give improved results.

A study performed by Chang & Wu (2011) offers a guideline for STAP algorithm selection for a practical realization and design of new processing methods. This study concludes that the Multi Stage Nested Wiener Filter (MSNWF) (Myrick & Goldstein 1999) provides the best performance but has dependency on the direction of arrival. The LMS algorithm has the next best performance but is not always practical. Recursive Least-Squares (RLS) and Simple Matrix Inversion (SMI) algorithms have next best performance to

MSNWF but with increased computational complexity. Since Power Minimization (PM) and reduced rank PM do not require knowledge of satellite direction, they are most practical. A different version of 2-D filtering called Space Frequency Adaptive Filter (SFAP) is discussed by Lu et al (2007) designed for multipath mitigation based on power minimization criteria.

The performance of the beamforming strongly depends on the number of elements in the array. With a higher number of elements, good performance can be achieved at the cost of increased processing complexity (Lijun et al 2007).

1.3.2 Issues in space-time processing

Antenna array processing techniques are studied in GNSS as effective tools to mitigate interference in spatial and spatiotemporal domains. However, without specific considerations, the array processing results in biases and distortions in the cross ambiguity function (CAF) of the ranging codes. In ***Space-time processing (STP)*** the CAF misshaping can happen due to the combined effect of space-time processing and the unintentional signal attenuation by filtering.

1.3.2.1 Biases

The CAF or CCF distortions are mainly introduced because of the temporal part of filtering (Church et al 2007). These biases vary based on the direction and also on the number of interference signals nullified by the filter.

1.3.2.2 Distortions

STAP does not provide a linear phase frequency response across the operating band due to its architecture (Shuangxun et al 2006), which leads to distortions, each one being unique for each desired signal. With distortions, the CCF is broadened (Shuangxun et al 2006, Hatke 1998). Unevenly broadened CCF will lead to an offset in code measurements. In spite of their advantages in interference mitigation, STP methods have a few disadvantages. Based on the type of optimization used in the weight computation, they not only introduce signal degradation in the form of measurement distortions but also deteriorate signal acquisition and tracking performance (Church et al 2007) for some satellites, which results in inferior position estimates (Fante & Vaccaro 2000). Distortions observed are different when different interference mitigation criteria are used (Shuangxun et al 2006). As seen in the literature, some studies have been done to characterize these distortions. Fante & Vaccaro (2000) have characterized the distortions in CCF for various interference and multipath conditions. The distortion in the CCF for a seven-element antenna array in the presence of two interferers was characterized by Myrick et al (2001). Here, the effect of the distortions in the position domain was not evaluated. As per Fante et al (2004) the error introduced in the correlation function will be about 5 ns (on an average, for a particular two interference scenario mentioned in the paper) and restricted to only some portion of the hemispherical gain pattern; this work also suggests that the distortion related biases depend on the number of interference signals and their spatial proximity to the desired signals.

The term space time adaptive processing (STAP) is widely used in the area of GNSS antenna arrays, even though it is not truly *adaptive* in nature. Even the work stated on

distortion characterization (in the previous paragraph) and mitigation techniques (in the upcoming paragraph) deals with *non-adaptive* space-time processing. The work done by Fante & Vaccaro (2000) and Myrick & Goldstein (1999) suggests that their methods could be extended to moving user scenarios, but results are given for space-time processing and STAP. Later research by Fante et al (2004) shows that distortion will increase when the interference and desired signal arrive from the same direction. This indicates that distortions will vary for a moving user or for moving interference source.

1.3.3 Attempts done for distortion mitigation

In general, distortion is an artifact that results when the signal reconstructed from the samples is different from the original continuous signal. There are several distortion mitigation methods proposed by researchers. One of the techniques proposed by Shuangxun et al (2006) uses a least squares inverse filter. This makes use of the complex coefficients of the designed STAP filter and the steering vector details. A compensating filter is required for each satellite signal. A 64^{th} order filter is used to compensate and the distortion effects can only be reduced but cannot be completely removed (Shuangxun et al 2006).

A faster convergence and reduced complexity method based on Normalized Least Mean Squares (NLMS) and MSNWF is proposed by Lu & Sun (2010); where it is proposed that NLMS introduces less distortion. Hatke (1998) has proposed a method for wideband interference mitigation mainly for the multipath and the distortion is reduced using minimum length equalizers. Based on the conjugate symmetry space-time pre-processor, Myrick et al (2000) proposed a method for distortion mitigation that was made

computationally efficient by changing the correlation matrix into real values. However, with reduced complexity some degradation in the nulling performance of the preprocessor was observed.

The distortion in the CCF in STP is due to the combined effect of signal attenuation and CAF misshaping in STP. Since the live real world signal received will always embed contribution due to noise, determining the individual contributions to CCF distortion is challenging and not addressed in the literature. Availability of a simulation test-bed that can generate noise-free signals would help in this scenario. Also, observing the work from other researchers, the contribution of these measurement distortions due to STP in the position domain is not analyzed.

1.4 Antenna arrays for interference due to terrestrial transmitters

Ground based transmitters are one of the main sources of GNSS interference. The harmonics and spurious emissions from Frequency modulation (FM), very high frequency (VHF) and ultra-high frequency (UHF) stations can enter GNSS bands and may degrade GNSS receiver operation. Sound signal carriers from the FM radio tower (narrow band signals) and TV tower emissions having narrowband or wideband signals are strong sources of interference for GNSS receivers (Borio 2008). VHF radio navigation and communication links used in aviation and maritime applications also pose potential threat to the GNSS receivers.

A pseudolite is a ground-based transmitter of navigation signals. The signals from these pseudolites are very similar to GNSS signals and can be much stronger depending on

the distance between transmitter and receiver. The data from pseudolites is mainly used for the following purposes (as identified during literature review):

- to get additional ranging measurements
- to send the correction details for the GPS measurements
- as a result of above two, to provide improved position accuracy
- when four or more pseudolites are deployed, can be used for independent navigation, generally called as Alternate Precision Navigation and Timing (APNT) (Czabaranek 2013).

In the pseudolite system paradigm, a receiver that has the capability to decode and use pseudolite signals is termed a *participating* receiver and one that does not have this capability is termed a *non-participating* receiver (Borio et al 2011). Pseudolites are used for augmentation in numerous applications such as tracking container movement in harbors and open-pit mining. In addition to augmentation, pseudolites are being considered for independent navigation and positioning in defense areas and for indoor navigation (So et al 2010, Wang 2002, Dai et al 2001). In all these applications *participating* and *non-participating* receivers should co-exist and be fully operational. Experiments conducted in the past suggest that pseudolites be developed to complement existing GNSS systems (e.g. GPS, Galileo) with continuous signal transmission which is different from the recommendation of Radio Technical Commission for Maritime services (RTCM). However, the use of a continuous signal adopting the same modulation used by existing GNSS signals does not provide any protection for *non-participating* receivers.

The 1559-1610 MHz band is used by GNSS as well as by augmentation systems and is intensively used for aeronautical radio navigation applications (International Civil Aviation Organization 2012). As per the RTCM SC-104 (Stansell 1986), pseudolite uses GPS L1 frequency with different pseudo random number (PRN) sequences to transmit the signals in the form of frequent, short (e.g.10% duty cycle) and strong pulses. At a distance of 50 m from a pseudolite transmitter, the pseudolite signal can be 60 dB above the nominal signal strength of the GPS signal (Stansell 1986)**.** This scheme has been tested in several designs and some modifications proposed. Even though pulsing helps reducing the effect of interference on GPS signals in the *near region*, it will result in inferior sensitivity performance in the *far region*. It is also quoted in a recent study that pulsing of the signal provides a certain level of interference mitigation without the need to modify the receiver (Borio et al 2011, Martin et al 2007). The major issue of the '*near-far*' problem and the interference observed due to pseudolites is widely discussed in the literature (Amt & Raquet 2007, Soon et al 2003, Wang 2002, Cobb 1997). There is ongoing research to overcome this problem and to avoid interference in the operating GNSS band (O'Driscoll et al 2011, Borio & Fortuny 2010).

As seen by Tsujii et al (2004), for a field test conducted by JAXA (Japan Aerospace Exploration Agency) a pseudolite is placed on a helicopter and an improvement in position accuracy is observed for a receiver on earth. Different defense and governmental agencies have performed real time tests with the pseudolites (Soon et al 2003) and also there is a mention of test beds available for testing pseudolite deployment.

Classical methods like pulse blanking are used in mitigating pseudolite interference (Konovaltsev et al 2008). However, signal removal due to blanking will have ill effects on

GPS sensitivity and this method cannot be applied to continuous pseudolites. A wavelet transform based interference mitigation scheme for distance measuring equipment (DME) interference is discussed in Paonni et al (2010). In Juang & Chang (2005) antenna array is used for pseudolite interference mitigation by employing block adaptation in spatial processing mode.

When pseudolite signal characteristics are known, a method that uses Successive Interference Cancellation (SIC) architecture for addressing this *near-far* problem is possible (Madhani et al 2003). However, when the thresholds for detection of pseudolite interference are not chosen properly, SIC can cause impairment on GPS signal processing such as acquisition failure. Moreover, this method cannot be extended to *non-participating* receivers, as these do not know the signal parameters like the pulsing sequence. SIC can be used for cancelling wideband interference due to pseudolites in *participating receivers*, even with a single RF channel (antenna).

1.5 Scope for further research

In the process of the above literature review, the following points were identified and these result in opportunities for further research:

a) It would be useful to generate a GNSS simulation platform that can also embed navigation data into the generated data. Subsequently, this would facilitate performance comparison in the position domain.
b) Distortion analysis was performed for space-time processing of real or simulated GPS signals. However, emphasis has not been given on the contribution from noise and losses due to cross correlation.

c) Few methods for CCF distortion have been identified but all of them claim that the distortion added due to array processing was reduced; however, position domain analysis was not done. This could be of interest for high accuracy applications when studied by a varying number of interference sources.

d) Space and space-time processing techniques with many antenna elements were mainly used for military applications. Space-time processing with fewer array elements can also provide considerable improvement in interference affected environments, mainly targeted to civilian applications.

e) Detailed studies on the use of antenna arrays for mitigating GNSS pseudolite interference have not been carried out. The mitigation methods presently available for pseudolite interference requires information about the pseudolite signal structure. But antenna array techniques can be used even without this knowledge. Proposed methods like pulse blanking and one based on SIC cannot be used in *non-participating* receivers.

f) Unlike other ground based interferers, pseudolites transmit their positions. Pseudolite position information has not been taken into account while computing the beamformer or during null steering. Also, not much work has been done on the use of antenna arrays with spatial and space-time processing for pseudolite interference reduction.

g) The standard STAP architecture uses Finite Impulse Response (FIR) structure in the path of each antenna array element. Therefore, distortion reduction can be explored by maintaining symmetry in the filter coefficients.

Given these open areas, objectives for further research are laid down in the next section.

1.6 Objectives and contributions

Considering the work of other researchers in the public literature, the planned objectives of the thesis and their implementations are now stated. The prime focus is to study space-time processing techniques for GNSS signal robustness in electronic interference environments. The objectives and the corresponding areas of research on space-time processing are shown in Figure 1-2.

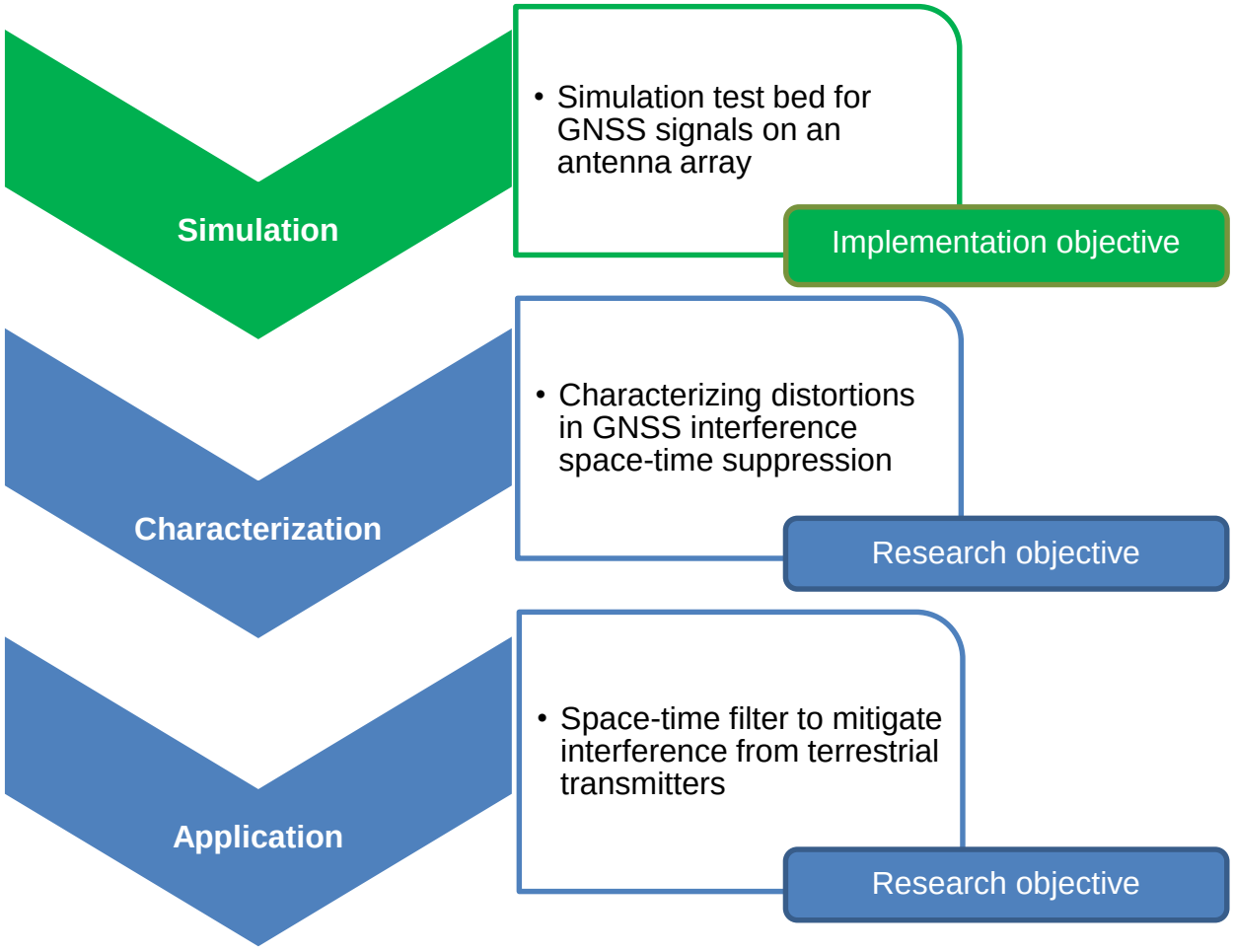

Figure 1-2: Mapping between areas of research and the objectives

The following subsections provide details on different tasks pursued to fulfill the objectives in Figure 1-2.

1.6.1 Antenna array simulation

The design of an antenna array simulation platform that can provide data samples corresponding to all types of scenarios is required. To develop this tool, the following steps will be carried out:

a) The challenges involved in generating interference scenarios will be assessed.
b) A method to simulate GNSS signals will be developed, that uses recorded data from single RF hardware simulator, and signal simulations will be performed for an ideal antenna array configuration, i.e. without mutual coupling, calibration errors, phase center variations and antenna element distortions.
c) The fidelity of the simulated signals will be inter-compared using signal tracking metrics like carrier Doppler and C/N_0 and these will be compared with the tracking metrics for two standard hardware simulators, namely the Spirent GSS-7700 and the Rohde & Schwarz SMBV-100. The tracking performance (considering the carrier Doppler and C/N_0 as comparison metrics) of the software simulator developed by the author as part of this research will be evaluated through a comparison with the above hardware simulators.
d) The capability of the simulator to generate antenna array signals will be demonstrated using the Minimum Power Distortion less Response (MPDR) beamformer and an improvement in processing gain will be shown.

e) An interference scenario with single continuous wave interference (CWI) will be simulated and the presence of interference in the simulated signal at the desirable direction will be validated with the help of array gain patterns.

1.6.2 Distortion characterization

The distortions due to space-time processing will be characterized for different methods, configurations of interference conditions and noise levels. In order to attain the objective, the following tasks will be carried out:

a) The need for having a simulation framework for performing distortion analysis will be discussed.

b) A *distortion metric* that would help to quantify the distortions in space-time processing will be introduced. The distortions observed for different PRNs and different number of taps will be tabulated and the contribution of these distortions to the position errors will be characterized.

c) Using single PRN noise free signal simulations, CCF distortions due to STP will be studied. Effects due to the presence of a higher number of interference sources and mitigation performance improvements by increasing the number of taps will be studied.

d) The effect of the spatial closeness of the interference source to the satellite signals and the effects observed in different beamforming methods will be analyzed.

e) Different space time techniques will be compared with focus on distortions. Real data collection using an antenna array with six elements for the case of a static user will be conducted. The desired interference sources will be simulated offline and added to

these samples. *Blind*, *semi-distortionless* and *distortionless* methods will be compared.

To get an insight on STP distortions, non-adaptive methods are considered in this thesis. Ultimately, it would be desirable to study these distortions for adaptive methods. However, it is strongly believed that the insight obtained from the study of non-adaptive methods will provide a detailed picture about STP distortions; hence, extending the characterization for adaptive methods will complete the study. This part of the research focusses on analysing the STP distortions but not on developing new beamforming methods. Therefore, non-adaptive methods that are suited for static scenarios are employed in this thesis; however, analyses can be repeated for adaptive methods for dynamic scenarios by considering the test cases and metrics used herein. Some of the findings in the thesis would likely apply to distortions in STAP.

1.6.3 Mitigate terrestrial interference

An interference mitigation method employing space time processing for interference due to high power terrestrial transmitters will be proposed. In order to attain these objectives, the following approaches will be considered:

a) Capability of an antenna array to mitigate interference due to high power pseudolites in the *near region* will be demonstrated through simulations. The results obtained with even a simple form of beamforming will demonstrate the suitability of the array processing methods for the interference impacted *non-participating* receivers.

b) The advantages of STP over space only processing will be demonstrated by comparing the acquisition status and antenna array gain patterns. Possible signal

enhancements to the GPS and pseudolite PRNs with a beamformer that uses a signal's angle of arrival approach, will also be demonstrated.

c) Furthermore, contribution of the above processing with additional measurements from pseudolites on the dilution of precision (DOP) will be studied.

1.7 Thesis outline

This thesis contains six chapters and the content of the five remaining chapters is detailed below.

Chapter 2 begins with an overview of GNSS vulnerabilities and signal models being used in subsequent sections. The different types of interference and their effect on different stages of receiver processing and countermeasures are discussed. The types of beamformers used in this research are formulated and the architectures of the receivers used for evaluation of the results are explained.

In Chapter 3, a new method for simulating GNSS signals corresponding to an antenna array is proposed and implemented in a software simulator. The results from this test bed are validated through comparison with two standard hardware simulators. The capability of the software simulator to generate different interference conditions and other GNSS signals (e.g. pseudolites) is studied.

The distortion of the CAF due to space-time processing is characterized in Chapter 4. Distortions are studied under different noise and interference conditions with a varying number of antenna array elements. Different space time methods are compared and analyzed for distortions. Real data collected using a static antenna array with six elements

is used. The desired interference sources are simulated offline and added to these samples.

Chapter 5 introduces a space-time processing technique for interference due to pseudolites. An illustration of how the method combats pseudolite interference in the *near zone* and recovers signals in the *operating zone*, is provided.

Chapter 6 provides conclusions and recommendations for future work.

The thesis organization is shown in Figure 1-3.

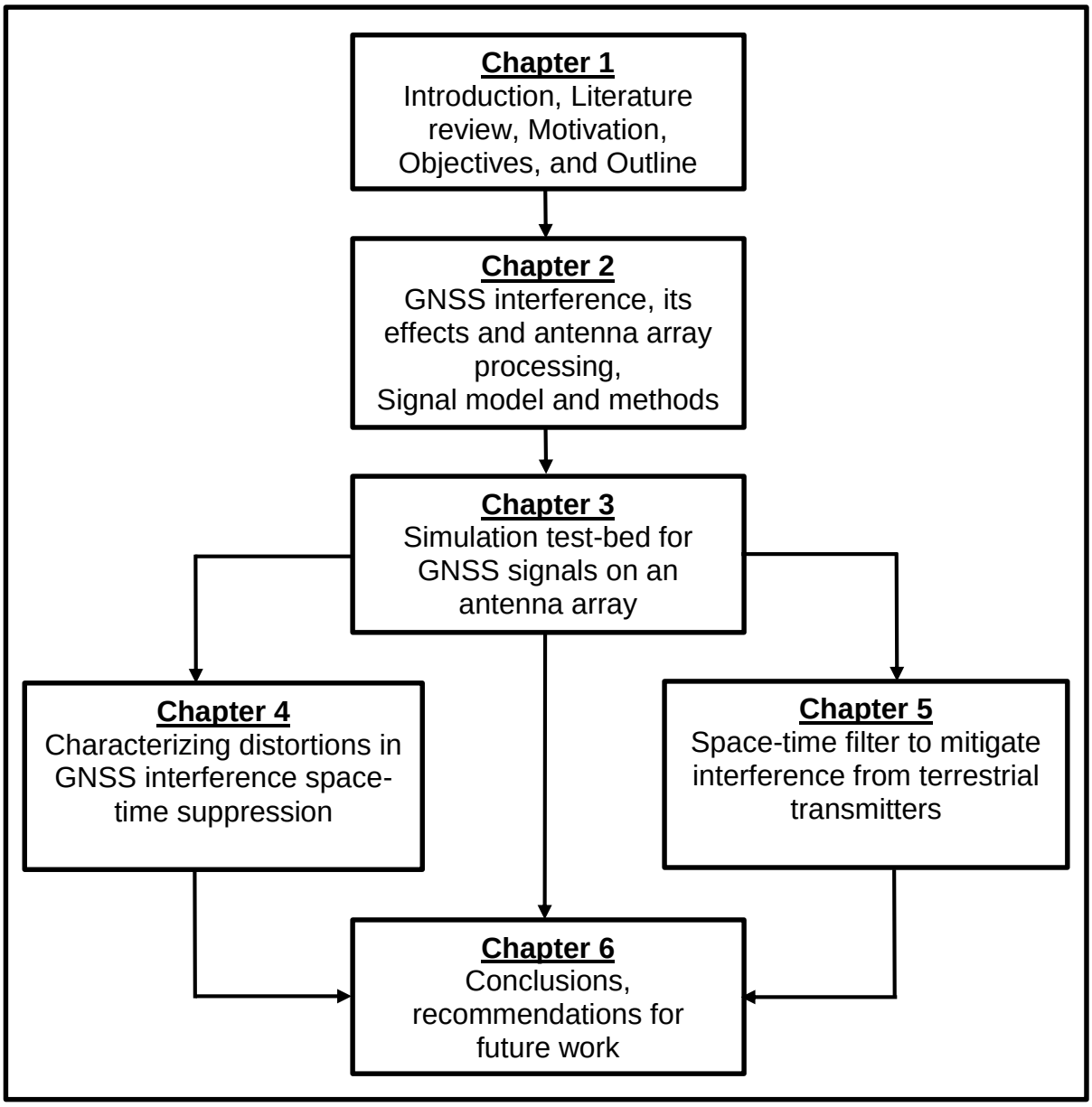

Figure 1-3: Thesis outline and information flow across chapters

CHAPTER 2: GNSS INTERFERENCE AND ANTENNA ARRAY PROCESSING

GNSS provide a variety of features enabling use in a plethora of applications. Specifically, GPS and GLONASS have following salient features – being active at all places on or near earth and at any time, unaffected by weather conditions, and provides inherent jamming immunity. However, the signals received on the Earth's surface are very weak. The satellites send the signals at a high power (about 27 W), but the level observed at the user segment is typically of the order of 10^{-16} W. GNSS employs DSSS modulation and this provides a feature whereby the signal before despreading is buried in noise. At low values of the signal power, GNSS signals are vulnerable to even very small disturbances or undesirable signals in their operating frequency band. To achieve higher performance like accuracy, precision, continuity, reliability, availability, the present day communication systems used for navigation embed transceivers of many wireless systems. To realize much functionality in a compact form factor and to include all desired functionalities within the available printed circuit board (PCB) area, the RF components of different wireless systems are packed in close proximity. This can cause inter-system RF coupling issues and result in inferior performance. Moreover, due to the wide bandwidth allowed in the front-end and the non-linearity of the components used for the hardware design, a GNSS receiver may observe undesirable signals in its reception port. The sources of this could be intentional or unintentional; their presence will degrade the GNSS performance. An illustration in Figure 2-1 demonstrates the low power of received GPS signals (Hoey & Benshoof 2005).

A 100 watt bulb is 10^{18} times more powerful than a GPS satellite signal at the receiver antenna

Figure 2-1: Illustration of low GPS signal power

2.1 Introduction to GNSS vulnerabilities and signal processing

Radio frequency interference (RFI) is defined in many ways. The International Telecommunication Union (ITU) defines RFI as "*the effect of unwanted energy due to one or a combination of emissions, radiations, or inductions upon reception in a radio communication system, manifested by any performance degradation, misinterpretation, or loss of information which could be extracted in the absence of such unwanted energy*" (Biggs 2013). A simplified definition is given by Kaplan & Hegarty (2006); it states that "*RF signals from any undesired source that are received by a GNSS receiver are considered interference*". Some of the GNSS interferences sources are – radio, TV, wireless communications, DME, RADAR, and pseudolites. The maximum signal levels for a user on earth is -158 dBW (for GPS L1) at a satellite elevation angle of 40° and minimum signal level of -160 dBW at the zenith and at the horizon (Parkinson & Spilker Jr. 1996). The average value is -158.5 dBW. Considering the example of a consumer grade GPS receiver operating with 2 MHz bandwidth and at ambient temperature of 300˚ K, one obtains a noise floor of -140.82 dBW. Here, the level of noise is higher than the signal power level. By allowing wider bandwidth higher noise will be allowed into the

system and noise floor further raises. Since GNSS (receivers) coexist with other wireless communication systems and they have small received power, they are much vulnerable to other disturbing signals.

2.1.1 Interference source categorization

All unwanted signals at the GNSS receiver front-end could be considered as interference. The different types of undesirable signals at the GNSS receiver front-end are due to:

- spoofing (GNSS like signals in the band of interest or due to transmission of artificial GNSS signals)
- meaconing (re-transmission of the earlier received GNSS signals)
- multipath/ghosting (GNSS signals reaching the receiver after single/multiple reflections from different surfaces)
- jamming.

Interference can be characterized based on a number of properties, namely interference type (as continuous wave, amplitude, frequency or phase modulated signals, noise), centre frequency (as in-band, near-band, out-of-band), bandwidth (as wideband, narrowband), power (as strong, weak – based on J/S or JNR), and time domain properties (as continuous, pulse with different pulse widths, pulse repetition frequencies and duty cycles) (de Bakker 2007). Two other ways of classification based on the type of interference source and based on spectral/time properties are given by Dovis (2011) as follows: (i) intentional (by using jammer devices) or unintentional (because of terrestrial communication signals or due to improper design issues), (ii) CWI, pulse interference,

chirp interference, wide band interference (narrowband if $B_{Interference} << B_{GNSS}$, wideband if $B_{Interference} \approx B_{GNSS}$, for $B = Bandwidth$).

Interference types listed above are described here with a few practical examples. Supposing a GPS receiver processes signal content present in ±5 MHz from the centre frequency of 1575.42 MHz, all interfering signals that fall within this band of 10 MHz are considered as in-band interference. If the interfering signal lies in the frequency band outside the above said band, the type of interference is said to be out-of-band interference.

The continuous wave interference is one in which interfering signals can be modeled using pure sinusoids. In communication systems, for long distance communication sinusoidal carriers are used and this necessitates use of a reference oscillator at the receiver end. The non-linearity and imperfections present in the electronic components used in the construction of oscillators may result in CWI. The pulsed signals have concentrated signal content in the time domain. A few of the present day communication systems that use pulsed mode of transmission are ultra-wideband (UWB) used for short-range communication, radar, DME used for landing operations, etc. These form potential disturbing signals for GNSS. The effect on GNSS signals due to the pulsed interference is determined by the periodicity of the pulsing sequence and duty cycle of the pulsing signal.

The narrowband matched sources follow a narrowband Gaussian probability distribution function. Disturbing signals can be modelled as Gaussian processes and in particular the qualifier *narrowband* is used for the reason that the spectrum of these disturbing signals occupies a relatively small portion of the receiver band (Borio 2008). These signals can

have a high bandwidth, lower compared to GNSS signal bandwidths. In case of swept interference, the disturbing signal sweeps over the GNSS signal frequencies. This type of interference can be observed in the near-zone of the VHF transmitters.

A few examples of practical interference scenarios are as follows (Borio 2008):

- *TV transmitters* - these can generate both wide and narrowband interference
- *Personal Electronic Devices (PED)* – with the introduction of new high data rate applications into PEDs, different types of interfering sources can be expected in future
- *satellite based navigation* – spurious harmonic emissions from the geo-stationary satellites.

Operation of jammers in many nations is illegal and may subject one to substantial penalties. Still, many GNSS jamming devices are available for purchase over the internet. These relatively cheap devices (some costing less than an inexpensive GNSS receiver), pose a significant risk to the normal operation of many systems reliant on GNSS (Mitch et al 2012). With the increased availability of UAVs or drones, a new type of intentional interference can be envisaged. Maneuverability and the unmanned nature of these systems might be explored to generate harsh and dynamic jamming conditions which might lead to a new class of interference, namely *drone-borne jammers.*

2.1.2 Effects of interference on GNSS signals

Due to the presence of interference overall receiver performance is degraded. Based on the type of interference the impact on different receiver parameters may vary. Generally, in the receivers, these effects can also be used to detect the presence of interference and

decide on the mitigation method to counter detected interference. de Bakker (2007) discussed some effects that could be observed in an interference impacted receiver. They are:

- front-end saturation: can cause saturation of first stage in the RF chain (improper receiver operation)
- acquisition failure: interference leads to partial or full failure of GNSS signal acquisition
- drop of measured signal strength
- loss of receiver tracking (failure in carrier and code tracking)
- errors in navigation data bit decoding (Curran et al 2016)
- pseudorange errors (increase in noise in the phase and code measurements, increased variances and biases due to errors in carrier and code tracking)
- increase in cycle slips in the carrier phase measurements
- position accuracy degradation.

In summary, interference poses a threat to accuracy and compromises position integrity. Interference can also affect the continuity and availability of navigation solution. The effects of interference are practically analyzed at different stages of a standard receiver operation namely acquisition, tracking and navigation (shown in Figure 2-2).

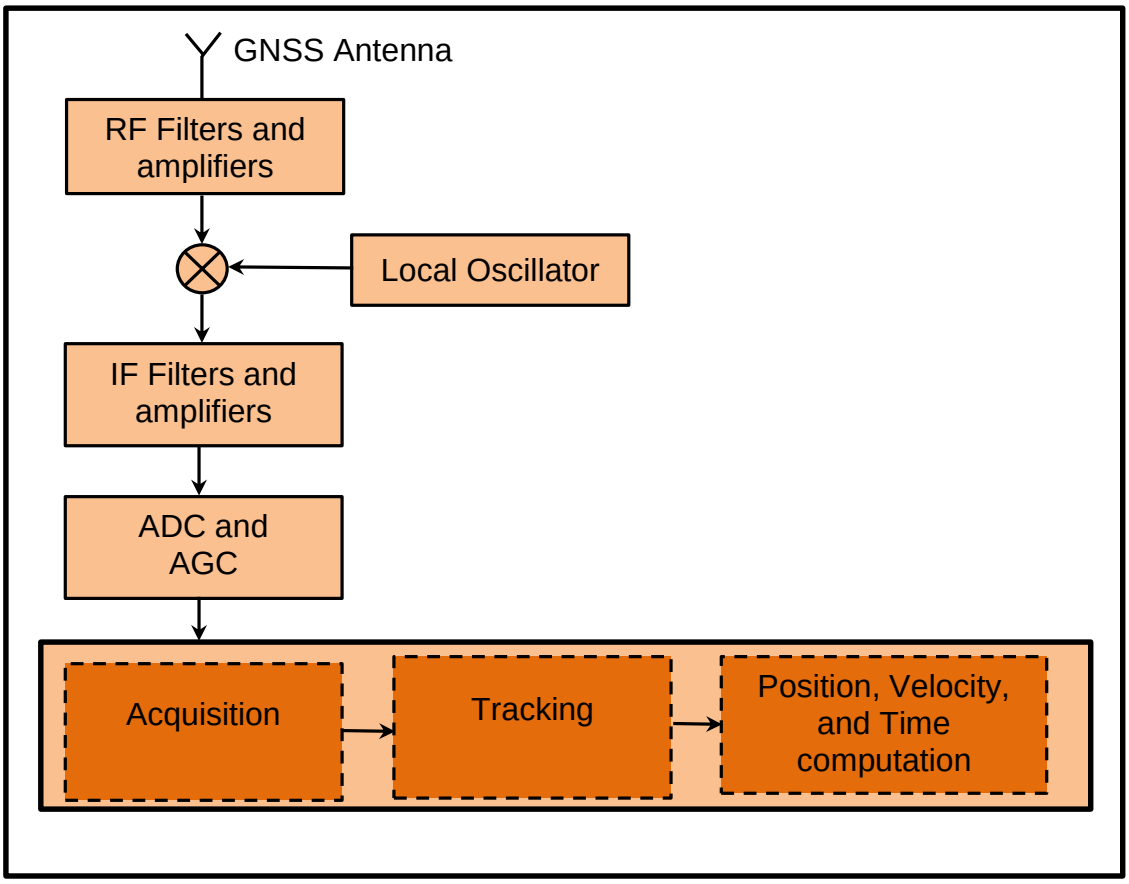

Figure 2-2: GNSS receiver stages vulnerable to interference

Before proceeding with the interference effects at different processing stages, the description of the test setup used to perform these tests is provided. The tests are performed in laboratory with GPS static scenarios by taking signals from a live antenna or from a hardware simulator (Spirent simulator GSS7700 in this case). Different components used and the flowchart based on which the tests are done are shown in Figure 2-3.

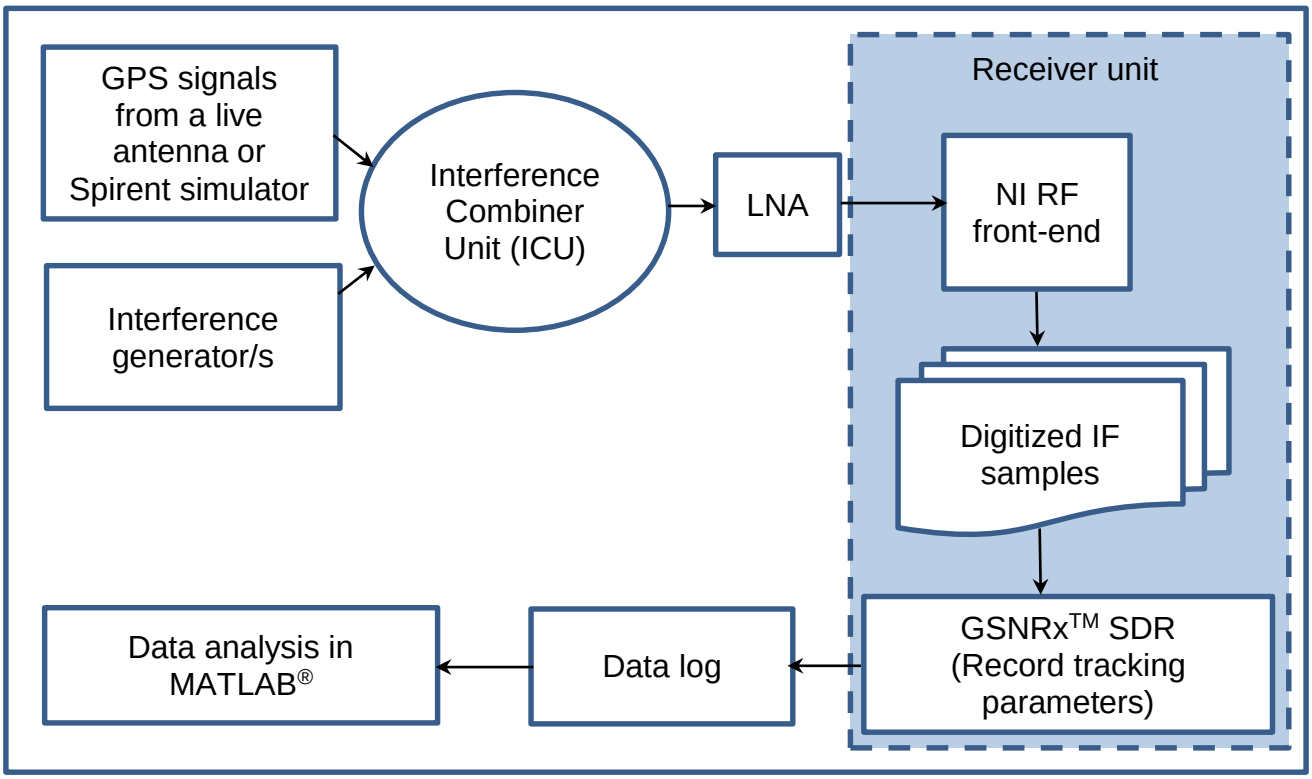

Figure 2-3: Test setup used for analyzing interference effects

The description of the components used for the analysis is given below.

GPS Signal Source **–** The signal source is chosen based on the type of test. The signals from a single or the multi-channel simulator or from the antenna are used. For evaluating the tracking performance of the signals in the presence of interference, the single channel simulator is used, to provide full control to the user on configuring the simulated dynamics. The position evaluation is performed using signals from the multi-channel simulator.

Interference source **–** The interference signals are simulated using the general-purpose signal generators from Agilent Technology. These provide an option to the user to choose the source as sinusoidal, pulsed etc.

Interference Combiner Unit (ICU) **–** Since the GPS signals and the interference are generated separately, they are combined using an external unit. For this, the GSS 4766 Spirent combiner is used in the test setup. At the output of the ICU, GPS signals which are subjected to interference are obtained.

Low Noise Amplifier (LNA) **–** The system's noise performance is improved by using an LNA module from Mini-Circuits. This will also compensate for the losses incurred due to the cable length.

RF front-end **–** The analog signal obtained at the output of LNA is down converted and sampled by a general purpose RF front-end designed by National Instruments (NI). After digitizing the signals, the front-end dumps the data into binary files. The details of the digitized IF file are given in Table 2-1.

Table 2-1: Details about IF and scenario duration

Sl. No.	Parameter	Description
1	Intermediate Frequency	420 kHz
2	Bandwidth	10 MHz
3	Log duration	25 – 30 seconds for tracking analysis 300 seconds for position analysis

Software GNSS receiver GSNRx™ **–** The standard version of the software receiver GSNRx™, developed by the PLAN Group (Petovello et al 2008), is used to monitor the tracking and positioning observations.

Interference effects are analyzed for pulsed and continuous wave (CW) interference. The interference signal details are provided in Table 2-2. The CW interference effects are analyzed at three different signal levels.

Table 2-2: Amplitude and frequency settings used to analyze interference effects

Input parameter settings	In-band interference	
	CW Interference	*Pulse Interference*
Frequency / Pulse Specification	1575.62 MHz	Period: 1 ms Width: 100 μs
Interference Signal Amplitude (dBm)	-105, -110, -115	-20
GPS signal level (dBm)	-130	-130

2.1.2.1 Acquisition domain

Thermal noise is inherent in the signals received by the antenna. The automatic gain control (AGC) block in the front-end not only maintains a constant gain but is also used to determine the threshold levels for quantization (Deshpande 2004). Presence of any interference increases the noise power in the receiver. The GPS signals near the user's antenna are very weak and in an interference free condition signals lie below the noise floor. Consequently, down converted IF samples are perfectly random in their occurrence and follow a Gaussian distribution (shown in Figure 2-4 (a) and (b)). Input data samples are highly correlated in the presence of high power interference. As seen in Figure 2-4 (c), the zoomed portion of the time domain samples corresponding to this condition, a sinusoidal variation is evident due to the presence of CW interference. A manifold increase in input signal may lead to signal saturation depending on the dynamic range of the analog to digital converter (ADC). Since 14-bit ADC is considered, ADC saturation is not present in the illustration. With interference, the histogram of the input samples not only deviates from the Gaussian curve, but also widens by a large amount (shown in Figure 2-4 (d)).

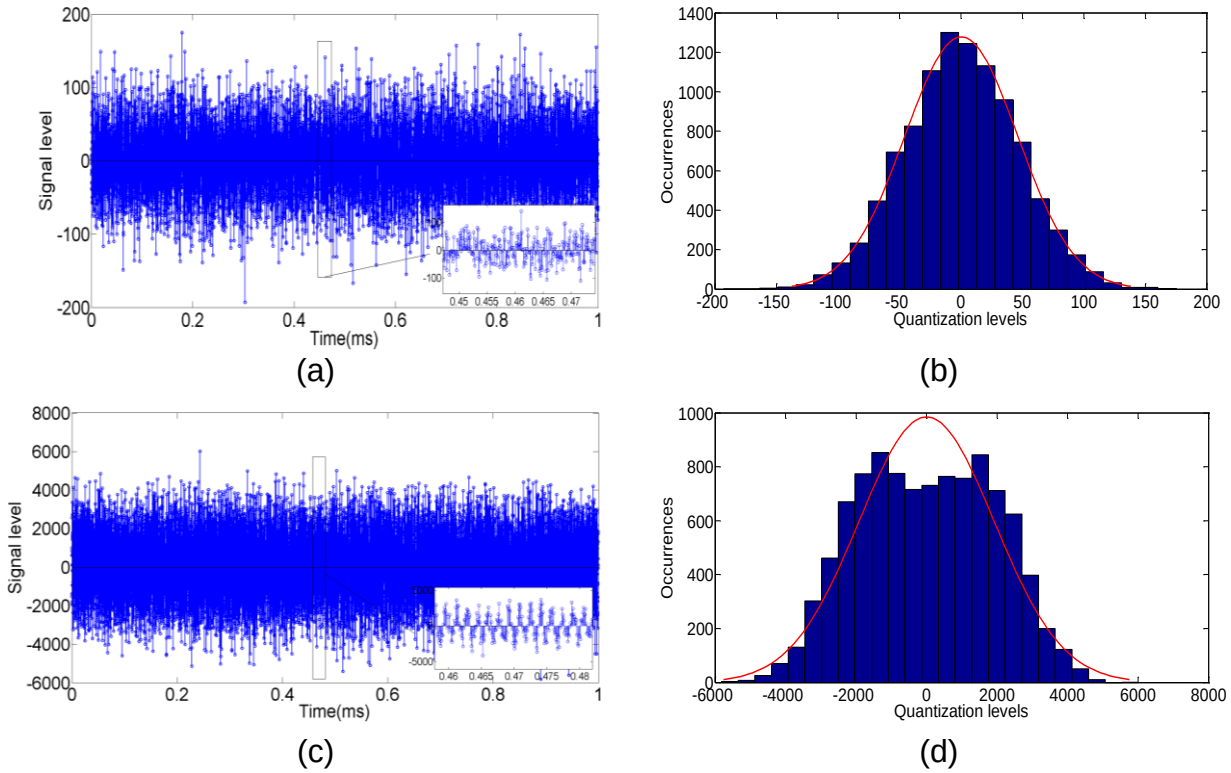

Figure 2-4: Comparison of interference effect on the recorded IF samples
(a) time domain representation of the clean IF samples: free from interference
(b) histogram of the clean IF samples: free from interference
(c) time domain representation of the IF samples with CW interference
(d) histogram of the IF samples with CW interference

An illustration of interference effects in the spectral domain is given in Figure 2-5. Here, the CAF of a particular PRN is analyzed for *interference free* and *with interference* conditions.

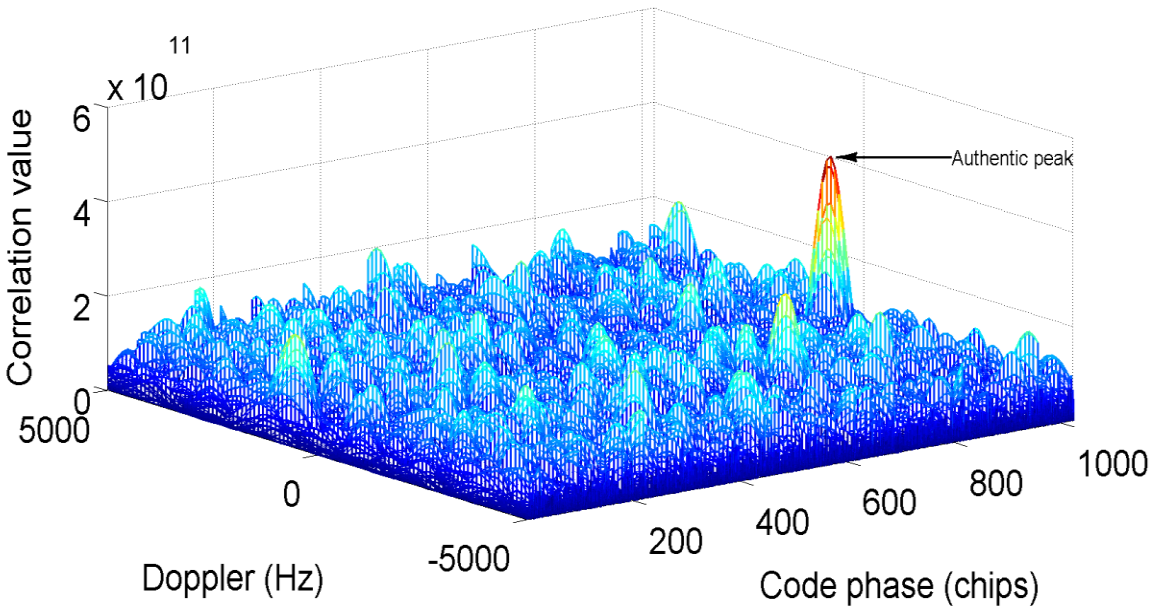

(a)

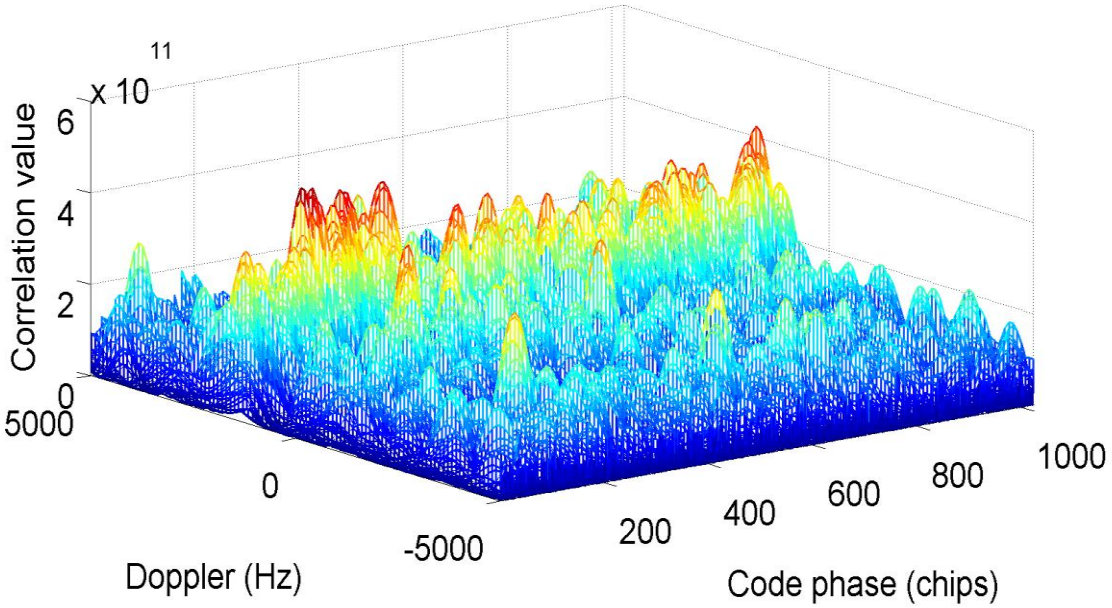

(b)

Figure 2-5: Cross Ambiguity Function (CAF) (a) Clean signal without interference (b) In the presence of CW interference at -105 dBm

Post-correlation analysis of the IF samples is performed using a two-dimensional search grid used for acquisition. CAF represents the variation of correlation values as a function of changing carrier Doppler and code offset. For the clean signal (free from interference) a clear and distinct correlation peak is visible (shown in Figure 2-5 (a)). When a CW interference having a magnitude of -105 dBm is present in IF, an overall increase in correlation values and a rise in the CAF noise floor is observed. This condition leads to false acquisitions and frequent tracking failures.

So far, in this section, interference effects in the acquisition domain were analyzed for single antenna receivers. There has been some research done in the context of array-based GNSS acquisition. The interested reader is referred to the following relevant publications: Arribas et al (2013, 2011), Fernandez-Prades & Closas (2009) and Torrieri & Bakhru (2008).

2.1.2.2 Tracking domain

RF interference can alter the C/N_0 for all or for some satellites. Similar to signal blockages, strong ionospheric scintillation and foliage attenuation, jamming can reduce the C/N_0. The noise power depends on the number of interfering sources and directly impacts measurement and position accuracy. This can also cause complete loss of lock for some satellites and impair navigation functionality. Figure 2-6 illustrates how the signal C/N_0 and the carrier Doppler vary in the presence of interference. In case of CW interference, as the power level of the interference source increases, C/N_0 ratio drops (refer to Figure 2-6 (b)). The same is illustrated for pulsed interference in Figure 2-6 (c). An experiment is done with a single channel simulation without any dynamics (user and satellite). For

this case, one should not expect carrier Doppler variations over time. However, the mean carrier Doppler is found to vary by a few hertz for different levels of CW interference (refer to Figure 2-6 (a)). Hence, it is important to observe that the presence of interference affects not only the tracking decision (i.e. success or failure), but also the quality of carrier tracking. This could be an issue of major concern for carrier phase measurement based positioning.

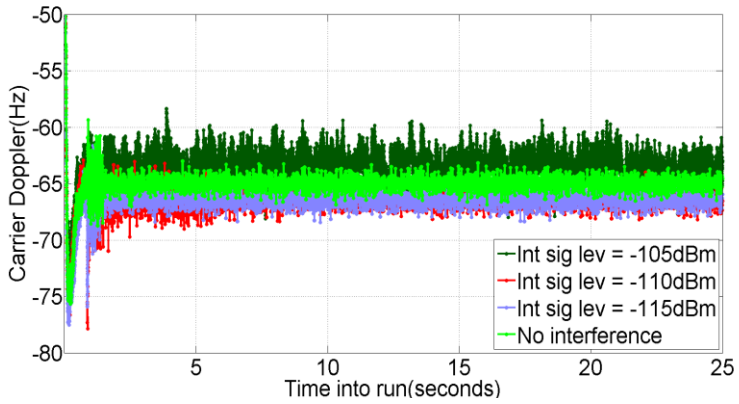

(a)

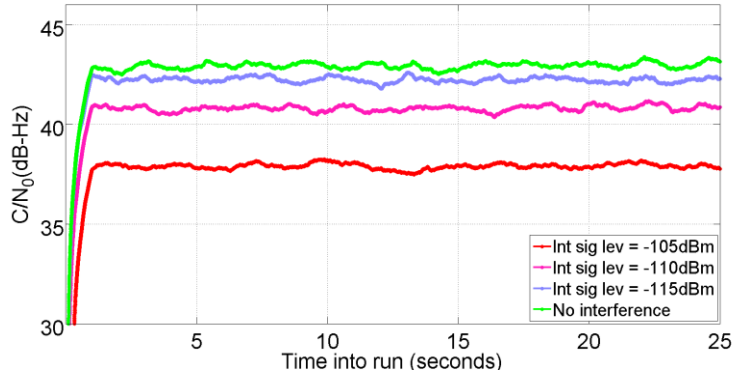

(b)

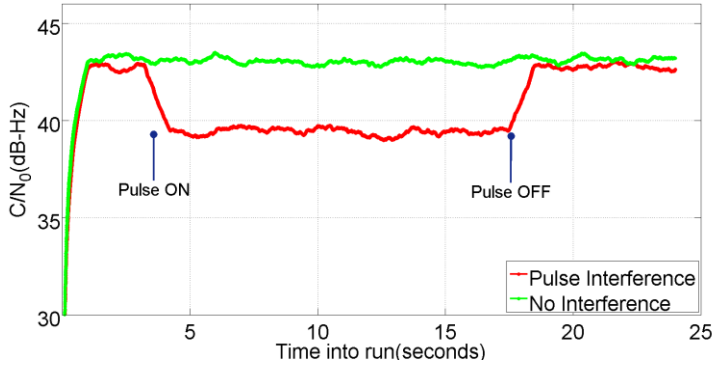

(c)

Figure 2-6: Comparison of interference effect on the signal tracking

(a) The carrier Doppler variation at different CW interference levels
(b) The C/N₀ profile at different CW interference levels
(c) The C/N₀ profile in the presence/absence of pulse interference

The tracking performance is quantitatively compared for different scenarios in Table 2-3. The carrier Doppler, carrier phase vacillation, C/N_0 ratio and the code phase variation indicate degradation in tracking in the interference presence.

Table 2-3 Comparison of statistics for tracking in the presence of different interfering sources with single channel simulator

Output Observable		**In-band interference**				
		No interference	*CWI*			*Pulse*
			-105 dBm	**-110 dBm**	**-115 dBm**	
Carrier Doppler (Hz)	Mean	-65	-63	-66	-66	-66
	RMS	0.61	1.11	0.71	0.63	0.82
Carrier phase	RMS	0.16	0.9	0.2	0.17	0.22
C/N_0 (dB-Hz)	Mean	42.9	37.9	40.8	42.2	40.7
Code phase	RMS	0.22	0.97	0.35	0.17	0.30

As seen from the Table 2-3, at different interference levels the carrier Doppler is found to differ from the expected carrier Doppler. The RMS value of phase errors increase with an increase in interference levels (however, not clearly conclusive in case of carrier phase) and C/N_0 value reduction is observed at higher interference.

2.1.2.3 Navigation domain

The degradations encountered in acquisition and tracking stage result in degradation of the position and velocity estimates. Based on the interference level, the following cases are possible: (a) receiver operation can be completely halted with failure to acquire minimum number of satellites required for positioning, (b) only a few satellites can be acquired leading to poor geometry and degraded DOP, or (c) all satellites can be tracked

as in the case of an interference free scenario but with degraded quality in signal tracking. Consequently, either a navigation solution cannot be computed (in the case (a) above) or inferior position/velocity estimates are computed (in (b) and (c) above). For a CW interference having a signal amplitude of -115 dBm the position and velocity estimates are compared against interference free scenario shown in Figure 2-7 (for example: north velocity is considered).

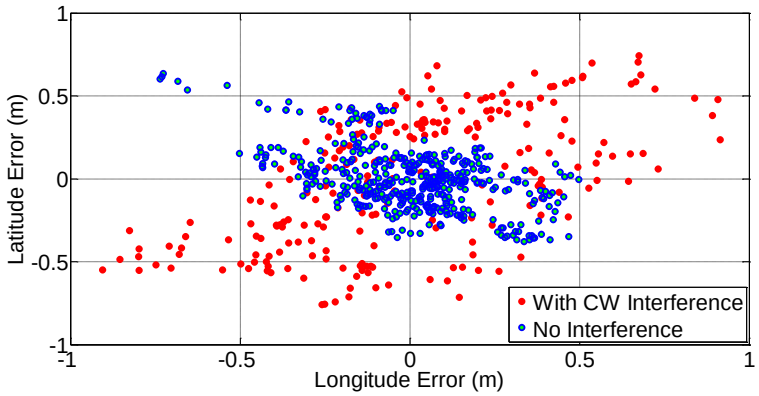

(a)

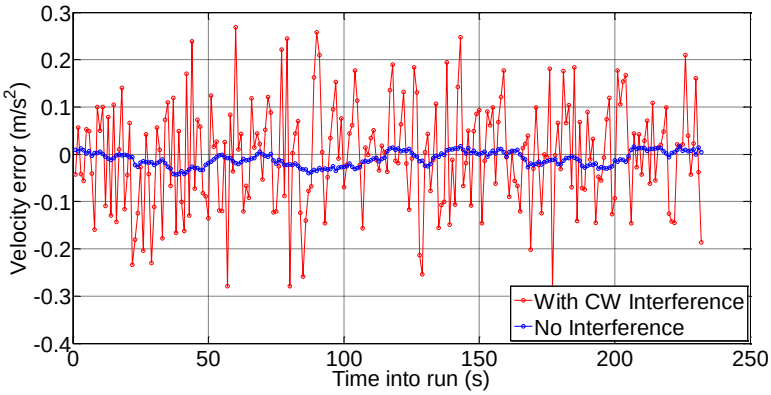

(b)

Figure 2-7 P-V errors in the presence of interference in the simulator mode with CWI (a) Horizontal position errors (b) North velocity errors

For an interference power of -115 dBm, there is a degradation observed in both position and velocity estimates. It was reported by Kuusniemi et al (2012) that for moderate

interference levels, degradations observed in the position domain were also moderate. It is also reported that position errors increased by a large amount and position solution availability decreased when interference signal power was increased by about 10 dB, as compared to a moderate case. As seen in Figure 2-7, even for moderate interference there are large velocity errors. In GNSS receivers, velocity estimates are computed using carrier Doppler measurements. The carrier Doppler results from the relative motion between the receiver and the satellite and it is a measure of the instantaneous rate of change of the signal's carrier phase and shift in the carrier being tracked (Deshpande 2004). The position estimates in this analysis are based on code phase pseudoranges. From Figure 2-7, it can be observed that, even at a moderate interference level, carrier phase measurements are affected to a greater extent than code phase measurements. Alternatively, interference effects are worse on the velocity than on the position estimates.

2.1.3 Overcoming interference

A robust receiver should have the capability to detect and mitigate interference signals before computing the navigation solution. Analyzing the RF spectrum in the process of interference characterization helps system designers to know the behaviour of the interfering sources. This information will in turn facilitate the selection of detection and mitigation strategies.

2.1.3.1 Interference characterization

Interference characterization is generally taken up before performing detection and mitigation of interference. In this process, all signal constituents of the IF samples are

analyzed to determine amplitude, phase and frequency characteristics. These are performed using temporal, spatial and spectral analyses. Depending on the signal environment, these analyses help in taking a judicious decision on selection of detection and mitigation methods. Metrics like noise levels of the input samples can be used to determine the presence of interference during GNSS interference characterization using spectral methods.

2.1.3.2 Interference detection and mitigation

GPS uses DSSS Code Division Multiple Access (CDMA) modulation to provide some level of protection against narrowband interference. Therefore, RF interference mitigation techniques are used only when necessary. Interference detection is a problem involving hypothesis testing, similar to the acquisition process. The temporal, spatial and spectral properties of the sampled data can be used to detect and classify the type of interference. The interference detection and mitigation can be done at various stages of the receiver processing using different techniques. Some of the stages where the mitigation could be done are listed below (Borio 2013):

- GPS receiver antenna (A)
    - Selection of antenna with desired gain pattern
- GPS RF front-end (B)
    - AGC design consideration
- In Digital Signal Processing (DSP)
    - Sample level (C)
    - Correlator level (D)

- Measurement level (E)
    - DSP based techniques are accomplished using Fast Fourier Transforms, Wavelet transforms, etc.

- Antenna based techniques (C) (D)
    - Having a gain pattern tailored for mitigation
    - Use of antenna arrays (antenna pattern controlled electronically – Spatial filtering)

The letters placed in brackets provide a mapping to the section of receiver blocks given in Figure 2-8.

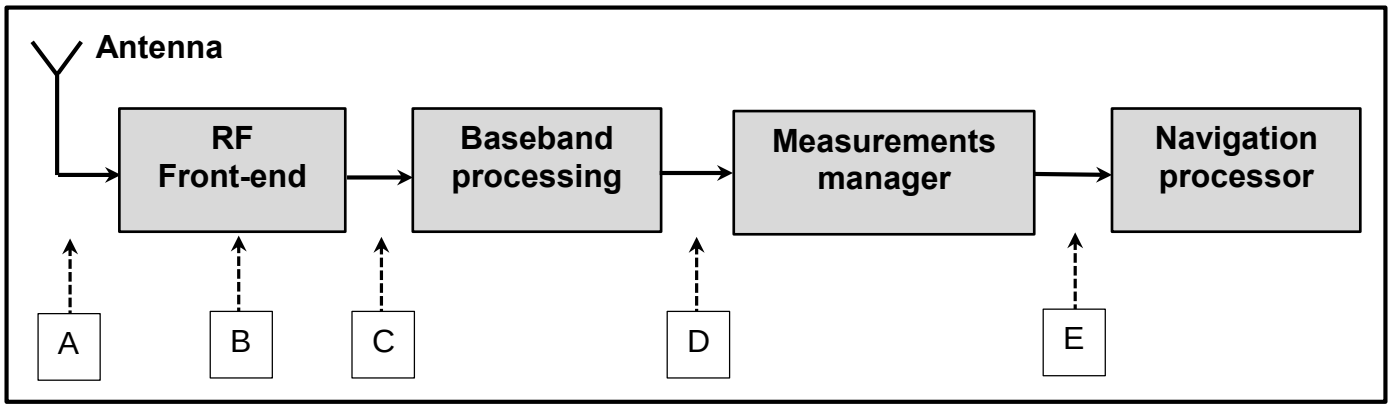

Figure 2-8: The different stages at interference detection and mitigation can be done

For detecting interference at the front-end, the AGC gain variation over time, and the distribution of the ADC output will be monitored. Additionally, increasing the number of bits in the ADC results in multi bit quantisation and thus the dynamic range provided to the incoming signal will be higher.

In case of pre-correlation techniques, the detection block is placed before the baseband processing. The strategies like pulse blanking and filtering are used. More processing power is required in the case of post processing techniques since detection and mitigation logic have to operate on each channel. In this case, analysis can be done on the carrier-to-noise ratio. The statistical analysis like the Chi-square goodness-of-fit test can be used for interference detection (Motella et al 2012).

In addition to the above techniques, selecting a particular type for the antenna to mitigate the interference plays an important role. The antennas with a desired gain pattern could be chosen knowing the source of interference.

The interference mitigation is a method to reduce the effects of disturbing signals. It is an estimation problem. Since a perfect mitigation method does not exist, 100% signal recovery is not possible. Also, a single interference countermeasure cannot be used as a common method for all types of interferences (Borio 2013). To ensure robustness, all possible mitigation methods should be considered in the receivers.

2.1.4 Illustrative study of interference detection and mitigation

In this section, for illustration purpose, only CW interference is considered. The results obtained for different levels of interference are presented. The interference detection is done using Fast Fourier Transform (FFT). In the case of CWI, mitigation is performed using following techniques:

- in the first approach, the FFT of the sampled IF signal is computed, then the maximum peak that corresponds to the interferer is stripped off by forcing the

sample to be zero and intermediate signal is reconstructed using inverse FFT (IFFT)

- in the second approach, the presence of the CW interference is detected using the frequency domain analysis. Then, a notch infinite impulse response (IIR) filter is introduced at the desired frequency.

2.1.4.1 FFT-IFFT method

In this method, the Fourier transform of the composite signal is taken. In the presence of the interfering signal the peak of the FFT output corresponds to that signal. This peak is removed from the dataset. This operation removes the CWI from the data. Then the IFFT of this filtered sequence is taken and in turn fed to the correlator for further processing. The signal corresponding to the GPS signals cannot be seen in the frequency spectrum because the signal is spread across the complete bandwidth. However, in case of the CWI a clean tone frequency could be seen corresponding to the CWI.

2.1.4.2 IIR Notch filter method

Another method used for mitigating CWI is the IIR based notch filter approach. This method is commonly used in commercial receivers. The notch filter is a non-linear device due to a non-linear phase response, with a transfer function that strongly attenuates only one particular frequency component. The discrete domain representation of the real interference signal is given as

$$i_i(n) = A_i \cos\left(\frac{2\pi f_i n}{f_s} + \phi_i \right), \tag{2-1}$$

where A_i is the interference amplitude, f_s is the sampling frequency, $f_i(n)$ is the interference frequency, n is the discrete-time index and ϕ_i is the phase of this signal. The aim is to remove the frequency content corresponding to this signal. This functionality can be achieved with a filter having following transfer function represented in z-domain:

$$H_{NF}(z) = \frac{1 - z_0 z^{-1}}{1 - k_\alpha z_0 z^{-1}}, \tag{2-2}$$

where k_α is the pole contraction factor (Range : $0 \le k_\alpha < 1$) and

$$z_0 = A \cdot \exp\left\{ j 2\pi \frac{f_i}{f_s} \right\}. \tag{2-3}$$

In case of multiple CW interference mitigations, such filters can be used in a cascaded fashion and the centre frequency of each filter depends on the corresponding CW's frequency.

The results corresponding to the two methods mentioned earlier are compared with the data from two commercial receivers from uBlox. One of the receivers (uBlox 6) has CW interference cancellation capability and the other one (uBlox 4T) does not. Table 2-4 provides a comparison of the position accuracies for different interference scenarios.

Table 2-4 Comparison of position errors for uBlox and GSNRx for different interference scenarios (CWI with power -90 dBm)

Sl. No.	Mode	Position RMS error (m)
uBlox receiver		
1	uBlox 4T in the presence of CWI	1.475
2	uBlox 6 in the presence of CWI	0.543
GSNRx receiver		
3	GSNRx without any interference	2.436
4	GSNRx in the presence of CW interference	4.493
5	GSNRx with interference mitigation using IIR notch filter approach	2.692
6	GSNRx with interference mitigation using FFT-IFFT approach	3.059

Since the uBlox 6 has some interference mitigation capability, successful interference mitigation was possible, unlike the uBlox 4T model. As a consequence, the position errors were relatively larger in the case of the uBlox 4. Similarly, the GSNRx results show that position accuracies were inferior when interference mitigation methods were not used.

2.2 Array signal processing

An *antenna array* is by definition a radiating/receiving configuration consisting of more than one antenna element. It is a group of elements arranged to provide the desired directional characteristics. The definition does not specify which elements are used to form the array nor how the spatial arrangement should be. This allows one to construct antenna arrays consisting of different elements, feeding configurations and spatial arrangements, hence resulting in radiating structures of different properties

(Allen & Ghavami 2005). Generally any combination of elements can form an array, however, regular geometry is usually used. Some of the configurations mostly used are shown in Figure 2-9. There is one more type of array configuration, namely the conformal array. In this configuration, the antenna array is composed of planar sectors (e.g. arranged in pyramid or in cone-shaped geometry) in order to allow tracking of either low elevation satellites or to capture the orientation/heading changes when the array is foreseen to change quickly.

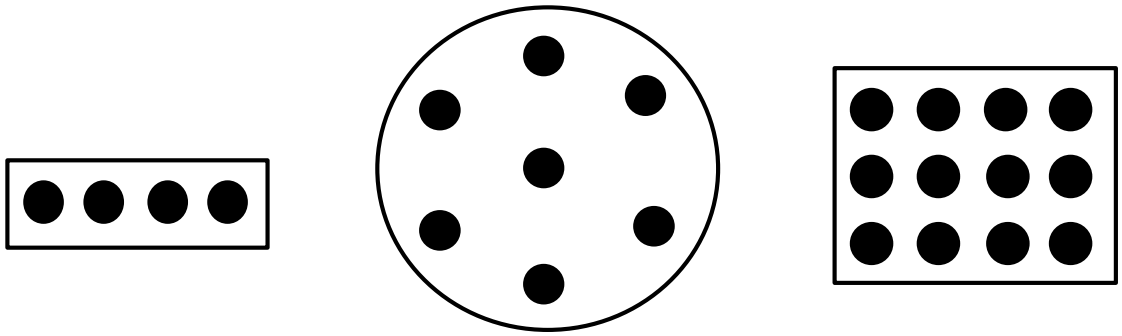

(a) (b) (c)

Figure 2-9: Different array configurations (a) Linear (b) Circular planar (c) Rectangular planar

Antenna arrays are becoming increasingly important in wireless communications. Some advantages of using antenna arrays are as follows:

- they are capable of generating steerable beams that are electronically controlled without moving the array physically
- they can provide a high gain / array gain by using simple antenna elements
- they provide a diversity gain, which can be exploited in acquisition enhancements and multipath mitigation
- they enable array signal processing.

The outputs from the antenna elements can be processed in a fixed or adaptive manner to respond to an unknown interference environment. Methods to optimize the performance of the system in some defined manner are also possible (Griffiths 1983). Precisely, the interest is in solving these problems in noisy environments i.e. in the presence of noise and interfering signals. Estimation theory is a basic and an important part of signal processing field where the prime focus is to estimate several system parameters based on measured or empirical data that has a random component. As the number of applications and the need for performance improvement increases, estimating temporal and spatial parameters becomes more important. Array processing emerged as an active area in the last few decades and is centered on the ability of using and combining data from different antenna elements in order to deal with a specific estimation task. The estimation framework can take advantage of the prior knowledge of the geometry of the array, in addition to the information extracted from the data.

Array processing is used in radar, sonar, and seismic explorations, anti-jamming and wireless communications. In GNSS, it is used for three applications namely beamforming, null steering and to obtain diversity gain. Beamforming encompasses electronically steering the beam (tuning the antenna gain pattern) in the desired direction. This provides improved SNR performance. In null steering, nulls are placed in the direction of the interfering sources. Beamforming and null steering are achieved by properly designed filter weights typically controlled in an adaptive fashion. An illustration of these two applications is shown in Figure 2-10. Antenna arrays are used to obtain diversity gain in harsh environments and fading channels (with known models) in applications involving acquisition performance improvements and multipath mitigation. Also, array processing

methods are used for AoA estimation and attitude determination. However, in all these applications the problems associated with array processing including array imperfections (e.g. mutual coupling, calibration mismatch etc.) should be judiciously accounted for.

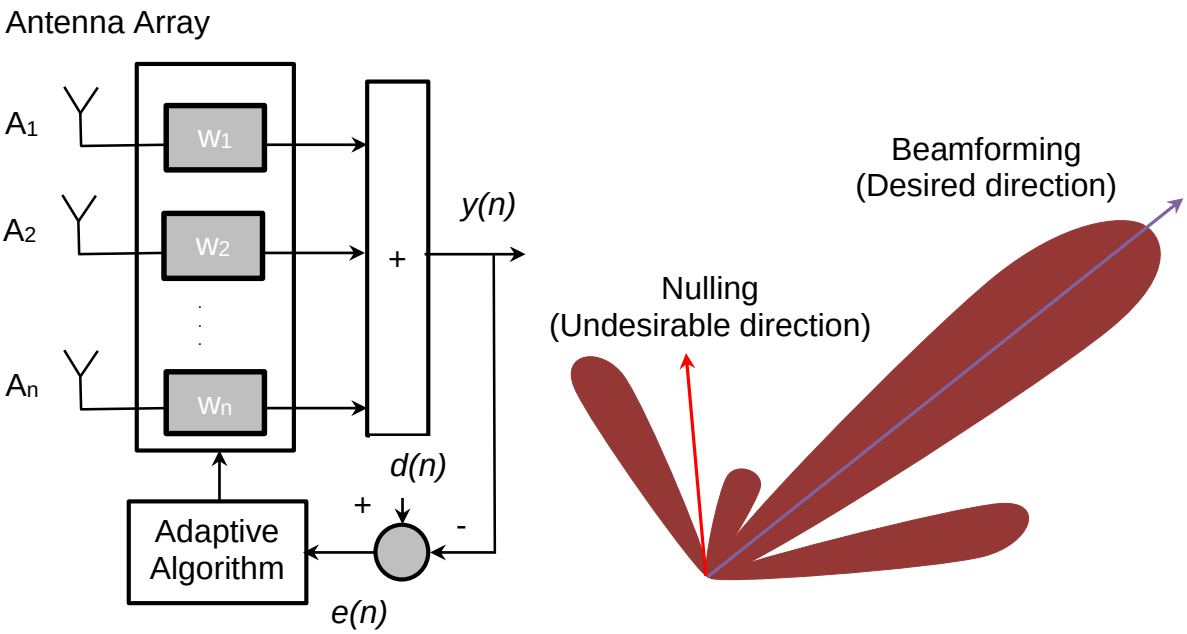

(a) Beamformer (b) Beam pattern

Figure 2-10: Block diagram of a beamformer and an illustrative beam pattern

Based on the properties of the parameters considered and the methods employed, antenna array processing can be categorized into the following sections: spatial processing, space time processing (STP), space time adaptive processing (STAP) and space frequency adaptive processing (SFAP). These methods are discussed further below. A previous contribution (Moore 2002) compared SFAP and STAP methods with equivalent computational burden and output SINR; this work concluded that SFAP distorted the desirable signal less than STAP as determined by comparing CCF peaks. Also, compared to SFAP, STAP is widely used as seen in literature. Therefore, SFAP is

not used in this thesis and is not discussed further; although not used, the STAP functionality is studied as an extension of STP.

2.2.1 Spatial processing

Spatial filters reject the interference during spatial domain processing, rather than time, and can achieve large anti-jam margins against interference waveforms, including broadband noise (Trinkle & Gray 2001). The simplest form of a spatial filter uses an antenna array to obtain a beamformer whose output feeds directly into a GNSS receiver. A beamformer can be considered as a single antenna element front-end with an adjustable beam pattern. The complex values of the filter weights determine the antenna beam pattern. These weights are fixed for Fixed Radiation Pattern Antenna (FRPA) and continuously updated by an adaptive algorithm for CRPA. The actual beamforming operation is implemented in the digital domain; this requires a separate down-converter and ADC for each antenna element.

One of the main limitations of spatial processing is cancellation of desirable signals arriving from the directions close to that of interference (Trinkle & Gray 2001). This limitation can be overcome with the help of space time processing, discussed in the following paragraph.

2.2.2 Space time processing

Before de-spreading, the GNSS signal is spread over a wide bandwidth (e.g. 2 MHz for GPS C/A). This permits excision of narrowband interference in the frequency domain without causing much loss of signal power. Such filters can be realized using time domain

filters with delay lines. The temporal domain filters are effective against multiple CW interferences. For such scenarios, combining temporal processing with the spatial processing can provide further enhancements. The enhancements achieved are mainly due to the increase in the array degree of freedom for narrowband interference cancellation. The algorithm calculates the complex weights by solving an optimization problem.

To implement a space time processor, FIR filters are placed after each antenna element. For an antenna array with *N* elements and *(M-1)* taps (used for TDLs), *NM* filter weights should be computed. A pictorial representation of a space time processor for an *N* element array with *(M-1)* taps is shown in Figure 2-11. In the case of spatial processing, filter weights corresponding to antenna elements are only estimated and time delay components will not be present.

A potential problem of the space time processing is that the additional temporal filtering can introduce timing errors into the GNSS signals. Spatial processing impacts the signal phase information but the temporal errors are not introduced. Therefore, utilizing STP for GNSS applications requires special considerations to avoid addition of biases in pseudorange and carrier phase measurements. Furthermore, since more filter coefficients (for space and time) are to be computed in STP, its computational complexity is more than that of spatial processing. Data from the test environment is gathered and essential information (e.g. data required to compute the covariance matrix **R**) is carefully extracted. However, the amount of data available to come up with an estimate is fundamentally limited. Hence estimates can be obtained on-the-fly which make the

methods work adaptively (Guerci 2003). This concept forms the basis of space time *adaptive* processing.

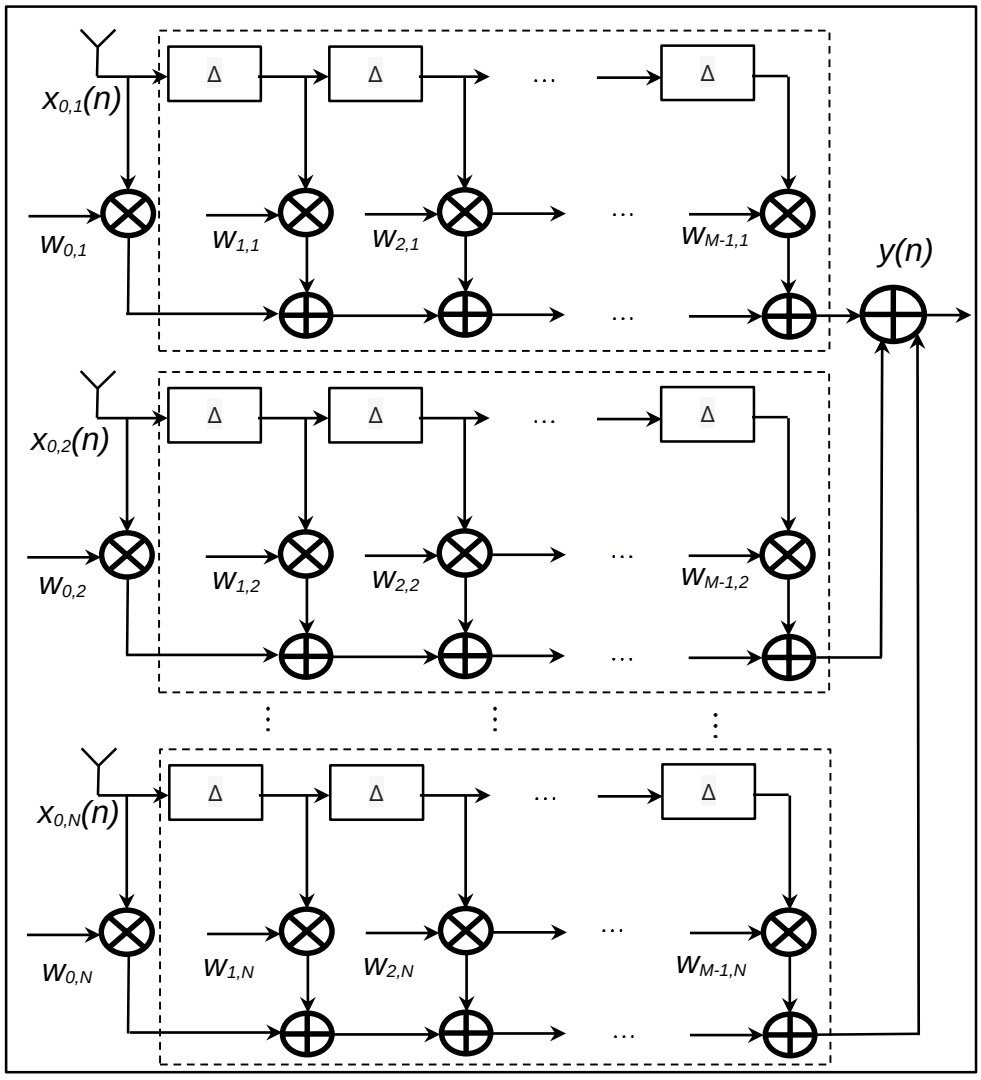

Figure 2-11: Block diagram of a generic space time processor

2.2.3 Space time adaptive processing

To solve the problems associated with the changing environments (e.g. fast sweeping interference due to a moving user or jammer), filter weights should be determined using adaptive algorithms in such scenarios. By incorporating *adaptation* into the STP methods,

space time adaptive processing can be achieved. The algorithm calculates the complex weights by solving an optimization problem adaptively. Several optimization criteria have been proposed, most of them are based on minimizing the output power of the array, subject to a given constraint. The adaptive algorithm continuously gets blocks of input data from which it calculates the optimal beamformer coefficients. Two approaches are considered for adaptation namely *block* adaptation and *continuous* adaptation (Van Veen & Buckley 1988). In the block adaptation method, optimum weights are estimated on blocks of temporal samples from input data. In continuous adaptation, filter weights are adjusted when the input samples arrive and the filter weights converge to optimum solution over time.

The optimum beamformer weight vector equations require knowledge of the *mean* of samples and the *correlations* between the components. These statistics are generally not known. However, by assuming that the test environment does not change rapidly, required statistics can be estimated from the available data and using these statistics, optimum weights can be estimated. The generic structure of an adaptive filter incorporated in STAP is depicted in Figure 2-12.

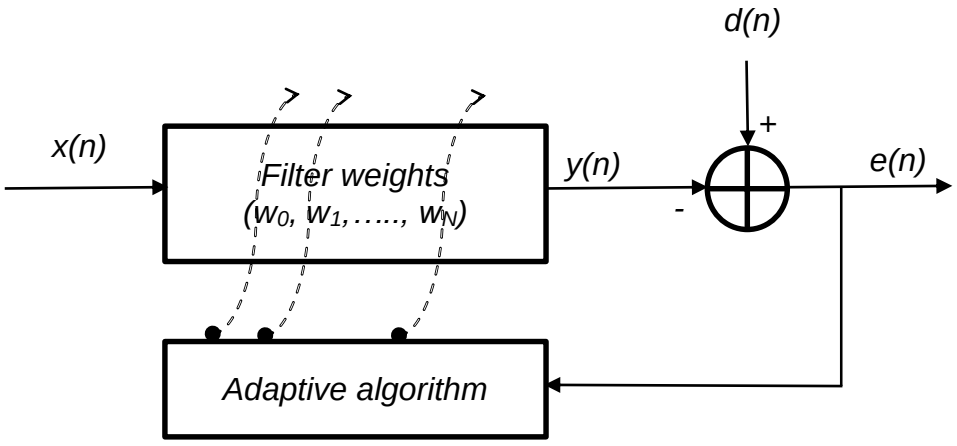

Figure 2-12: Basic block diagram of an adaptive filter

As shown in the block diagram, a sample from the digital input signal *x(n)* (from the down-converter connected to the antenna element) is fed into a filter structure called *adaptive filter* that computes a corresponding output signal sample *y(n)* at time *n*. The output signal is compared to a second signal *d(n)* called the desirable response signal. One gets the error signal *e(n)* by subtracting *y(n)* from *d(n)* i.e. $e(n) = d(n) - y(n)$. The error signal is fed into a procedure which alters or adapts the parameters of the filter from time *n* to (*n+1*) in a well-defined manner. This process of adaptation is represented by the curved arrows piercing the adaptive filter block in Figure 2-12. As the time index *n* is incremented, it is hoped that the output of the adaptive filter becomes a closer match to the desired response signal through this adaptation process, such that the magnitude of *e(n)* decreases over time.

2.3 Signal model

In this subsection, a general signal model of an antenna array and some basic beamformers are presented.

Assume a GNSS signal impinges on an antenna array with *N* isotropic antennas. In describing the system model, arbitrary positions are assumed for antenna elements. In a Cartesian coordinate system, the positions of these elements are shown with vectors $\mathbf{d}_1^{ant}$,$\mathbf{d}_2^{ant}$, …, $\mathbf{d}_N^{ant}$ which are pointing from the origin of the coordinate system to the antenna elements as shown in Figure 2-13. Without loss of generality, it is assumed that the origin of the coordinate system is located at the position of the first antenna element.

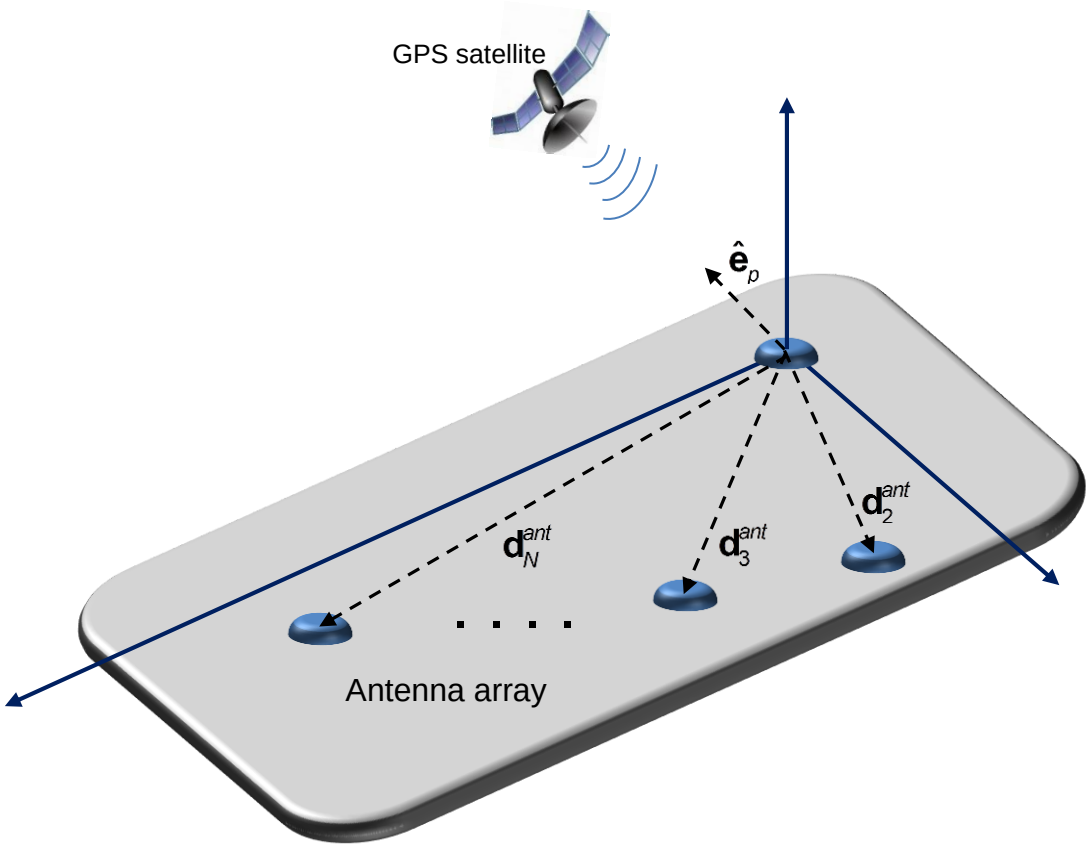

Figure 2-13: Plane wave impinging on an antenna array with *N* elements

The received baseband signal vector at an antenna array can be expressed as

$$\underset{N\times 1}{\mathbf{x}} = \begin{bmatrix} x_1 \\ x_2 \\ \vdots \\ x_N \end{bmatrix} = \sum_{p=1}^{P} s_p \underset{N\times 1}{\mathbf{a}_p} + \sum_{l=1}^{L} i_l \underset{N\times 1}{\mathbf{b}_l} + \underset{N\times 1}{\boldsymbol{\eta}}, \tag{2-4}$$

where P and L are the number of satellites and the interfering sources respectively, s_p and $\mathbf{a}_p$ are the signal waveform and the steering vector of p^{th} signal, i_l and $\mathbf{b}_l$ are the waveform and the steering vector of l^{th} interference signal, $\boldsymbol{\eta}$ is the white Gaussian noise vector, and x_n indicates the received signal at the n^{th} antenna element.

For an antenna array with *N* elements and *(M-1)* taps, *NM* weights should be computed (referring to Figure 2-11). At every time epoch, *NM* samples comprising of antenna elements and the TDLs for a $NM \times 1$ received signal vector are given as

$$\vec{\mathbf{r}} = [\quad x_{0,1} \quad x_{0,2} \quad \cdots \quad x_{0,N} \quad \cdots \quad x_{(M-1),1} \quad x_{(M-1),2} \quad \cdots \quad x_{(M-1),N} \quad]^T, \tag{2-5}$$

in which $x_{M,N}$ is the m^{th} delayed sample and $m = 0,1,2,\ldots,(M-1)$ at the n^{th} antenna element with range $n = 0,1,2,\ldots,N$.

Considering Equation (2-5), the space-time correlation matrix can be obtained as

$$\underset{NM \times NM}{\mathbf{R}_{\vec{\mathbf{r}}}} = E\left\{\vec{\mathbf{r}}\vec{\mathbf{r}}^H\right\}. \tag{2-6}$$

This correlation matrix contains information about the sources in space (number, strength, direction) and time and can be used for detection and separation of the sources. The number of independent spatial and temporal signals at the input of array and the *rank (* $\mathbf{R}_{\vec{\mathbf{r}}}$*)* is the same. Singular values decomposition (SVD) of $\mathbf{R}_{\vec{\mathbf{r}}}$ gives the information about the signal subspace, which is necessary for subspace based AoA estimators and beamformers. This correlation matrix is employed in the optimization for different beamforming methods.

The assumptions made and used in the rest of this thesis are as follows:

- there is uniform propagation in all directions of isotropic and non-dispersive medium
- for far field array processing, the radius of propagation is much greater than the size of the array and there is plane wave propagation

- there is a zero mean white noise, which shows lack of correlation (i.e. the noise term in Equation (2-4) is a spatially and temporally white zero mean complex vector with covariance matrix $\sigma^2 \mathbf{I}_N$), and
- undesired signals (i.e. interference) are considered unknown deterministic signals.

2.3.1 Beamformers

In general, the quality of a beamformer depends on the overall information available to it. The information about the AoA of the desirable signal or the interference signal might be available or not. In a simpler form of a beamformer, interference can be mitigated with power minimization. When the AoA of a desirable signal, i.e. satellite direction in case of GNSS, is available, the beamformer's performance can be improved by making use of AoA. Further, the use of AoA of interference provides improved null steering and hence SINR performance. In case of GNSS, receivers generally have the capability to store satellite ephemeris and almanac. Given the availability of ephemeris and almanac and through exploring their extended validity, receivers can determine the satellite AoAs. Because of the very nature of interference (i.e. being undesirable), assuming that the AoA of the interference signal is known in advance is an inappropriate assumption. Considering this practicality, in this thesis, AoA characteristics of the desirable signals are either used or not used, based on the beamformer being considered; however it is not assumed that the AoA of the interfering signal is known.

The beamformers used in this thesis are now described.

2.3.1.1 Eigen vector beamformer

In a Blind Eigen vector beamformer, neither the directions of arrival of the satellite signals nor that of interference signals are used in determining the space-time filter weights and this beamformer is extensively addressed in the literature (Daneshmand et al 2015b**,** Van Trees 2002**,** Monzingo et al 2011**,** Citron & Kailath 1984). The presence of unintentional nulls in this case may cause failure in the acquisition of some satellite signals.

The projection matrix **P** (with matrix dimension $(NM-L)\times NM$) into the interference free subspace can be obtained by applying an Eigen Value Decomposition (EVD) of the correlation matrix $\mathbf{R}_{\tilde{\mathbf{r}}}$ of the input samples as

$$\mathbf{R}_{\tilde{\mathbf{r}}} = \begin{bmatrix} \underset{NM\times L}{\mathbf{U}_{Int}} & \underset{NM\times(NM-L)}{\mathbf{U}_{Null}} \end{bmatrix} \begin{bmatrix} \underset{L\times L}{\mathbf{\Lambda}_{Int}} & 0 \\ 0 & \underset{(NM-L)\times(NM-L)}{\mathbf{\Lambda}_{Null}} \end{bmatrix} \begin{bmatrix} \underset{NM\times L}{\mathbf{U}_{Int}^{H}} \\ \underset{NM\times(NM-L)}{\mathbf{U}_{Null}^{H}} \end{bmatrix}, \tag{2-7}$$

where $\mathbf{U}_{Int}$ and $\mathbf{U}_{Null}$ are the eigenvector matrices of the interference and interference-free signal subspaces respectively, $\mathbf{\Lambda}_{Int}$ and $\mathbf{\Lambda}_{Null}$ are the corresponding eigenvalue matrices. By isolating eigenvectors corresponding to the bigger eigenvalues, interference-free subspace (i.e. noise signal subspace) can be calculated. Using **P**, the STP filter weights are computed such that they suppress high power interference (i.e. minimize the filter's output power) and are given by

$$\mathbf{w} = \mathbf{P}^{T}\mathbf{g}, \tag{2-8}$$

where **g** is a gain selection vector which can be **1** (all one vector) for equal gain combining or can be chosen based on the selection gain combining criteria (Marathe et al 2015b).

In its general form, an Eigen vector beamformer utilizes the received data to estimate the signal subspace and the noise subspace. In the context of interference impacted GNSS

signals, the signal subspace actually contains interference and the noise subspace represents both the noise and GNSS signal subspaces, as the GNSS signal levels are lower that the noise levels. The correlation matrix is estimated from the input data. When the correlation matrix is written in terms of Eigenvalues and Eigenvectors, large values correspond to interference. The Eigenvectors corresponding to remaining smaller eigenvalues relates to a noise subspace and contain the GNSS component. The filter weights for interference suppression are a set of vectors that span the noise-plus-GNSS signal subspace.

2.3.1.2 Simple power minimization (SPM) beamformer

The optimization problem in this case is defined as

$$\mathbf{w}_{opt} = \underset{\mathbf{w}}{\arg\min}\left\{\mathbf{w}^{H}\mathbf{R}\mathbf{w}\right\}, \tag{2-9}$$

$$\text{such that } \mathbf{w}^{H}\mathbf{q} = 1$$

with the constraint vector

$$\mathbf{q} = \begin{bmatrix} 1 & 0 & \cdots & 0 \end{bmatrix}^{T}, \tag{2-10}$$

and a solution to the above problem is given by

$$\mathbf{w}_{opt} = \mathbf{R}^{-1}\mathbf{q}\left(\mathbf{q}^{H}\mathbf{R}^{-1}\mathbf{q}\right)^{-1}, \tag{2-11}$$

where **R** is the space-time covariance matrix defined in Equation (2-6) and $\mathbf{w}_{opt}$ is the beamformer weight vector. In this optimization, the constraint vector avoids the trivial solution i.e. $\mathbf{w}_{opt} = 0$. The above linear constraint optimization problem is solved by employing the method of Lagrange multipliers.

2.3.1.3 Minimum Power Distortion less Response (MPDR) beamformer

The optimization problem in this case is defined as

$$\mathbf{w}_{opt} = \underset{\mathbf{w}}{\arg\min}\left\{\mathbf{w}^{\mathbf{H}}\mathbf{R}\mathbf{w}\right\}, \quad \text{such that } \mathbf{w}^{H}\mathbf{a}_{p} = 1 \tag{2-12}$$

A constraint vector that incorporates AoA is used in finding a solution to this problem (Van Trees 2002). The steering vector is given by

$$\underset{N\times 1}{\mathbf{a}_{p}} = \begin{bmatrix} e^{j\left(\frac{2\pi}{\lambda_c}\right)\left(\hat{\mathbf{e}}_p^T\mathbf{d}_1^{ant}\right)} \\ e^{j\left(\frac{2\pi}{\lambda_c}\right)\left(\hat{\mathbf{e}}_p^T\mathbf{d}_2^{ant}\right)} \\ \vdots \\ e^{j\left(\frac{2\pi}{\lambda_c}\right)\left(\hat{\mathbf{e}}_p^T\mathbf{d}_N^{ant}\right)} \end{bmatrix}, \tag{2-13}$$

where λ_c is the carrier wavelength, $\hat{\mathbf{e}}_p$ is a vector pointing in the direction of the desired signal given by

$$\hat{\mathbf{e}}_p = \begin{bmatrix} \cos(\theta_{El}^p)\sin(\phi_{Az}^p) \\ \cos(\theta_{El}^p)\cos(\phi_{Az}^p) \\ \sin(\theta_{El}^p) \end{bmatrix}, \tag{2-14}$$

$\mathbf{d}_j^{ant}$ is the antenna coordinates vector given as

$$\mathbf{d}_j^{ant} = \begin{bmatrix} d_{j_x}^{ant} \\ d_{j_y}^{ant} \\ d_{j_z}^{ant} \end{bmatrix}, \tag{2-15}$$

where θ_{El}^{i} is the elevation angle of the p^{th} signal direction , ϕ_{Az}^{p} is the azimuth angle of the p^{th} signal direction, p=1,2,….,P is an index for the desirable signal directions, j=1,2,….,N is an index for the antenna elements.

A solution to the above problem is given by

$$\mathbf{w}_{opt} = \mathbf{R}^{-1}\mathbf{a}_p \left(\mathbf{a}_p^H \mathbf{R}^{-1}\mathbf{a}_p\right)^{-1}. \tag{2-16}$$

The above linear constraint optimization problem is solved by employing the method of Lagrange multipliers (Van Trees 2002)**.**

In this thesis, when using the beamforming methods which use the AoA of satellites, it is assumed that perfect knowledge on the AoA characteristics are available and they are not estimated explicitly.

2.3.2 Antenna array gain pattern

For a space-time filter, the gain pattern (in dB) is calculated as

$$AG = 10\log\left(\left|\mathbf{h}^H(f)\mathbf{a}_p\right|^2\right), \tag{2-17}$$

where AG is the antenna array gain, $\mathbf{h}^H(f)\mathbf{a}_p$ is the response of the filter to the input signal with the steering vector $\mathbf{a}_p$ at frequency f. From Equation (2-17), it is clear that the array gain pattern is a function of frequency and signal's AoA.

An illustrative array gain pattern is shown in Figure 2-14. The beam pattern, which is a function of three variables i.e. frequency, azimuth and elevation, is represented with a two-dimensional plot by fixing the frequency. The variation of the antenna gain in dB (which varies in the plane perpendicular to the paper) is shown using a color-bar besides the figure. An interference at 200 Hz is considered; hence a null is placed for corresponding frequency, azimuth and elevation, shown with a black dot.

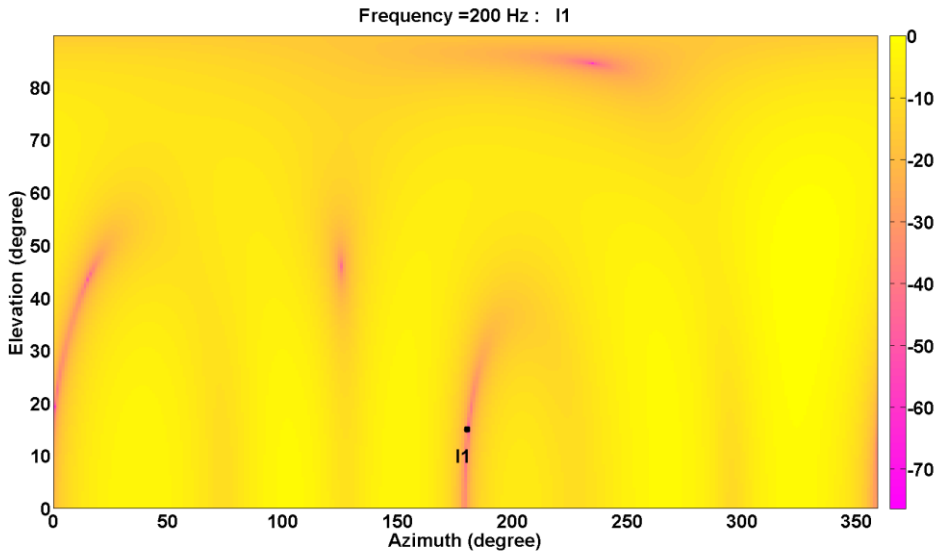

Figure 2-14: Illustration of beam pattern for single interference scenario

An interference signal is placed at an azimuth angle of 180° and an elevation of 15°. A simple power minimization criteria is used to obtain the array filter weights. The AoA characteristics of neither satellites nor that of interference source were used to obtain the gain patterns. Use of the power minimization criteria leads to attenuation in the gain corresponding to interference source direction, which is also referred to as nulling out the interference signal. The filter weights are not designed to provide high gain in any particular direction; therefore, pointed beams with high gain in specific direction were not

observed. The antenna gain patterns are used as effective illustrative tools to analyse the performance of the designed spatial or space-time filters. The antenna gain patterns are appropriately used in the relevant sections of the following chapters to illustrate the results.

2.4 GNSS Receivers

A receiver constitutes the *user segment* of the GNSS system and is responsible for processing the signals coming from the satellites. The satellites transmit signals with pseudo randomness embedded in them. Receivers search for the presence of desirable signals i.e. the visible satellites and if they are found, they demodulate and extract measurements and navigation information and estimate the user position, velocity and time.

2.4.1 Single antenna receiver

Receivers are tailored and engineered for different GNSS signals and applications. However, the basic building blocks of a generic receiver remains the same. The architecture for a single antenna receiver is given in Figure 2-15.

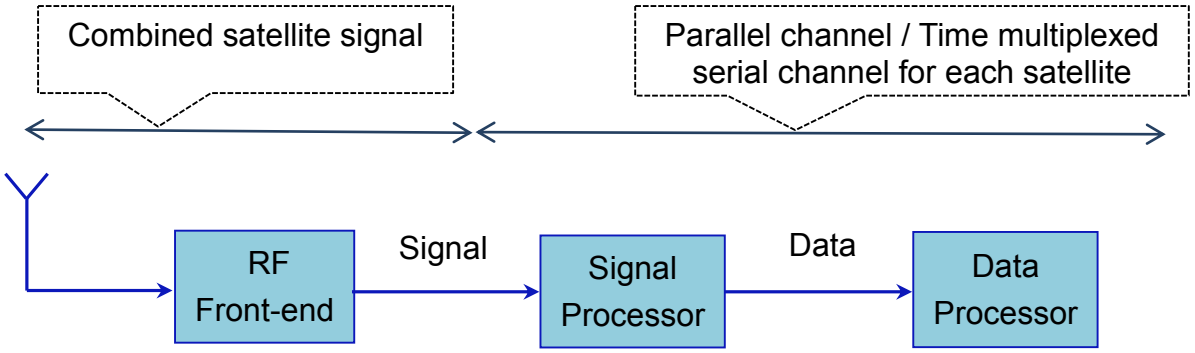

- Antenna and cable
- Low noise amplifier (LNA)
- Mixers and local oscillators
- Amplifiers and filters
- Frequency synthesizer
- Reference clock/oscillator
- Automatic gain controller
- Analog to digital converter

- Local code generator
- Local carrier generator
- Delay lock loop
- Costas loop

- Software algorithms on a computing platform

Figure 2-15: A typical GNSS receiver architecture

The functions performed by each of the receiver block is briefly explained here.

RF stages (Front-end): The purpose of the receiver front-end is to filter and amplify the incoming GNSS signals. As the received signal is very weak, front-end of the receiver provides about 30-55 dB of gain.

Frequency down conversion and IF amplification: After amplification in the front-end, the signal is down converted to a lower frequency namely IF. Down conversion will not affect the bandwidth. Increasing the ratio of bandwidth to center frequency permits use of band pass filters with sharp cutoff frequencies. Down conversion also makes the sampling more feasible for digital processing. Down conversion is accomplished by multiplying with local oscillator frequency using mixers.

Digitization: Digital signal processing is used to track the signals and make the pseudorange and delta range measurements, and to demodulate the 50 Hz data stream. For this purpose, the final IF analog signal is sampled and digitized using an ADC. Sampling frequency must be chosen such that there is no spectral aliasing.

Base band signal processing: Base band signal processing refers to the high speed real time algorithms for acquiring and tracking the signals, and decoding the 50Hz navigation data.

Navigation data processing: Performs satellite data extraction and measurement generation. Subsequently, user position estimation is computed along with the generation of satellite corrections, satellite visibility computation and integrity monitoring tasks.

2.4.2 Multiple antenna receiver

Along with the functionalities achieved with a single antenna receiver, to enable array processing, some sections of the receiver are altered and some more functional blocks are added in a multiple antenna receiver. The modified receiver architecture for multiple antenna functionality is shown in Figure 2-16.

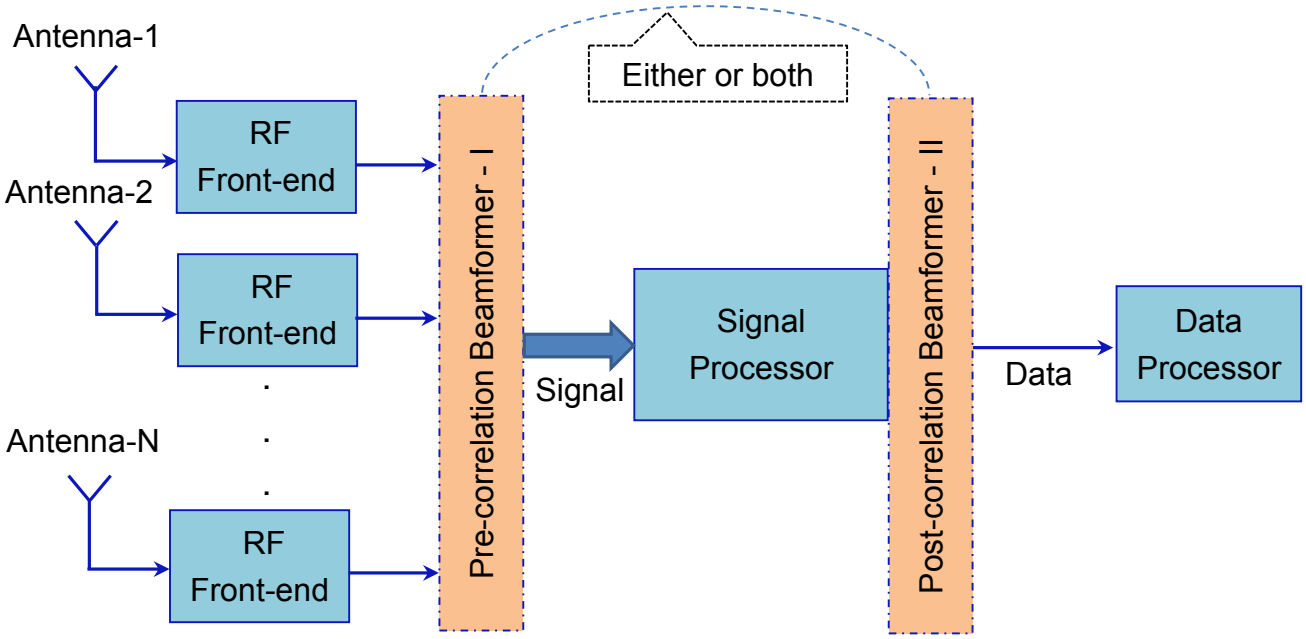

Figure 2-16: Receiver architecture for multi-antenna processing

Signals from each antenna are down-mixed and converted from analog to digital domain for baseband processing. In the case of pre-correlation beamformers at baseband, the signals received at the antenna elements are multiplied with the complex beamformer weights and summed. The filter coefficients (weighting factors) are chosen in such a way that the received signals from each antenna element cancel out in the direction of the interferers (nulling). Additionally, for advanced digital beamforming, the gain is increased in the direction of the satellites by forming individual beams to each satellite. Similar to pre-correlation methods, beamforming can be performed in the tracking domain, after baseband processing. In case of pre-correlation methods, since the signal is still under acquisition, data from all antenna elements is jointly considered. However, in the case of post-correlation methods, individual tracking channels need to be maintained for each antenna element for each satellite. The pre-correlation methods run at higher update

rates since they operate at sampling frequency. The post-correlation methods run at comparatively lower update rates.

2.5 Summary

In this chapter, the following were studied and discussed: introduction to GNSS vulnerabilities, their categorization, effects and countermeasures; different array signal processing techniques; signal model and mathematical formulation of different beamformers used in this thesis; and two receiver architectures.

The major research contributions are presented next.

CHAPTER 3: SIMULATION TEST BED FOR GNSS SIGNALS ON AN ANTENNA ARRAY

Vulnerability of GNSS signals to strong RF signals has resulted in new research needs. Based on the type of interference various mitigation schemes have been proposed. Antenna array processing is one of the powerful methods for interference mitigation. However, data collection using real antenna arrays to develop and test array processing methods is considerably complex. Therefore, it is very useful to develop a simpler way of obtaining array data using a simulation platform.

This chapter introduces a new approach to simulate GNSS signals for an antenna array. Employing the user trajectory information recorded using a single antenna hardware simulator and the known physical configuration of the antenna array, GNSS signals are simulated for each antenna element. Additionally, directional interference signals can be generated and added to the GNSS signals. Fidelity of generated signals for each antenna is evaluated by comparing the tracking parameters from this simulator with two commercially available GNSS simulators, namely the Spirent GSS-7700 and Rohde & Schwarz SMBV-100. Simulations are verified by evaluating C/N_0 values, carrier Doppler and code phase. Two approaches of array signal generation i.e. one based on a reference antenna and another based on independent antenna's signal parameters, are explained and compared. Capability of the simulator to generate interference scenarios is demonstrated with several examples and comparisons of acquisition metrics, position errors and beam patterns.

3.1 Introduction

Broadly, for an array-based processing three different simulation approaches can be considered, namely a) using only software, b) using only hardware, and c) using hardware and software. Employing software simulations to generate signals is an alternative to expensive hardware simulators and provides full control of the simulation environment. Simulations can be done completely in software as proposed by Pinto et al (2012). A simulator implemented completely in software requires access to stored ephemeris over a communication link or access to internet archives of ephemeris. Additionally, satellite position computations should be done in the software, which consumes some processing time. However, by having the simulations partially in hardware and in software most of the satellite data related computations can be done in the hardware simulator, and the parameters required for signal simulations in software are readily available from the hardware simulator. Furthermore, since the models used for simulating errors in pseudoranges (e.g. atmospheric errors, clock offsets, multipath etc.) are available in the hardware simulator, those errors can be enabled/disabled in the hardware simulator before recording the pseudoranges. Subsequently, these pseudorange measurements can be directly used in the software simulator without having to model the errors.

From the previous discussions and the one outlined in Section 1.2, following points can be made:

- having full control during signal simulations makes it easier to evaluate new algorithms developed for GNSS applications
- the process of generating GNSS and interference scenarios simultaneously is challenging

- there is an increased focus on antenna array methods for interference mitigation but array signal simulators used to evaluate these methods are expensive.

The work presented in this chapter addresses these issues.

A new approach to simulate GNSS signals for an antenna array is introduced; for brevity, this approach will be referred to as SimPLAN in the rest of this thesis. The user trajectory information recorded from a single antenna hardware simulator and a known physical configuration of the antenna array are used to simulate GNSS signals for each antenna element. Signal generation is achieved using phase delays obtained using the assumed steering vectors. A similar approach might be possible with real data i.e. by recording live signals, extracting its parameters and regenerating them in the form of array signals. However, signals generated in this way can be inaccurate due to the presence of errors from multipath and the atmosphere; the proposed simulation scheme is free from these errors since the measurements are taken with a hardware simulator. Signal degradations and other interference like jamming and multipath can be generated and added to the GNSS signals as required.

In order to analyze and validate the array data simulations, two types of array processing methods are used. Firstly, the SPM method, which does not take into account the AoA of the signals. In this method, a single set of beamformer weights is estimated and can be used for acquiring all available satellites. Secondly, the MPDR method where the signals' AoAs are incorporated while solving the optimization problem; individual beamformer weights for each signal that maximize the SNR in the desired direction are computed.

3.2 Simulation methodology

Even though the proposed simulation approach can be extended to other GNSS signals, the specific case of GPS signals is considered in the rest of this chapter.

Whenever GPS signals on an antenna array are to be simulated, one should know the signal details and the antenna array configurations *a priori*. Herein, the signal details are obtained using a single antenna hardware simulator, GSS-7700, a hardware simulator from Spirent Communications. Even though the simulations in this thesis are performed using the GSS-7700, this simulation approach is applicable to other hardware simulators that log the required signal parameters. The user position and array configuration are selected by the user. These are the inputs required for simulating antenna array signals. The steps involved in the proposed signal simulation scheme are shown in Figure 3-1. Corresponding to the simulation start time and expected total run duration, user position and satellite positions are recorded and taken from the GSS-7700. The specific signal details like carrier Doppler, pseudorange, code offset are derived from these simulator data log files. This enables precise and accurate multi-antenna scenario generation to maintain high fidelity. Since the exact locations of the satellites are known *a priori*, precise steering vectors can be generated. Likewise, the data corresponding to each antenna element’s position is recorded.

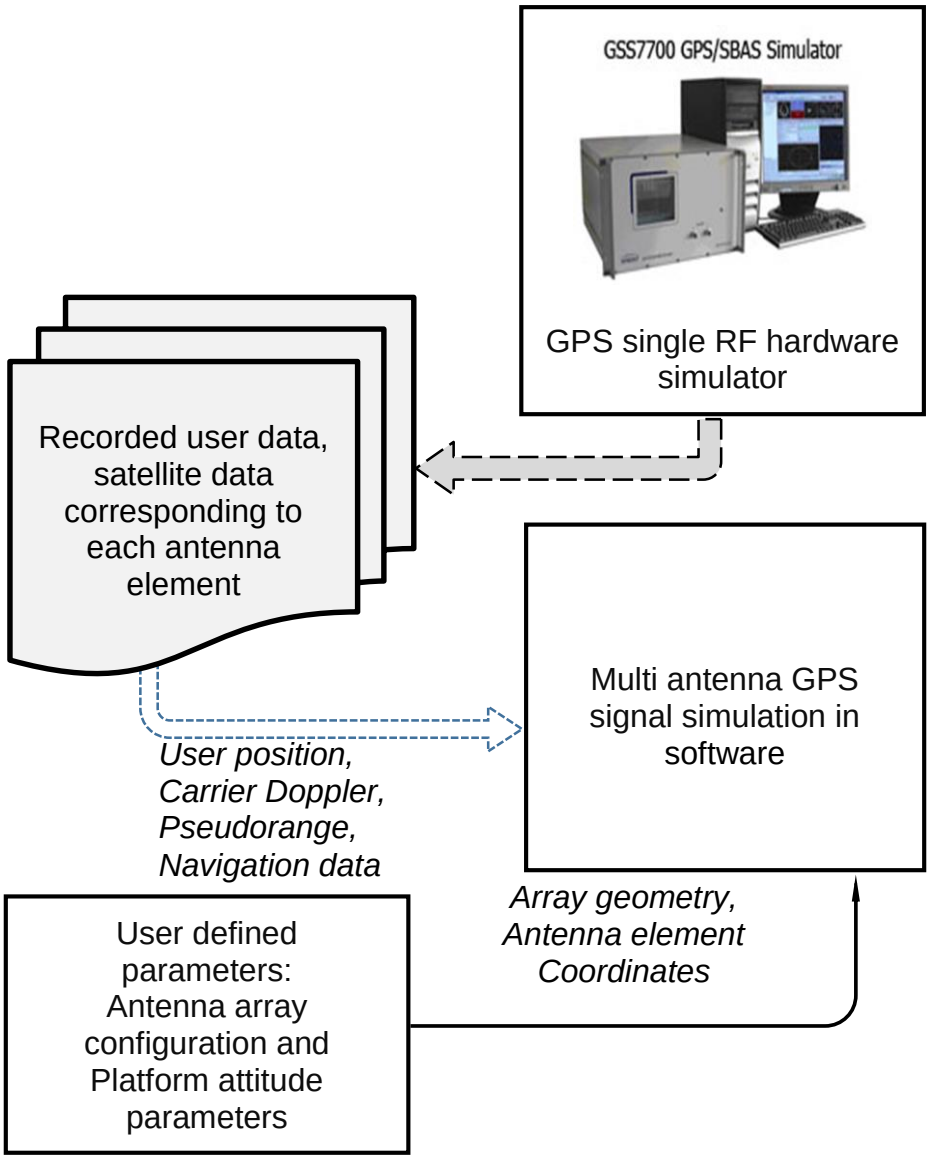

Figure 3-1: Steps involved in the proposed GPS signal simulation scheme

An antenna array can be considered a physical entity with its coordinates aligned in a three dimensional Euclidean space. For simplicity, a particular case corresponding to a static user is considered for simulations. Here, the X_B, Y_B and Z_B components of the array in the body-frame coordinate system are assumed to be aligned with the X, Y and Z components of the Earth Centred Earth Fixed (ECEF) frame, which is the reference frame used for computing the satellite and user positions. However, by incorporating the array

attitude information (roll, pitch and yaw) and a few rotation transformations, the same simulation scheme can be extended to dynamic scenarios. User defined parameters namely array configuration and the platform attitude are used to configure the antenna element positions

3.3 Theory and System Model

The GPS signals transmitted by the satellites consist of three parameters, namely

- navigation data
- C/A code
- carrier signal.

Navigation data consists of satellite's position details and correction terms to compensate for the clock mismatch between the satellites. The satellite positions are time tagged and enable user position estimation. The C/A code spreads GPS signals over a wider bandwidth while providing cross correlation margins and enables the receiver to achieve despreading gain. Additionally, the C/A code provides a way to estimate the pseudorange between the satellite and the user using a time of arrival (TOA) approach. The long distance signal transmission using modulation of navigation data and C/A code is made possible using a carrier signal.

3.3.1 GPS signal simulation for a single antenna

The signal model of the GPS signal received at the user receiver antenna for p^{th} satellite can be modelled as

$$s_p(t) = \sqrt{2A_p} \cdot d_p(t - \tau_p) \cdot c_p(t - \tau_p) \cdot \cos\left(2\pi\left(f_p^{RF} + f_p^d\right)t + \varphi_p\right). \quad (3\text{-}1)$$

The descriptions of the symbols in Equation (3-1) are given in Table 3-1.

Table 3-1: Description of GPS signal model parameters

Parameter	Description
A_p	Amplitude of the generated signal. This can be controlled by setting the desired value of SNR
$d_p(t)$	Navigation data
$c_p(t)$	C/A code (Spreading code)
τ_p	Code offset
f_p^{RF}	Carrier frequency
f_p^d	Carrier Doppler frequency, determined by the relative motion between user and satellite.
φ_p	Carrier phase

3.3.2 GPS signal simulation for an antenna array

The simulated signals at each of the antenna array elements are distinct due to the array geometry, and signal characteristics vary as a function of antenna separation and signal AoA. The single antenna signal generated as per Equation (3-1) is used to generate the array signals by using the multi-antenna signal model described in Section 2.3.

3.4 Results and Analyses

A scenario corresponding to a static user with good visibility of GPS satellites is chosen for simulations. The signal details required for simulation are logged with the GSS-7700. The tracking performance of the software simulator is evaluated using single antenna simulations. Functioning of the multi-antenna signal simulations is demonstrated using

the MPDR beamformer described in Section 2.3.1.3. Finally, a few applications of the proposed simulation method are discussed and corroborated with results.

The simulations and analyses performed are categorized into three sections as follows:

- single antenna simulation of GPS signals
- multiple antenna simulation of GPS signals
- examples of potential applications of the simulator.

The open source MatLab® based single antenna software receiver developed by Borre et al (2007) was modified to achieve multi-antenna receiver functionality. Acquisition, tracking and position computation blocks of the original software were also modified. The interference mitigation capabilities were added to the receiver by incorporating both spatial and temporal processing. The simulated Intermediate Frequency (IF) samples from the array were processed with this multi-antenna receiver. Single antenna IF samples for SimPLAN, GSS-7700 and SMBV-100 simulators were collected using NI front-end and the samples were processed using a single antenna software receiver.

Figure 3-2 shows the positions of the satellites with respect to the user during simulations. The locations of satellites are shown as a function of azimuth and elevation angles.

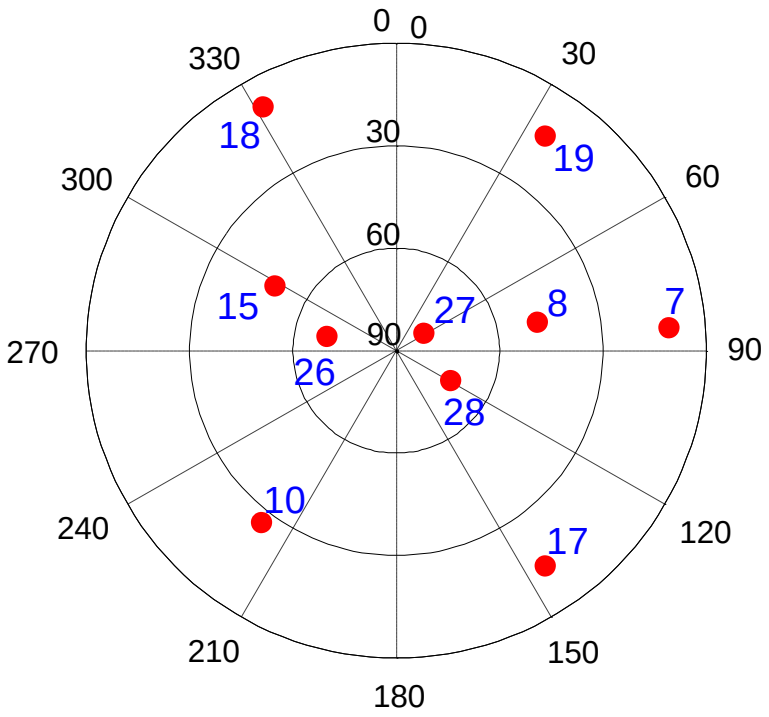

Figure 3-2: Visibility of GPS satellites during simulations

3.4.1 Single RF simulations

The tracking performance of SimPLAN data is evaluated in single antenna mode. The fidelity of SimPLAN can be evaluated by observing the carrier and code tracking performance. The carrier tracking and code tracking performance can be quantified by observing carrier Doppler and Carrier to Noise Density ratio. Evaluations are done using the software receiver implemented in MatLab® with single antenna processing capability. The results obtained for the data generated using SimPLAN are compared with the data from the GSS-7700 and SMBV-100 simulators, wherever applicable. The IF data from these two hardware simulators are collected using a NI RF front-end, with the settings given in Table 3-2.

Table 3-2: Parameter settings used in simulators and front-ends

	Simulator		
Parameter	*GSS-7700*	*SMBV-100*	*SimPLAN*
Intermediate Frequency[*]	420 kHz	420 kHz	-500 Hz
Number of bits used in quantizer	14		
Number of channels	12		
Atmospheric errors	No error		
Reflections and multipath errors	No error		

[*] *this is the IF set in NI front-end for signals from GSS-7700 and SMBV-100*

3.4.1.1 Code generation validation

The input parameters i.e. the reference signal details from the recorded hardware simulator files, are available at intervals of every 10 ms. In SimPLAN, signal simulation is done at the rate of 1 ms. Since reference samples are available at a lower rate, code and carrier phases of the generated signals were propagated from the current simulation epoch to the next simulation epoch to maintain signal's phase continuity. A comparison of the reference signal's code phase to the generated code phase for a particular PRN is given in Figure 3-3.

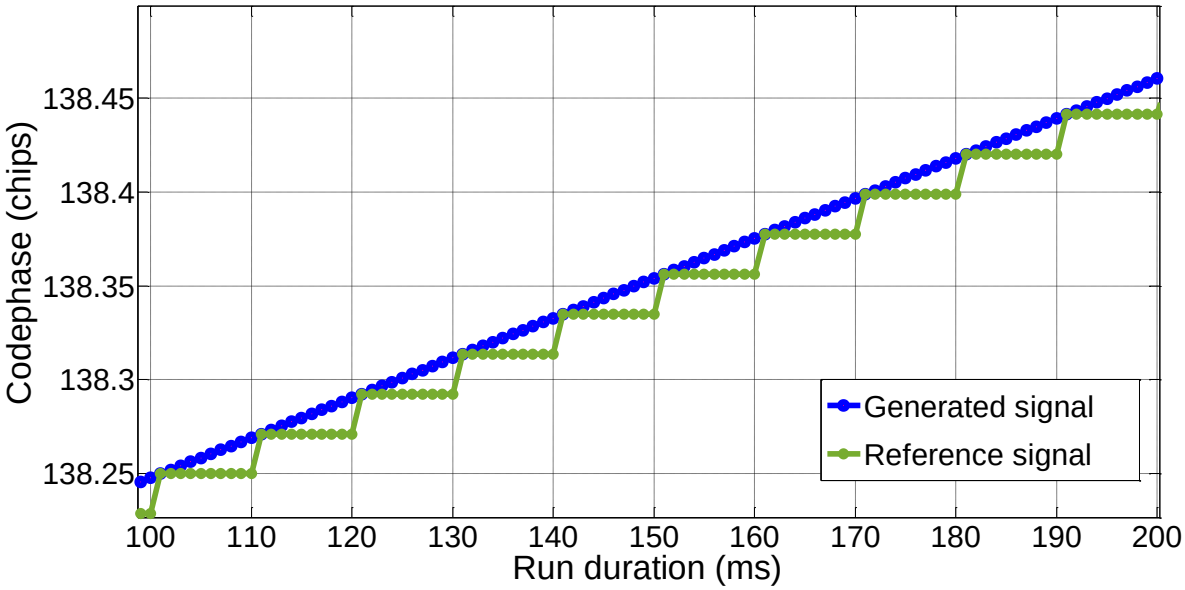

Figure 3-3: Comparison of generated code phase with reference

3.4.1.2 Carrier tracking

The carrier Doppler values for PRN 26 in GSS-7700 and in SimPLAN are compared in Figure 3-4. The fine tracking details are shown in the in-plot. Taking all tracking satellites into account, the standard deviations in carrier Doppler were found to be 0.51 Hz for both GSS-7700 and SimPLAN.

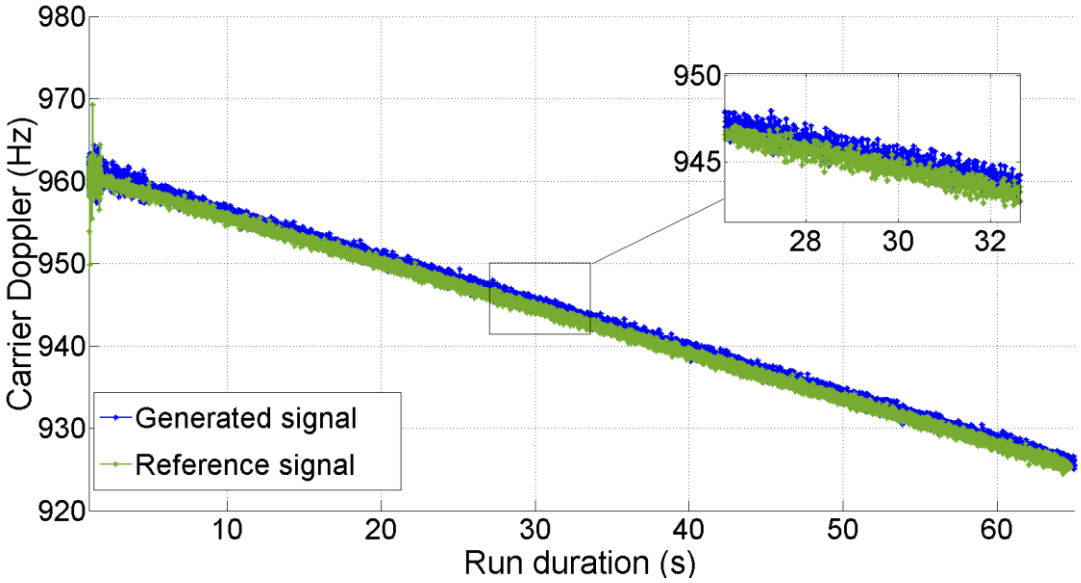

Figure 3-4: Comparison of carrier tracking performance for simulated data using carrier Doppler

3.4.1.3 Code tracking

The C/N_0 of a tracking signal is used to evaluate code tracking performance (Kaplan & Hegarty 2006, Bao & Tsui 2000). The C/N_0 for all PRNs for GSS-7700, SMBV-100 and SimPLAN are given in Figure 3-5, for the data collected using the in-built clocks available with the instruments (i.e. simulator, front-end). There are three distinct bands and each band consists of C/N_0 for all tracking PRNs in that simulator mode. It is conclusive that the SimPLAN code tracking performance is comparable with that of the hardware simulators; considering all tracking channels, the standard deviations in C/N_0 were found to be 1.1 dB-Hz, 1.5 dB-Hz and 1.2 dB-Hz for GSS-7700, SMBV-100 and SimPLAN, respectively. The magnitude differences between different simulators are due to the signal power setting differences; however, the C/N_0 variations over time are comparable.

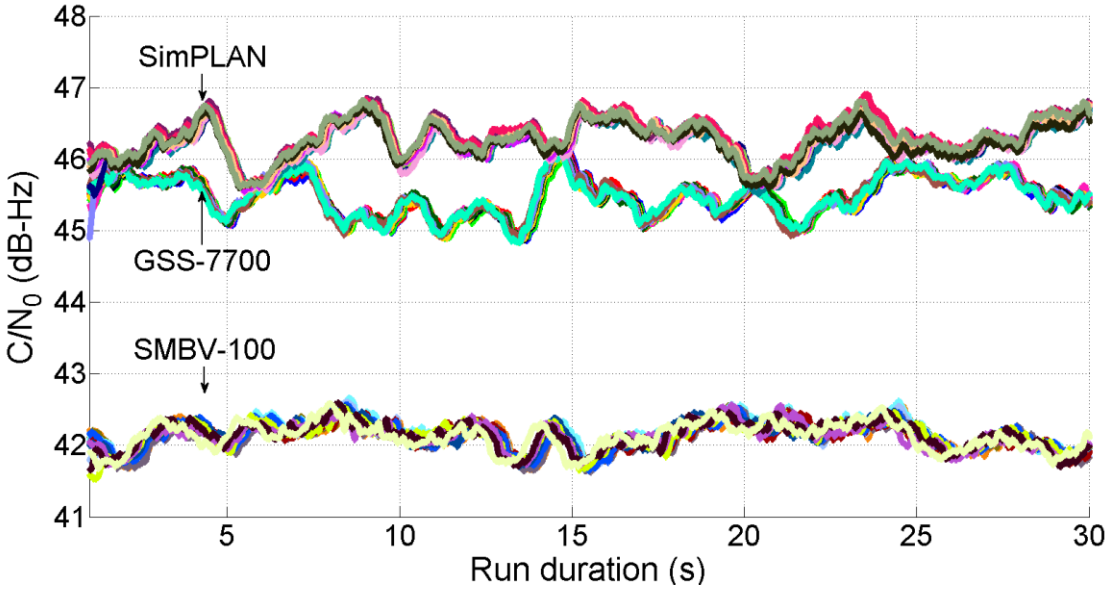

Figure 3-5: Comparison of C/N_0 code tracking performance for simulated data

3.4.2 Array signal simulations

As in single antenna mode, a static GPS data is simulated corresponding to six antenna elements placed in a uniform circular fashion of radius equal to half a wavelength (of GPS L1 signal) and three antenna elements placed in a triangular fashion. The array configurations are given in Figure 3-6.

The array is considered to be placed in the *X*-*Y* plane facing in the direction of the *Z*-axis.

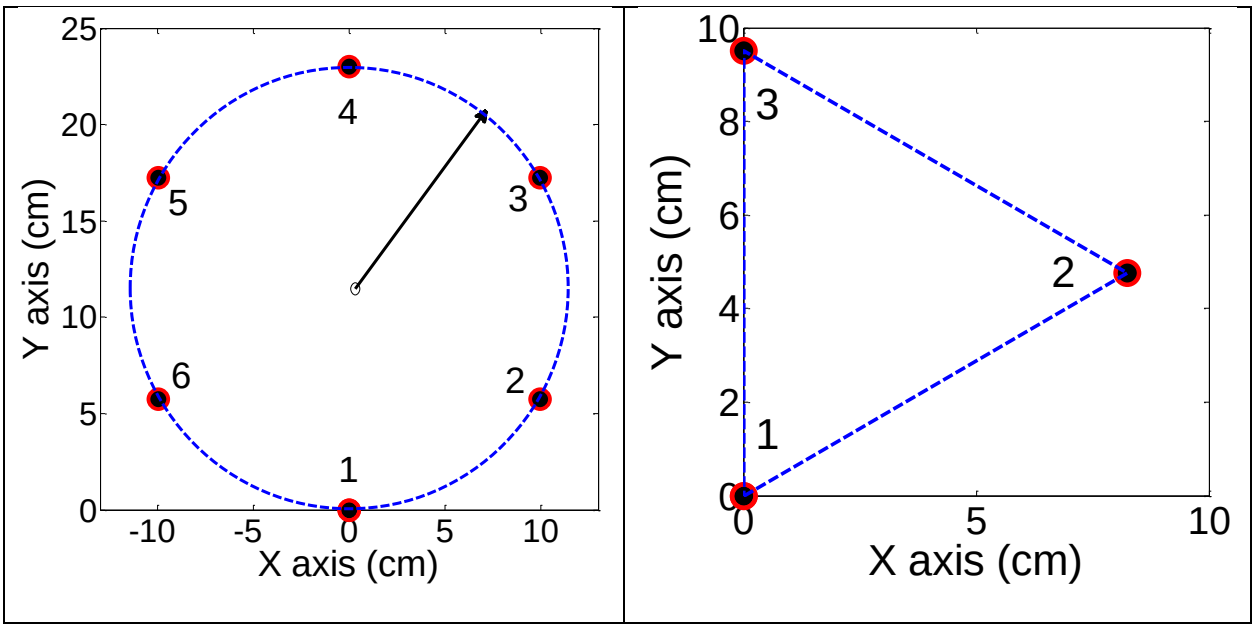

(a) (b)

Figure 3-6: Array configurations for multiple RF simulations (a) 6-element circular (b) 3-element triangular

For evaluations, the SPM beamformer and MPDR beamformers are used and these are described in Section 2.3.1.

As discussed earlier, use of the CRPA beam steering can be done electronically in the desired direction. The MPDR beamformer is used here for beam steering. The use of signal's AoA in the MPDR beamformer not only directs the beam in the desired direction but also passes the desirable signal in an undistorted manner.

The focus is now to demonstrate the functioning of antenna array signal simulation for GPS signals. Multiple antenna signals were simulated and the IF samples were processed using the multiple antenna receiver software. Unless explicitly mentioned, all results described below are obtained for the array data generated using a six element circular array. The MPDR beamformer was used; as a result of using AoA of the signals,

an improvement in the C/N_0 was observed with the antenna array processing. The theoretical value of coherent gain one can expect for a six antenna array is approximately 7 dB (i.e. $10\log_{10}(6)$). Considering all tracking satellites, a C/N_0 of 47 dB-Hz was seen for single antenna processing and that for multi antenna processing with MPDR was recorded as 53.3 dB-Hz, demonstrating a gain of 6.3 dB. These values are indicative of the gain offered by an antenna array; however, absolute values may vary based on the noise levels and the run duration.

Different approaches used for array signal simulations are now discussed. Array signal simulations can be done using only geometric phase shifts captured in the steering vector $\mathbf{a}_p$, with the following approximation: array dimensions are much smaller than the transmitter to receiver path lengths which is the pseudorange; therefore, code phase, carrier Doppler, and navigation data remains the same for all array elements. In this particular approach data corresponding to a single (reference) element is used to generate array data. Such array data works well for many applications. However, in dynamic user applications (e.g. if antenna array is moving/ rotating or if body frame of the array is placed at an inclination with respect to the reference frame), pseudoranges, change in carrier and code Doppler can vary across array elements. These subtle differences in signals at different elements can be captured by following an alternate simulation approach which does not consider any approximations. In this second approach, signal details of each antenna element are independently used to simulate data for an antenna array.

In general, the overall position accuracy of the receiver is determined by the geometric DOP and RMS of measurement errors from all satellites used in the position estimation (Kaplan & Hegarty 2006, Misra & Enge 2001). In order to compare the two approaches mentioned above, measurement biases for both methods were considered and observed biases are recorded in Table 3-3, for the simulations done in a three element triangular array configuration.

MPDR beamformer is used to combine the array data and the biases introduced due to array processing, which can be the same or different for different satellites, are computed as

$$\Delta\rho^{p} = \rho_{MPDR}^{p} - \rho_{c}^{p}, \tag{3-2}$$

where $\Delta\rho^{p}$ is the measurement bias (in m), ρ_{MPDR}^{p} is the pseudorange measurement corresponding to array processing and ρ_{c}^{p} is the pseudorange measurement for a single antenna (single RF front-end) signal for the p^{th} satellite.

For this comparison, single satellite *noiseless* scenarios were simulated for PRN8 and PRN10 separately.

Table 3-3: Comparison of pseudorange biases for different simulation approaches

		PRN	
		8	*10*
$\Delta\rho^{p}$ **(m)**	*Using data from single element (Approach-1)*	0.03	0.02
	Using separate data for each element (Approach-2)	0.15	0.20

The measurement biases were computed for C/A code based measurements. If the signal spectrum remains same at all array elements, one can expect same biases for both approaches. However, for signal simulation using single reference element approach and for the approach that uses positions of each antenna element separately, biases seen are different. Similar results are observed with the six-element circular array. Therefore, array simulation based on individual elements might be required in order to evaluate high performance receivers (for e.g. ones that combine code and carrier phase measurements). Also, this approach (i.e. *Approach-2*) might be very much necessary for simulating signals that do not strictly follow *narrowband* approximation. For e.g., Galileo E5 AltBOC signal which has an entire transmitted bandwidth of 92 MHz.

3.4.3 Applications

Examples of some potential applications of the proposed simulator are now discussed.

3.4.3.1 Simulation of GPS-interference combined signals

Combined GPS interference scenarios were simulated and the descriptions of different interference scenarios are given in Table 3-4. Each in-band interference source has a jamming-to-noise power ratio (JNR) of 15 dB over a bandwidth of 10 MHz. The directional details of the interference sources were incorporated while simulating.

Table 3-4: Interference scenarios

Scenario	Description of parameters (Angles in degree and frequency in Hz)
Scenario 3(a)	One CW Interference, Azimuth = 180 Elevation = 15 Frequency offset = 700
Scenario 3(b)	Three CW Interference Azimuth = 180, 25, 80 Elevation = 15, 30, 15 Frequency offset = 700, 3500, 5000
Scenario 3(c)	Five CW Interference, Azimuth = 180, 25, 80, 245, 320 Elevation = 15, 30, 15, 40, 10 Frequency offset = 700, 3500, 5000, 5500, 6700

Scenario 3(a) was used to compare the acquisition performance and gain patterns. Due to the presence of high JNR interference and resulting rise in the noise floor, GPS signal acquisition failed with the single antenna receiver. Subsequently, the IF samples from the antenna array were processed using the multiple antenna receiver. The SPM (in STP mode with six taps) and MPDR beamformers were used and acquisition metrics obtained in both methods are shown in Figure 3-7. In SPM, a single set of beamformer weights that can be used to acquire all available satellites is estimated; however, maximum gain for all PRNs is not guaranteed. The MPDR method of beamforming is effective as beams are directed to all desirable directions but it is computationally expensive. The corresponding antenna gain pattern for SPM and MPDR (for PRN28) are given in Figure 3-8 (a) and Figure 3-8 (b) respectively.

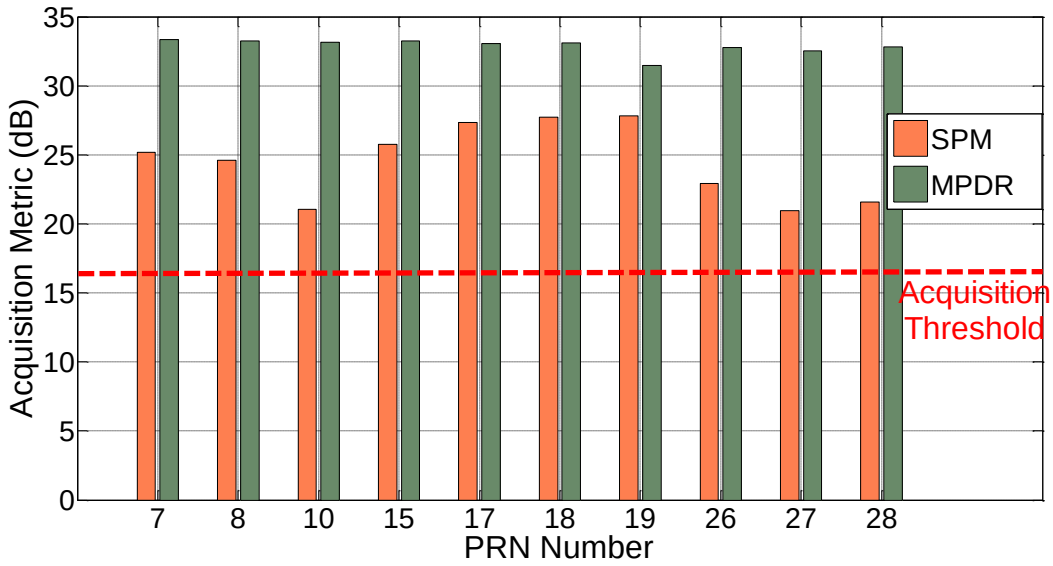

Figure 3-7: Receiver performance comparison for GPS interference combined scenario using acquisition metric for SPM and MPDR for different PRNs

In Figure 3-8 (a), a deep null is placed in the interference direction and maximum gain is not present in the direction of all satellites. A directed beam for MPDR with high gain in the direction of PRN28 in Figure 3-8 (b) validates the method of incorporating directional details during simulations.

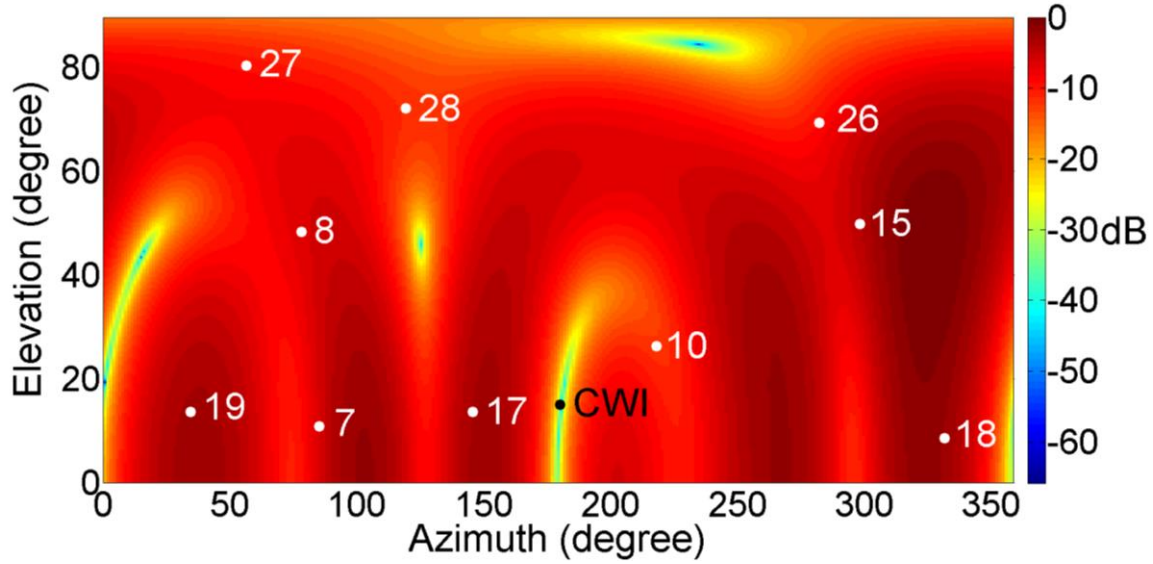

(a)

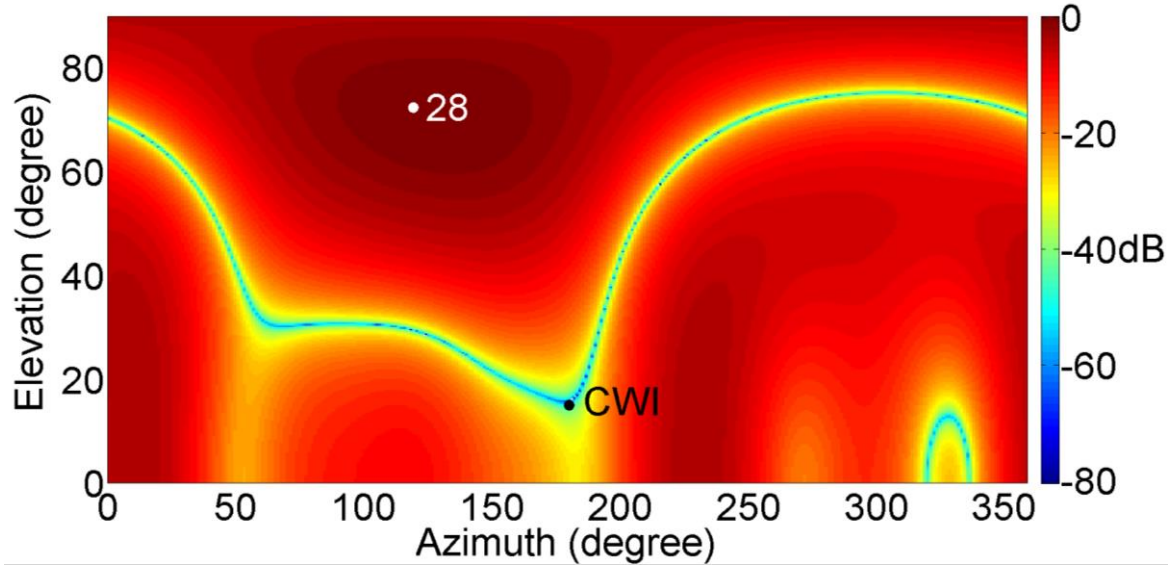

(b)

Figure 3-8: Normalized array gain patterns comparison for GPS interference combined scenario: (a) SPM beamformer – for all PRNs, (b) MPDR beamformer – for PRN28

Position domain results were analyzed for all scenarios given in Table 3-4 by comparing the RMS values of errors in east (E), north (N) and up (U) directions and are given in Table 3-5.

Table 3-5: Comparison of GPS position errors for different interference conditions

Position errors (m)		**Beamforming method**	
Scenario	**Direction**	*SPM*	*MPDR*
Scenario 3(a)	*E*	-2.8	-3.6
	N	-1.8	-2.3
	U	-1.0	-1.4
Scenario 3(b)	*E*	2.8	-3.6
	N	1.8	-2.3
	U	1.1	-1.4
Scenario 3(c)	*E*	-23.2	-7.4
	N	-14.8	-4.7
	U	-8.7	-2.8

SimPLAN enables analysis of results in the position domain as the actual navigation data bits are embedded during signal simulations. The results of Table 3-5 show that position degrades in both methods as the number of interference sources increases. For higher interference sources, as satellite signals AoAs were used in MPDR lower position errors were observed compared to SPM.

3.4.3.2 Simulation of single PRN and noise-free signals

Based on the method used for beamforming, antenna array processing can result in distortion in the GPS signals or pseudorange measurements. As discussed in Section 1.3.2, especially in the case of space-time processing, some additional distortions

can be present due to the temporal filters. These distortions can be due to the following sources: cross correlation function (CCF) misshaping, attenuation and noise domination and measurement biases (Marathe et al 2015b). Firstly, during STP filtering, CCF gets widened asymmetrically and results in an error component in pseudorange measurements. Secondly, when proper design considerations are not employed in STP, unintentional nulls may occur and desired signals may get attenuated, which will also be reflected in the shape of the tracking CCF. Thirdly, due to the non-linear nature of space-time filters, different satellite signals experience different delays through the filter leading to erroneous position estimates.

As the simulator proposed here provides full control on the signal simulations (for e.g. generation of single satellite signals, addition of noise), distortions in STP due to each of the above contributors can be characterized with reasonable accuracy. Detailed analysis of these distortions and use of SimPLAN to generate different scenarios is done in Chapter 4; however, an example illustration is added here for completion of the potential applications.

To illustrate above capabilities of SimPLAN, two scenarios were generated as follows: a single PRN scenario *without noise* and a multiple PRN scenario *with noise*. The CCF for PRN10 for the above scenarios is given in Figure 3-9 and compared against the triangular shaped reference CCF (shown as dotted line). For the *noiseless* case the CCF misshaping is only due to STP; whereas for the *noise* case, CCF distortions are due to noise, attenuation and PRN cross correlation.

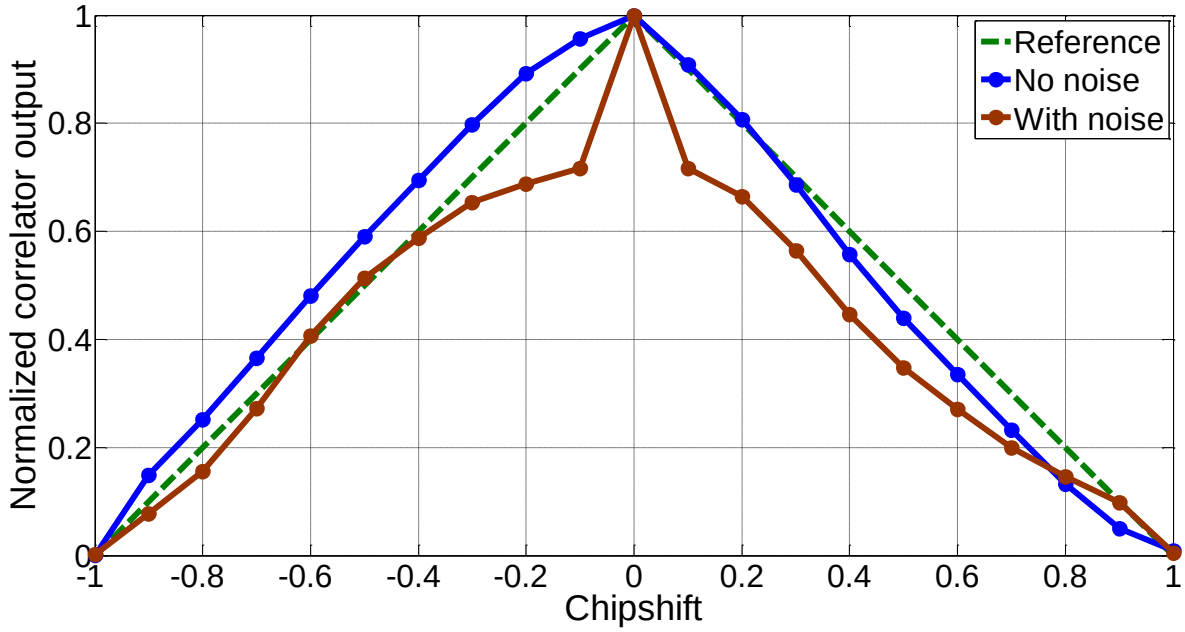

Figure 3-9: CCF comparison for PRN10

In addition to the features discussed above, SimPLAN can be used to generate spatially displaced interference with single or multiple PRN scenarios. This can be particularly handy to study the effects of interference incidence angle with respect to the AoA of the desirable satellite signal.

3.4.3.3 Simulation of other GNSS signals

As signal simulations can be controlled in software, SimPLAN can be used to generate signals corresponding to other constellations or GNSS like signal transmitters. To illustrate this capability, pseudolite signals were simulated using SimPLAN. At shorter distance from the pseudolite transmitters, the pseudolite signals are overpowered. Therefore, these interfere with the GNSS signals and degrade receiver performance. Since pseudolites jam GNSS in the *near zone*, simulating the pseudolite signals is very

useful for research on pseudolites. An antenna array based solution to *near zone* problem is proposed and signals for this study are generated using the proposed simulator. This application of the simulator is described in Chapter 5.

3.5 Summary

Following the discussions about the challenges involved in generating interference scenarios, a new method to simulate GPS interference signals was presented. The fidelity of the simulated signals was compared using carrier Doppler and C/N_0 and these were compared with the tracking metrics for commercially available hardware simulators, i.e. GSS-7700 and SMBV-100. It was demonstrated that the tracking performance of the new simulator matches the performance of the hardware simulators. Capability of the simulator to generate antenna array signals was demonstrated using the MPDR beamformer and an improvement in processing gain was shown. The need for simulating signals corresponding to each antenna element separately was analyzed by comparing measurement biases. Examples for three possible application areas where the proposed simulator can be used were discussed. Different interference scenarios were simulated along with GPS signals and navigation data embedding capability of the simulator was demonstrated using a comparison of the position domain results. The presence of interference in the simulated signal at the pre-set direction was shown with the help of array gain patterns.

Given the scope of this chapter, simulations were restricted to static user scenarios. The dynamics observed due to satellite motion were accounted for appropriately. However, the simulation methodology proposed can be extended to dynamic or moving user

scenarios. Since the parameters recorded from the hardware simulator are used, any desired user motion can be embedded while recording, and array data is simulated as per the recorded information. As the simulations are carried out on a computer platform, there are no restrictions on the dynamics limits (for e.g. there are upper limits on allowable dynamics in hardware simulators due to maximum acceleration or jerk). However, the computational time for SimPLAN depends on the performance of the computer on which it is running.

CHAPTER 4: CHARACTERIZING DISTORTIONS IN GNSS INTERFERENCE SPACE - TIME SUPPRESSION

This chapter focuses on characterizing the STP distortions for different controlled signal scenarios and for live data from an antenna array. The antenna array simulation method introduced in Chapter 3 enables one to perform accurate analyses in the field of STP. The effects of relative placement of the interference source with respect to the desired signal direction are shown using overall measurement errors and profile of the signal strength. Analyses of contributions from each source of distortion are conducted individually and collectively. Effects of distortions on GNSS pseudorange errors and position errors are compared for *blind*, *semi-distortionless* and *distortionless* beamforming methods. The results from characterization can be useful for designing low distortion space-time filters that are especially important for high accuracy GNSS applications in challenging environments.

4.1 Introduction

STP combines information available from both spatial and temporal domains and can be used in receivers to mitigate both narrowband and wideband interference while preserving the GNSS signals. Compared to space-only processing, the enhancement achieved is mainly due to an increase in the array's degree of freedom (Sklar 2003). However, this mitigation technique may deteriorate signal acquisition and tracking performance, and degrade the signals by introducing some distortions (Zhao et al 2006). In C/A code phase based GNSS receivers, pseudorange measurements are generated from the CCF, which is the time domain form of the CAF. In a receiver, a local replica of

the C/A code is generated to track the incoming signal continuously. The peak tracking value (Prompt (P) value) of the correlator is decided based on the shifted local replicas (i.e. Early (E) and Late (L) correlator arms). For proper code tracking, the mid-point between E and L arms gives the location of the peak (P) (Kaplan & Hegarty 2006, Misra & Enge 2001). A non-linear behavior in the phase response of the space-time filter may result in distorted CCFs and biased pseudorange measurements (De Lorenzo et al 2011). In general, space-time processing does not provide a linear phase frequency response across the operating band due to the architecture of the space-time filter (Shuangxun et al 2006). In contrast to the other fields such as Radar and wireless applications (e.g. SNR based methods), it is critical to reduce the array processing borne distortions to maintain error-free pseudoranges because erroneous values have a direct impact on achievable accuracy and integrity requirements (De Lorenzo et al 2011, Fante & Vaccaro 2000, Hatke 1998)**.** Some efforts to characterize and reduce these distortions have been completed (Fante & Vaccaro 2000, Myrick et al 2000). Fante & Vaccaro (2000) characterized the distortions in CCF and its widening for interference and multipath conditions. Distortions in the CCF for a seven-element antenna array in the presence of two interferers were characterized by Myrick et al (2001). However, effects of the distortions in the position domain were not evaluated.

In general, beamformer is a processor that performs filtering in the spatial (or spatial-temporal) domain by linearly combining spatially (or spatially and temporally) sampled data from each antenna (Van Veen & Buckley 1988). Considering distortions as a criterion, beamformers can be classified as *blind*, *semi-distortionless* and *distortionless* (Daneshmand et al 2015a). In case of *blind* beamformers, the AoA of satellite signals are

not used while designing a space-time filter; achieving the interference cancellation while maintaining a linear phase of the filter might be challenging. In such cases, the phase delays for different satellite signals through the space-time filter can be different and it introduces biases in the pseudorange measurements. Furthermore, occurrences of the unintentional nulls may affect receiver performance. *Semi-distortionless* STP methods employ steering vectors that use AoA to avoid unintentional nulls and reduce the distortions (Konovaltsev et al 2008, Zhao et al 2006, Myrick et al 2001). Nonetheless, due to the lack of explicit assumption on the linearity of space-time filter response, these methods do not guarantee distortionless responses for GNSS signals. A few other proposed methods effectively reduce the induced bias errors (De Lorenzo et al 2011, O'Brien & Gupta 2011); however, they do not guarantee phase linearity. In the *distortionless* methods, not only are the steering vectors incorporated, but also the filters are designed to have a linear phase or zero phase and theoretically provide a distortionless response (Daneshmand et al 2015b, Fante & Vaccaro 2000). In one approach, an additional filter is cascaded with the original filter. The frequency response of this filter is the conjugate of the frequency response of the space-time filter and therefore the resulting frequency response is real and has zero phase (Fante & Vaccaro 2000). In another approach, filter coefficients are designed such that the filter is linear phase and at the same time interference is suppressed (Daneshmand et al 2015b). It is conclusive from these discussions that attempts are done to minimize the distortions by combining the information from steering vectors and by forcing the filter to have linear phase frequency response. The magnitude of the filter-induced biases depends on many factors, including the beamforming method and the angle of incidence of the interference

source (O'Brien & Gupta 2011). Bias introduced in the code phase measurements due to array processing can be of the order of a few metres in simple interference scenarios to several hundred metres in harsh interference environments (Daneshmand et al 2015a, Chuang & Gupta 2013, O'Brien & Gupta 2011, Fante et al 2004). Hence, it is important to understand the characteristics of the biases introduced during array processing to assess the quality of the measurements in interference scenario.

4.2 Simulation Methodology

Due to regulations, outdoor RF power transmission in the GNSS bands is prohibited. Therefore, research involving interference from jammers and other transmitters is generally performed in a simulation environment. The array signal simulator described in Chapter 3 is used to generate both interference and satellite signals for evaluating interference mitigation methods. The distortions in STP are characterized herein mainly by using an antenna array simulation test bed, which is developed based on the accurate data recorded from a single antenna hardware simulator. This simulation platform enables one to evaluate the different aspects of distortions due to STP.

In this chapter, the GPS L1 C/A code is used for simulations and analyses; the methods and analyses presented here are applicable to other signals. The simulation test bed is used to obtain the GPS scenarios and simulate signals as received by an antenna array and add interference signals like CW / WB jammers. The block diagram in Figure 3-1 in Section 3.2 is modified to add an additional block corresponding to interference generator and shown in Figure 4-1.

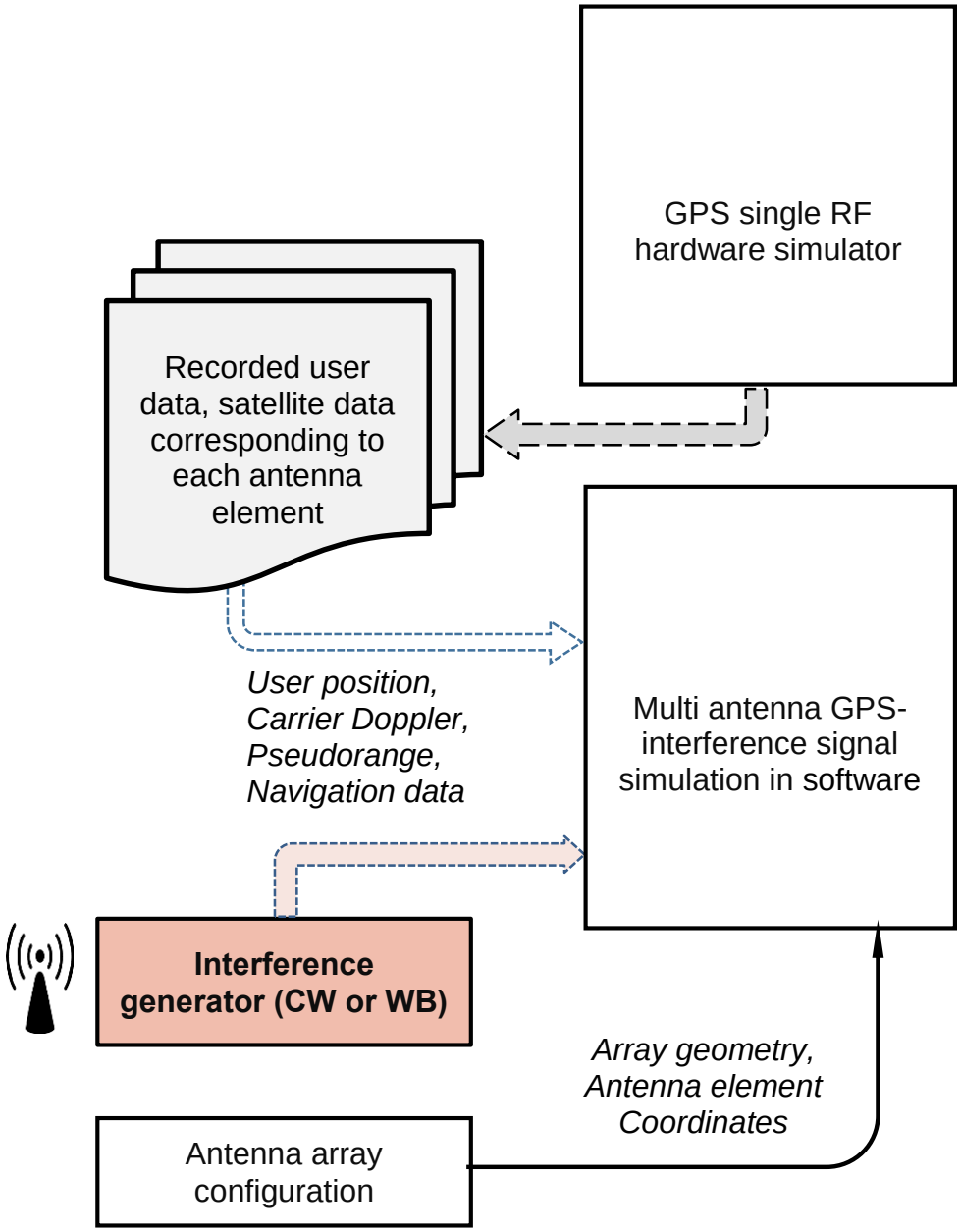

Figure 4-1: Multi antenna GPS-interference simulation scheme

Let τ_n be the time delay between the reference antenna element and the n^{th} array element, for n = 0,1,2,… (N-1) with $\tau_0 = 0$. GPS signal frequency for L1 carrier is 1575.42 MHz, the signal bandwidth is small (generally, 2 MHz to 20 MHz). For the signal model in Equation (3-1) substitute $t = t - \tau_n$. Since the bandwidth of GPS envelope is small,

$$s_p(t-\tau_n) = \sqrt{2A_p}\cdot d_p(t-\tau_p-\tau_n)\cdot c_p(t-\tau_p-\tau_n)\cdot\cos\left(2\pi\left(f_p^{RF}+f_p^d\right)(t-\tau_n)+\varphi_p\right), \quad (4\text{-}1)$$

can be approximated as

$$s_p(t-\tau_n) \simeq \sqrt{2A_p}\cdot d_p(t-\tau_p)\cdot c_p(t-\tau_p)\cdot\cos\left(2\pi\left(f_p^{RF}+f_p^d\right)(t-\tau_n)+\varphi_p\right), \quad (4\text{-}2)$$

such that $B_s\cdot\Delta T_{\max} \ll 1$, where B_s is the maximum envelope bandwidth and $\Delta T_{\max}$ is the maximum time required for the signal to traverse the array (Van Trees 2002).

With the approximation in Equation (4-2), which is also known as *narrowband assumption*, signal delays are approximated by phase shifts and the array steering vector, which is a function of the signal's AoA, carrier frequency, and the array configuration, as given by Equation (2-13).

The assumptions made for signal simulations are given in Section 2.3.

4.3 Theoretical Analysis of Distortions and Beamforming Methods

Distortions are analyzed for following methods: space–time blind Eigen Vector beamformer, MPDR beamformer, extended MPDR (E-MPDR) and Cascade Distortionless (C-DL) beamformer. Space-time Eigen Vector beamformer is a *blind* beamformer (Monzingo et al 2011, Citron & Kailath 1984). The MPDR is a spatial only

beamformer that incorporates a steering vector; this beamformer provides a *distortionless* response for carrier phase measurements (Van Trees 2002). The E-MPDR is an extended version of MPDR for space-time processing to increase the array degrees of freedom (DoF) (Daneshmand et al 2015a, Marathe et al 2015a). Due to the presence of distortions from the temporal filter, this is considered a *semi-distortionless* method. The C-DL method incorporates satellite steering vectors and is designed to provide zero phase, providing a *distortionless* filter response (Fante & Vaccaro 2000). Space-time blind Eigen Vector, E-MPDR and C-DL are used in space-time mode and MPDR is used to observe the results for the space-only processing mode (hence, CCFs and position solutions do not experience any distortions due to temporal filtering in MPDR). The system model and the four mentioned beamforming methods are discussed in the remainder of this chapter.

4.3.1 STP distortions

Interference mitigation using STP allows three types of GNSS signal degradations, namely CCF misshaping, attenuation and noise domination, and measurement bias. Firstly, the ideal shape of a typical GNSS signal's CCF is triangular; however, misshaping (asymmetric widening) of the CCF after STP will introduce an error component in the pseudorange measurements. Secondly, when a space-time filter is used for interference mitigation, it is designed to strip off a designated portion of the input (typically interference). Without proper considerations, due to the unintentional nulls being introduced, some portion of the desired signals is attenuated. Based on the magnitude of the attenuation, this may lead to rounding of the CCF tip and a drop in the correlator

output value. Thirdly, due to the non-linearity of the space-time filter, different frequency components (in GNSS, corresponding to Doppler frequencies of different satellite signals) experience different delays passing through the filter, which leads to biases in the pseudoranges. Having different biases for different satellite pseudoranges leads to inaccurate position estimates. On the contrary, if the biases are the same across all satellites, it will be absorbed in the receiver clock offset and an accurate position estimate is obtained (Kaplan & Hegarty 2006, Misra & Enge 2001, Bao & Tsui 2000). Temporal filters in STP can be independently constrained to obtain linear phase by using typical construct of FIR filters (i.e. by forcing coefficients to have conjugate symmetry (Abdizadeh 2013)). Even then, maintaining phase linearity in STP is not easy, as the information from spatial (signals from different antennas) and temporal (delayed signals) domains are combined.

Because of the STP filter structure shown in Figure 2-11, without special considerations it does not provide a linear phase frequency response across the operating band. Consequently, it is possible that the filter will introduce distortions to the input GPS signals (Fante & Vaccaro 2000). Fante & Vaccaro (2000) and Peng et al (2012) provided a detailed mathematical framework for analyzing the distortions in the GPS CCF. In GPS receivers, the ranging delays are estimated by cross correlation of the received signal with a known signal generated locally. Then the correlation function for the signal after space-time filtering, despreading and Doppler removal can be written as

$$R(\tau) = \int_{-\infty}^{\infty} H(f)P(f)e^{-j2\pi f\tau}df, \tag{4-3}$$

where *P(f)* is the power spectrum of the signal, which is a symmetric function of *f* , and *H(f)* is the frequency response of the space-time filter defined as $H(f) = \mathbf{h}^H(f)\mathbf{a}_p$, $\mathbf{h}(f)$ is the frequency response vector of the TDLs and $\mathbf{a}_p$ is the steering vector of the satellite signals. Because of the addition of *H(f),* the correlator peak can be shifted and the correlator function can be potentially broadened. Only with proper design considerations bias errors and phase shifts can be corrected.

Adding antenna array processing adds biases in code and carrier phase measurements. The phase delays experienced by the signals impinged on different elements of the array can be precisely modelled in the steering vectors. By employing methods such as MVDR or MPDR, the carrier phase delays can be compensated. Hence carrier phase measurements can be bias-free, irrespective of the presence or absence of interference in the data being processed. Conventional MVDR cannot however compensate for code phase based measurements and may cause shifting and widening of the cross correlation function. Depending on the array configuration and signal AoA, this may add measurement biases that can vary between negligibly small values to a few metres; such biases are present in pseudorange measurements that are generated using real antenna arrays. In this chapter, array signals are simulated using GPS signals corresponding to a single antenna and then phase translation is performed to obtain signals for other elements of the array. Therefore, code phase pseudoranges are free from biases, as code

offsets are not simulated. This simulation method, which uses phase translations, enables one to accurately assess STP filter's temporal distortions.

All the types of distortions that show up due to the presence of *H(f)* in the GPS processing chain as shown in Equation (4-3) are considered for analysis in this chapter.

4.3.2 Blind Eigen Vector Beamformer

A Blind Eigen vector beamformer, as described in Section 2.3.1.1 is used. Beamforming is performed in the pre-despreading stage of the receiver where the satellite signal arrival details are still unknown (not extracted). Therefore, a single set of filter weights that works well for all satellites is designed. Looking at the steps involved in this method, it can be seen that no consideration is given towards the satellite signal directions/locations while designing the filter weights. The lack of AoA constraint can result in distortions of the desired signal.

4.3.3 Minimum Power Distortionless Response (MPDR) beamformer

This method incorporates satellite signal steering vectors in the filter as a constrained optimization problem (Van Trees 2002)**,** as given in Section 2.3.1.3. For spatial processing, the correlation matrix is constructed only using spatial samples leaving the matrix dimensions as $N \times N$ (only one tap corresponding to zero delay is used).

The MPDR method uses signal arrival details ($\mathbf{a}_p$) in the filter design and consequently all spatial phase differences are compensated. Due to the use of AoA in the constraint of the MPDR, the phase of the GPS signal would not get affected and the signal would pass

through the filter undistorted; additionally, due to the fact that it is used in a *spatial-only* configuration, it is free from the distortion contributions from temporal filters.

4.3.4 Extended MPDR (E-MPDR)

This is the extended version of the MPDR for space-time processing. Compared to MPDR, this approach provides additional DoF (Daneshmand et al 2015a)**.** The optimization problem for the extended MPDR can be expressed as

$$\mathbf{w}_{opt} = \underset{\mathbf{w}}{\arg\min}\left\{\mathbf{w}^{\mathbf{H}}\mathbf{R}\mathbf{w}\right\}, \tag{4-4}$$

such that $\mathbf{w}^{H}\mathbf{c} = 1$. The vector $\mathbf{c}$ is defined as

$$\underset{NM\times 1}{\mathbf{c}} = \begin{bmatrix} \underset{N\times 1}{\mathbf{a}_p^T} & \underset{N\times 1}{\mathbf{0}^T} & \cdots & \underset{N\times 1}{\mathbf{0}^T} \end{bmatrix}^T. \tag{4-5}$$

Like MPDR, this method also incorporates satellite signal steering vectors in the structure of the space-time filter as a constrained optimization problem; consequently, the distortions due to the spatial phase mismatch are reduced. A non-zero constraint is added to the first tap. The filter response is not necessarily a linear phase and as a result it may lead to possible CCF widening and distortion errors, due to the added temporal filters.

4.3.5 Cascade Distortionless(C-DL) beamformer

As discussed in Section 4.3.1, distortions are introduced due to the beamforming/null steering filter. The C-DL method explores the possibility of distortion reduction by cascading an additional filter to achieve linear phase (precisely, zero phase in this method) from the filter (Fante & Vaccaro 2000). In the filter response *H(f)*, distortions due to spatial processing are reduced by using the steering vectors. However, a linear phase

response is not assured. To remove the phase non-linearity of the space-time filter, it is cascaded with another filter whose frequency response is the conjugate of the frequency response of the space-time filter. Designing a cascaded filter with proper considerations, a symmetric impulse response is obtained that provides the same shift to all satellite pseudoranges; however, the correlation peak can be broadened. The frequency response of the resulting filter is given as $H(f)H^{*}(f) = |H(f)|^{2}$.

A summary of comparison of the above methods is given in Table 4-1.

Table 4-1: Comparison of few features offered by beamformers

	Beamforming method			
Parameter description	*Blind Eigen Vector*	*MPDR*	*E-MPDR*	*C-DL*
Use of steering vector	No	Yes	Yes	Yes
Computational complexity	Less	Moderate	High	High
Space(S) or Space-time (ST)	ST	S	ST	ST
Distortions	Maximum	No distortion	Moderate	Minimum
Number of filter weight sets	Single	Multiple*	Multiple*	Multiple*

* separate steering vector is used for each satellite

The performance of beamformers depends on the overall information available to them, for e.g. AoA. Based on the design criteria, the available information is used in the beamformers for interference mitigation to maintain maximum gain in the desired direction, to reduce the distortions and to maintain linear phase.

4.4 Simulation Results and Analyses

Static GPS data is simulated for six antenna elements placed in a uniform circular fashion with radius equal to half a wavelength (of GPS L1 signals). Each of the simulated interference scenario has a JNR of 20 dB over a bandwidth of 10 MHz. A set of GPS satellites providing a good DOP is chosen for the simulation. The PRN codes and azimuth and elevation angles of the satellites are given in Figure 4-2. The user is assumed static and the satellite motion and corresponding Doppler changes have been incorporated into the simulations.

PRN	Az (degree)	El (degree)	Sky plot
7	85	11	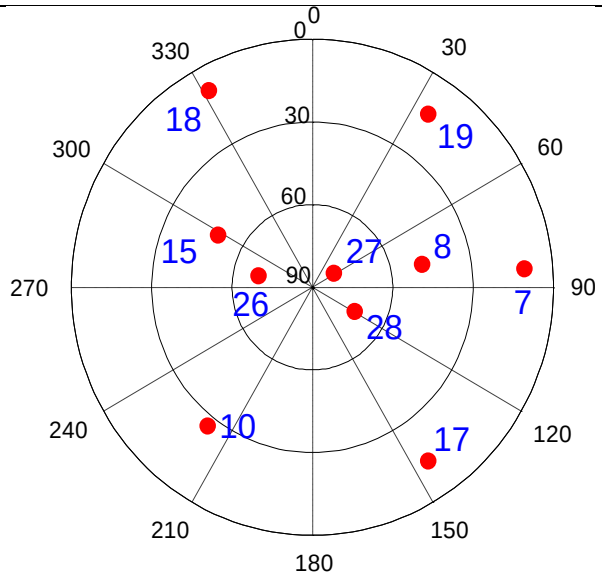
8	78	48	
10	218	26	
15	298	50	
17	146	14	
18	332	9	
19	34	14	
26	282	69	
27	57	80	
28	119	72	

Figure 4-2: Satellite visibility during test – Simulator data

Four interference scenarios are considered for the simulations. Table 4-2 lists different parameters corresponding to the interference sources. CW sources are simulated such that they are present in the GPS L1 main lobe bandwidth.

Table 4-2: Interference scenarios

Scenario	Parameters description (Angles in degree and frequency in Hz)
Scenario 1	One CW Interference Varying azimuth Varying elevation; details are in Section 4.4.1 Frequency offset = 500
Scenario 2	One CW Interference Azimuth = 190 Elevation = 45 Frequency offset = 1500
Scenario 3	Two CW Interference & One Wideband Interference Azimuth = 190,25,40 Elevation = 45,30,70 Frequency offset = 1500,3500
Scenario 4	Six CW Interference Azimuth = 190,25,80,245,320,345 Elevation = 45,30,15,40,10,55 Frequency offset = 1500,3500,5000,5500,6700,7500

An open source MatLab® based software receiver, which is described in Section 3.4, was used. One of the antenna array elements was chosen as a reference and the local signal replicas corresponding to this antenna path were used to measure the relative amplitude and phase values of the signals at other antennas. Hence, the estimated discriminator outputs at different antennas differ only in amplitude and phase.

Several metrics that indicate performance of the receiver's operation at different stages are used for comparison. Distortions in the CCFs are quantified using a distortion metric, the total error in the GPS pseudoranges due to array processing is measured using overall measurement error (or measurement bias), effective C/N_0 indicates the quality of code tracking, and the contributions of the measurement errors are observed by

comparing the East North Up (ENU) position errors. The number of satellites tracked is given wherever applicable.

Distortion metric (DM)

The metric shown in Figure 4-3 is used to quantify the distortion in the CCF shape compared to the clean CCF shape (Marathe et al 2015b). Due to the asymmetric widening of the CCF, the prompt (P) derived using E and L arms will have an offset from the P value of the clean signal, leading to GPS measurement errors. The error introduced only due to CCF misshaping is termed a *distortion metric (DM)* and is measured in metres. Due to asymmetry in widening, the distortion metric depends on the correlator spacing chosen for code tracking. During simulations ideal signal conditions are considered; distortions due to multipath are not present in the metric.

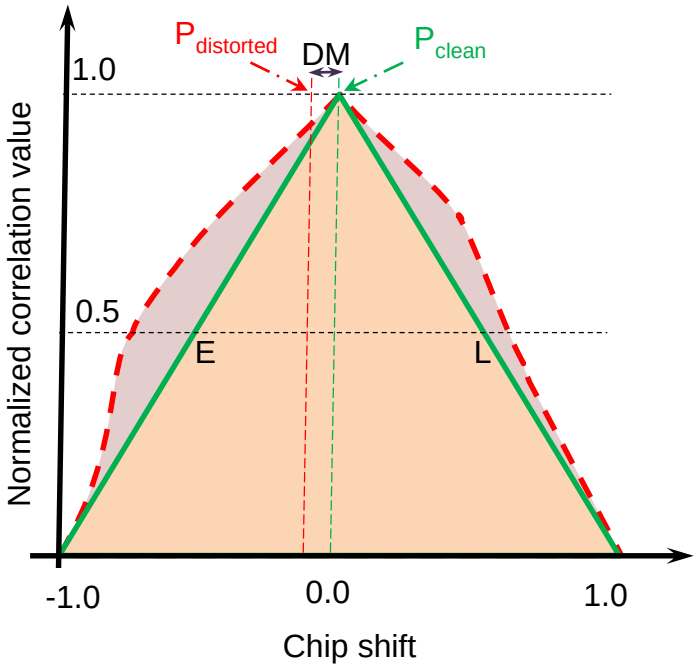

Figure 4-3: CCF distortion metric

Overall measurement error (Measurement bias)

In the CCF distortion metric explained previously, the bias added only by CCF misshaping was measured. However, the absolute biases introduced due to space-time processing, which can be same or different for different satellites, were not quantified. These are computed as per the Equation (3-2) where ρ_c^p is the pseudorange measurement for a single RF clean signal without any interference and without any spatial-temporal processing for p^{th} satellite. Generally, $\Delta\rho^p$ comprises a fixed part $\Delta\rho_F^p$ and a variable part $\Delta\rho_V^p$. For a linear phase FIR filter with conjugate symmetric coefficients, the variable part $\Delta\rho_V^p = 0$ and the fixed part can be given by

$$\Delta\rho_F^p = T_s C\left(\frac{M-1}{2}\right), \tag{4-6}$$

where T_s is the delay due to one tap (in units of time), C is the speed of light (m/s) and M is the number of taps used in the temporal filter.

Effective C/N_0

To measure the effect of interfering signals on the quality of the prompt code tracking channel of a GPS receiver, a metric called *effective C/N_0* is considered and it is calculated based on the following equation (Betz 2001):

$$\left(\frac{C}{N_0}\right)_{eff} = \frac{C_s \int_{-\beta_r/2}^{\beta_r/2} G_s(f)df}{N_0 \int_{-\beta_r/2}^{\beta_r/2} G_s(f)df + C_j \int_{-\beta_r/2}^{\beta_r/2} G_j(f)G_s(f)df}, \tag{4-7}$$

where C_s is received power of the desired signal, $G_s(f)$ is the normalized power spectral density (PSD) of the desired signal and N_0 is the thermal noise power density. C_j is the interference power and $G_j(f)$ is the normalized PSD of the interference signal. β_r is the receiver front-end bandwidth. Assuming that the front-end bandwidth is wide enough to pass all the signal and interference frequency components, Equation (4-7) reduces to

$$\left(\frac{C}{N_0}\right)_{eff} = \frac{C_s}{N_0 + C_j \int_{-\beta_r/2}^{\beta_r/2} G_j(f)G_s(f)df}. \tag{4-8}$$

Equation (4-8) can be extended for array processing and the expression for effective C/N_0 is

$$\left(\frac{C}{N_0}\right)_{eff}^{Array} = \frac{(A_{BF})C_s}{N_0 + \sum_{l=1}^{L}\left((A_{NS})_l C_l \int_{-\beta_l/2}^{\beta_l/2} G_l(f)G_s(f)df\right)}, \tag{4-9}$$

where A_{BF} is the beamforming gain and $(A_{NS})_l$ is the loss due to null steering at l^{th} interference signal. C_l is the interference power and $G_l(f)$ is the normalized PSD of l^{th} interference signal having bandwidth β_l. Effective C/N_0 for array signals given in Equation (4-9) will be referred to as C/N_0 further in this chapter.

4.4.1 Effects based on interference source incident angle

Array processing methods primarily process the signals in the spatial domain and the performance of the beamforming process depends on the relative angles between the desired and interference signals. Here, the effects of the interference source incidence angle on receiver performance are evaluated. To analyze the effects of spatial closeness between the desirable and interference signals, a CW interference source is placed at different spatial separations (as per Scenario 1 given in Table 4-2) from a GPS satellite signal, i.e. PRN27 located at an elevation of 80° and azimuth of 57° with respect to a static user on earth. The interference source position is simulated to be at different azimuths and elevations from the user with a step size of 60° in azimuth and 30° in elevation, forming a grid of interference incident angles around PRN27. In addition to these angles, two more azimuth-elevation pairs that are close to PRN27, namely (30°, 70°) and (40°, 85°) are simulated. Single PRN scenarios (for PRN27) are generated for each interference location separately and generated array data is processed using a Blind Eigen Vector beamformer with seven taps, for each case. The overall measurement errors, C/N_0 and distortion metrics are measured for each case and are tabulated. The overall measurement errors are computed using Equation (3-2) and the constant delay due to TDLs, namely $\Delta\rho_F^p = 104.93\,\text{m}$, is removed. The measurement errors, C/N_0 and distortion metrics for all cases are given in Table 4-3, Table 4-4 and Table 4-5, respectively. It is evident from Table 4-3 and Table 4-4 that when the interference is spatially away from the PRN, a very small bias gets added into the measurements and a high C/N_0 value is maintained. As the interference source approaches the satellite signal, the signal strength drops by a value of up to 6 dB and errors of up to 132 m occur in the

measurements. The errors and the C/N_0 variations as a function of interference location are shown in Figure 4-4 and Figure 4-5. The satellite signal is shown as a circled star and the simulated positions of the interference sources are indicated using a plus symbol in the figures.

Table 4-3: Changing interference placement – Overall measurement errors ($\Delta\rho_V^p$)

(in metres)		**Azimuth (degree)**							
		0	*60*	*120*	*180*	*240*	*300*	*30*	*40*
Elevation (degree)	*0*	0.2	-0.8	-1.0	0.6	0.2	-0.9	*	*
	30	-0.4	-0.1	-0.1	0.5	0.3	-1.0	*	*
	60	1.2	1.6	1.2	0.0	0.0	0.0	*	*
	90	-114	-114	-114	-114	-114	-114	*	*
	70	*	*	*	*	*	*	-102	*
	85	*	*	*	*	*	*	*	-132

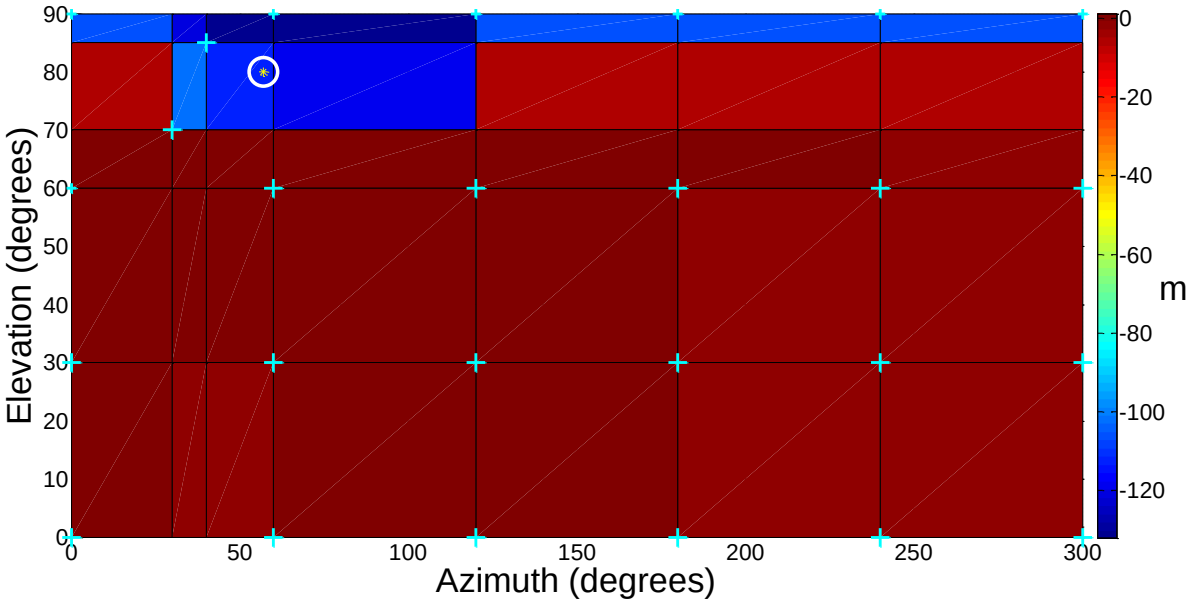

Figure 4-4: Changing interference incident angle – Variation of $\Delta\rho_V^p$

Table 4-4: Changing interference incident angle – C/N$_0$

(in dB-Hz)		Azimuth (degrees)							
		0	*60*	*120*	*180*	*240*	*300*	*30*	*40*
Elevation (degrees)	*0*	54.5	54.7	54.6	54.7	54.9	54.7	*	*
	30	54.8	54.9	54.9	54.5	54.7	54.5	*	*
	60	54.2	52.8	54.4	55.1	55.0	55.0	*	*
	90	49.5	49.5	49.5	49.5	49.5	49.5	*	*
	70	*	*	*	*	*	*	51.1	*
	85	*	*	*	*	*	*	*	49.0

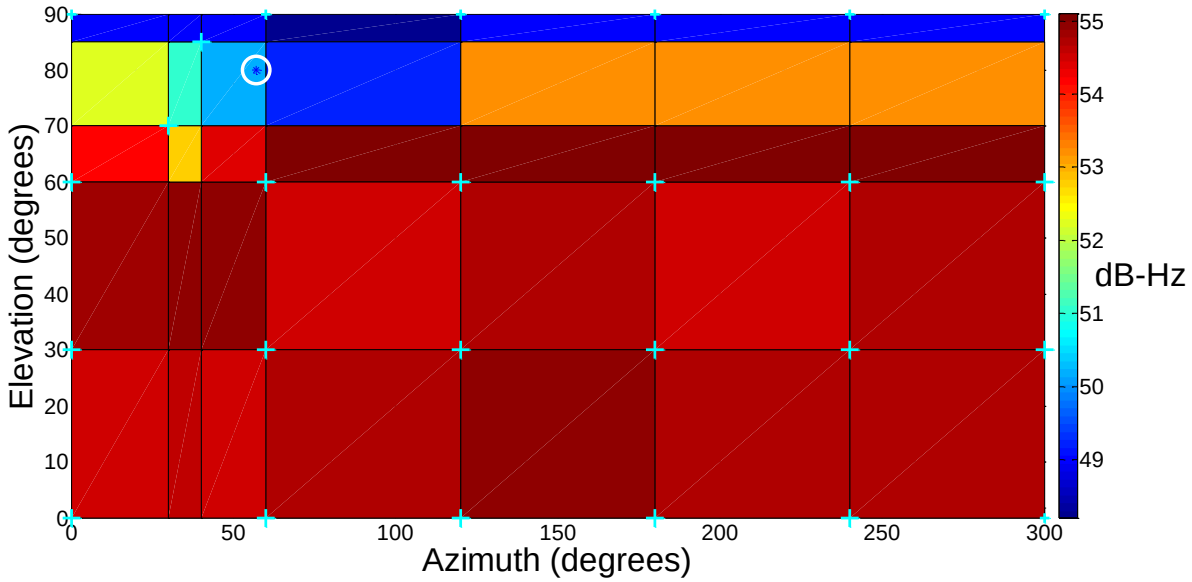

Figure 4-5: Changing interference incident angle – Variation of C/N_0

As discussed previously, asymmetrical widening of the CCF results in distortions. The amount of degradation depends on correlator spacing. To understand this behavior, distortion metrics were measured for chip spacing of 0.2 and 0.5 and are given in Table 4-5. Because of close proximity of the PRN and interference, errors up to 50 m are introduced due to CCF misshaping and the distortions were observed to be higher at 0.5 chip spacing compared to 0.2 chip spacing.

Table 4-5: Changing interference incident angle – Distortion metric

(in metres)			Azimuth (degree)							
		Correlator chip spacing	*0*	*60*	*120*	*180*	*240*	*300*	*30*	*40*
Elevation (degree)	*0*	*0.5*	2.0	0.4	0.8	0.3	0.4	0.7	*	*
		0.2	2.0	0.8	1.0	0.2	0.1	0.8		
	30	*0.5*	2.4	0.6	0.1	0.4	0.6	0.9	*	*
		0.2	2.3	0.6	0.3	0.1	0.3	1.1		
	60	*0.5*	1.3	0.9	0.3	0.1	0.1	0.2	*	*
		0.2	1.5	0.5	0.3	0.3	0.2	0.1		
	90	*0.5*	53	53	53	53	53	53	*	*
		0.2	26	26	26	26	26	26		
	70	*0.5*	*	*	*	*	*	*	51	*
		0.2							14	
	85	*0.5*	*	*	*	*	*	*	*	41
		0.2								31

Based on the results obtained with the Blind Eigen Vector method, it is apparent that the interference effects (as observed using C/N_0 and the errors) mostly do not change when the interference source is spatially away from the satellite. Therefore, for other beamforming methods, analysis of the interference placement effects is done only at a few sample points close to the desirable signal and results are given in Table 4-6. Results from the previous method are also added for the sake of comparison.

Table 4-6: Changing interference placement – Comparison of different beamformers

		Beamforming method			
(Azimuth, Elevation) pair	***Parameter***	*Blind Eigen Vector*	*E-MPDR*	*C-DL*	*MPDR*
(30,70)	*C/N_0 (dB-Hz)*	51.1	52.3	50.8	51.4
	DM (m)	51	26	3.9	0.2
(40,85)	*C/N_0 (dB-Hz)*	49.0	51.8	47.8	45.8
	DM (m)	41	6.2	3.0	1.0
(60,90)	*C/N_0 (dB-Hz)*	49.5	52.2	50.7	50.8
	DM (m)	53	11	2.6	1.5

Since a single CW interference was used, MPDR introduced minimal distortions over a large space close to the interference source location, with some variation in the signal strength. The E-MPDR provided an improved C/N_0 but higher distortion errors due to the temporal filter occur. As some DoF are consumed to maintain phase linearity in the C-DL method, smaller errors due to CCF misshaping were observed, compared to the blind method and E-MPDR. It can be seen that C/N_0 values for the C-DL method (distortionless STP) are lower compared to the E-MPDR method (semi-distortionless STP). This is owing to the fact that distortionless STP methods, in addition to steering the main lobe of the array beam pattern towards the direction of the received signals, apply a constraint to maintain the linearity of the filter phase response.

4.4.2 Effects of different STP distortions

Three different signal degradations that occur on GPS signals after performing STP are analyzed. The results obtained for different test cases are given here. These are categorized based on the distortion source in the following order:

- CCF misshaping only due to STP: This is analyzed using *without noise* scenarios generated for each PRN separately to avoid losses due to cross correlation. Six CW sources (as in Scenario 4 in Table 4-2) are simulated.
- Effects of noise and PRN's cross correlation: This is analyzed with multiple satellite scenarios *with noise*. Results are compared for one CW and six CW interference scenarios.
- Effects of CCF misshaping, bias, noise and PRN's cross correlation: Combined effects due to above sources and the position error bias are given for one CW and six CW scenarios (Scenario 2 and 4 in Table 4-2).

In order to characterize the effects of CCF misshaping and noise, one should have control to enable or disable noise in the generated signal. This is achieved by simulating signals *without noise*. Since the GPS is a Direct Sequence CDMA system, even if the effect of thermal noise is nullified during signal simulation, losses due to cross correlation between signals from different PRNs still persist. As a consequence, clean lossless GPS signals cannot be generated in a multi-satellite environment. To address this, single PRN scenarios were individually generated for a few satellites. The proposed multi-antenna simulation platform enables one to perform all the tests mentioned above and determine the contributions due to each part.

While generating the results, the deviations seen in the CCF are translated to distance (as measured using distortion metric) and tabulated for comparison. An early-late (E-L) correlator spacing of 0.2 chips is used in all experiments. These data sets are processed using a space-time filter adopting the Blind Eigen Vector beamformer. The number of taps changes from 2 to 4, 6 and 8 for analyzing purpose.

CCF misshaping only due to STP

The CCF widening does not result in errors if widening occurs symmetrically but asymmetrical widening does. The interference scenario considered here contains six sources of interference. The single PRN scenarios for PRNs 8, 10, 17, 18 and 27 are simulated independently and the distortion metric used for the STP with different tap numbers is reported in Table 4-7.

With a lower number of taps, complete signal recovery from interference could not be achieved for all PRNs and a frequent loss of tracking was observed. Interference mitigation was partially successful for 2 and 4 taps. By increasing the number of taps, better interference mitigation was observed which in turn led to improved acquisition and tracking. In spite of a widened CCF, an overall decrease in the distortion error was seen, due to improved mitigation performance.

Table 4-7: Measurement errors using distortion metric without noise (Six CW Scenario 4)

(in metres)				
SV ID	**Number of taps**			
	2 tap	*4 tap*	*6 tap*	*8 tap*
8	43.2	20.4	8.1	5.2
10	54.1	36.2	8.1	6.5
17	*	36.4	8.3	7.0
18	*	*	*	4.6
27	60.5	19.3	9.0	5.9

* *tracking with frequent loss of lock*

Since the distortions are prominent even in the *without noise* case, it can be concluded that there is significant CCF distortion due to STP alone. A lesser distortion was observed with higher tap numbers; this could be due to an increase in the available temporal DoF in the space-time filter for interference mitigation. The CCF is further distorted due to the presence of noise and cross correlation losses and these are analyzed further.

Effects of noise and PRN's cross correlation

In this case, since signals for all PRNs are present, the noise floor increases due to the cross correlation. These are the most practical scenarios one encounters. Analysis is carried out on two multiple PRN scenarios, one with a single CW source (interference Scenario 2) and another with six CW sources (interference Scenario 4).

In the case of one CW, due to a favorable DoF, good quality interference mitigation is possible. Figure 4-6 shows a widening of the CCF with increasing taps for PRN10. The

measurement errors due to the CCF distortion for all PRNs are reported in Table 4-8. Though not clearly conclusive, the trend observed suggests a distortion decrease at higher taps.

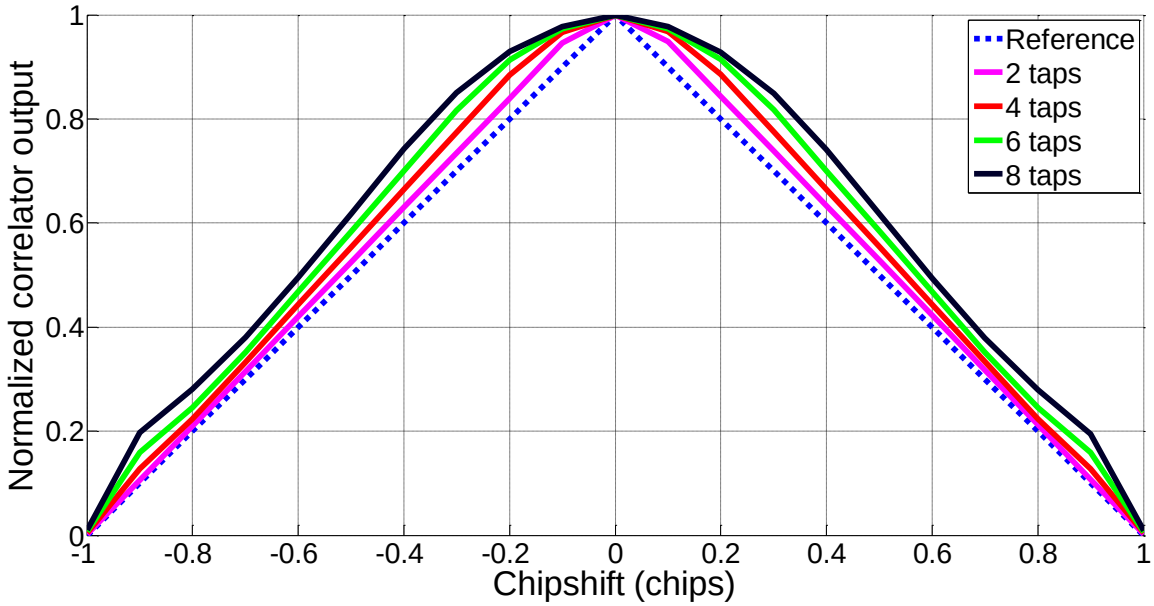

Figure 4-6: CCF distortions for PRN10 – Scenario 2

Table 4-8: Measurement errors using distortion metric: For One CW and Six CW (in metres)

SV ID	Scenario	Number of taps			
		2 tap	*4 tap*	*6 tap*	*8 tap*
10	*2*	0.3	0.1	0.1	0.1
	4	*	*	27.7	26.2
17	*2*	0.6	0.2	0.5	0.5
	4	*	*	26.1	22.5
18	*2*	0.4	0.3	0.7	0.8
	4	*	*	22.1	26.6
27	*2*	1.2	1.5	3.2	2.3
	4	*	*	32.9	23.1

** tracking with frequent loss of lock*

Similar distortion analysis was carried out for another multiple PRN scenario with comparatively intense interference conditions (Scenario 4). Due to the combined effect of PRN's cross correlation loss, noise and STP, maximum impact is observed on the CCF distortion. The CCF for PRN10 is shown in Figure 4-7 where with six CW, the CCF distortion is higher compared to that in the presence of one CW. Improved GPS signal recovery is seen with a higher number of taps. A five to seven times increase in distortion errors is observed in the six CW case, as compared to the one CW scenario case.

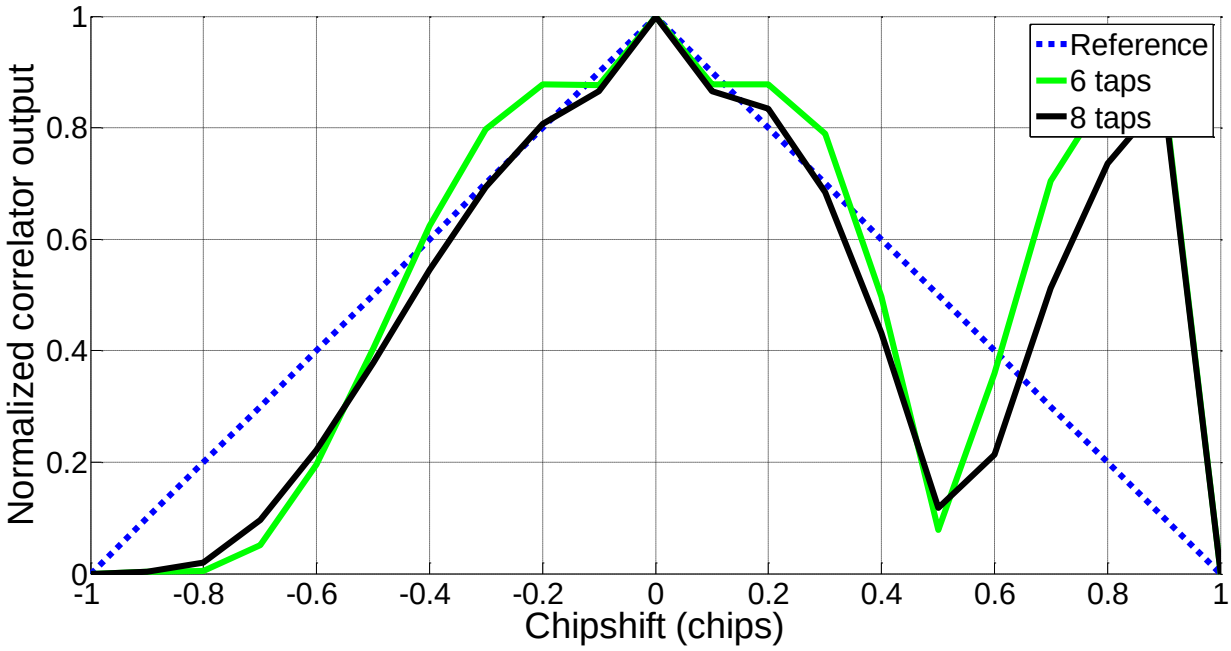

Figure 4-7: CCF distortions for PRN10 – Scenario 4

Effects of noise and cross correlation, CCF misshaping and bias

Here, the combined effect of all the distortion sources on the position errors is compared for different delays in the temporal filter of STP. The position accuracy of the receiver is determined by using the geometric DOP and RMS of measurement errors from all the satellites used for the position estimation (Misra & Enge 2001). The distortions present in each of the satellite measurements collectively contribute towards an increase in position errors. Typically, the position errors in east (E), north (N), and up (U) directions increase when the receiver antennas are exposed to a higher number of interferers as shown in Table 4-9.

Table 4-9: Position errors in the presence of distortions for different TDLs: For One CW and Six CW

(in metres)						
	One CW (Scenario 2)				Six CW (Scenario 4)	
	2 tap	*4 tap*	*6 tap*	*8 tap*	*6 tap*	*8 tap*
E	-2.8	-3.0	-2.3	-3.2	-100	-69
N	-1.8	-1.9	-1.5	-2.1	-64	-29
U	-1.1	-1.1	-0.9	-1.2	38	21

Considering the previous discussions and looking at the position errors (for one CW scenario) given in Table 4-9, the measurement errors due to biases dominate the errors due to the CCF distortion and errors seem to increase as the number of taps increases. This leads to a position error increase (e.g. higher ENU errors for 8 taps compared to 6 taps in Scenario 2). Each addition of a TDL provides an increase in the number of temporal DoF available for interference mitigation. When the signal environment contains a higher number of interference sources, adding TDLs improves interference cancellation performance and in turn improves the acquisition and tracking behavior. For the specific case of six CW sources (interference Scenario 4), partial success in acquisition/tracking of all PRNs was seen in the space-time filter with 2 and 4 TDLs and therefore position computation was not possible. The acquisition and tracking performance improved for 6 and 8 TDLs, increasing the number of satellites that can be used in the position computation. In Scenario 4, for the space-time filter with eight taps, an increase in the satellite count leads to a DOP improvement and in turn a reduction of position errors. The above observations suggest that the use of an *optimal* number of taps to achieve

successful interference mitigation and at the same time maintain good position accuracy by maintaining less filter-biases is needed to achieve best results.

Effects of noise and cross correlation were studied for the Blind Eigen Vector beamformer, as it is widely used in real world applications due to fact that it does not require signal's AoA information compared to other methods considered in this research. Even though the results corresponding to noise analysis and varying number of taps are not presented and compared for other methods, one can expect a similar trend in results, possibly with different absolute values. In the following sections, distortions, biases, C/N_0 and position errors for different beamforming methods are compared for various simulated and live signal scenarios.

4.4.3 Comparison of distortions in beamformers

Distortions and their contributions in the position errors are analyzed for three different interference scenarios listed in Table 4-2. GPS signals are simulated as per the information of Figure 4-2. Array data corresponding to these scenarios are processed using the four beamforming methods listed previously. For space-time processing six taps were used. Variable part of the overall measurement error ($\Delta\rho_V^p$) and DM are obtained for each beamformer and the results corresponding to PRN15 and PRN26 are reported in Table 4-10 for all scenarios.

Table 4-10: Distortions: For (One CW), (Two CW + One WB) and (Six CW)

(in metres)		Scenario 2		Scenario 3		Scenario 4	
Beamforming method	*Parameter*	***PRN***		***PRN***		***PRN***	
		15	*26*	*15*	*26*	*15*	*26*
Blind Eigen Vector	$\Delta\rho_V^p$	1.4	-0.2	-215	-77	146	-151
	DM	1.8	0.5	53	1.7	6.7	5.8
MPDR	$\Delta\rho_V^p$	0.3	-0.3	0.3	-0.4	--	--
	DM	0.5	0.2	0.2	0.6	--	--
E-MPDR	$\Delta\rho_V^p$	1.3	0.6	17	11	131	138
	DM	3.1	2.6	20	14	25	21
C-DL	$\Delta\rho_V^p$	0.6	0.2	-2.6	1.9	-3.3	-4.2
	DM	1.3	0.3	0.6	1.1	1.2	0.4

The results of Table 4-10 show that DM values for Blind STP are on the average higher for all scenarios. For the simple scenario (Scenario 2), DMs for all methods are mostly the same and have small magnitudes. The C-DL method reduces the CCF distortions in all scenarios. For the MPDR beamformer, since array data is collected from six elements, only five uncorrelated interference sources can be mitigated. Therefore, results are not obtained for Scenario 4. Non-equal measurement biases can be observed from the $\Delta\rho_V^p$ values recorded in Table 4-10. Measurement biases increase for all methods with an increasing number of interferences. In addition to the reduction of DM values, the C-DL method results in smaller biases. Even though there are only three interference sources in Scenario 3, significant biases are observed. This could be due to the presence of

wideband interference, which generally consumes more DoF during mitigation than CW interference.

Table 4-11 lists position errors in the ENU coordinate system for all three scenarios after employing the beamformers described in Section 4.3. For Scenario 2, the position error magnitude is almost the same for the different beamformers. The Blind Eigen Vector method provides an accurate position for the mild interference scenario and large position errors for harsh scenarios. The MPDR beamformer is only based on spatial processing and the CCFs and position solutions do not experience any distortion due to time filtering. Results in Table 4-11 verify the fact that the MPDR beamformer can suppress one interference (Scenario 2) and three interference sources (Scenario 3) without generating significant ENU errors but is not able to mitigate six uncorrelated narrowband interference signals (Scenario 4). The E-MPDR method successfully mitigates six interference sources as a result of additional DoF from temporal filters, but introduces some bias, leading to position estimates that are inferior to MPDR. Results show that the C-DL method not only provides extra DoF for narrowband interference mitigation compared to MPDR but also keeps the CCFs less distorted and measurements less biased. Therefore its positioning performance is considerably better than that of the other STP methods. Similar to the observations made in Section 4.4.1, C/N_0 values for the C-DL method are lower compared to corresponding MPDR and E-MPDR values. The C/N_0 values also indicate the gain achieved (or the losses incurred) during array processing. This gain can be analyzed using antenna array gain patterns. The space-time filter gain pattern is calculated as per Equation (2-17).

Table 4-11: GPS position domain results for different methods and interference scenarios (for simulated GPS signals)

Beamforming method	*Scenario*	Position errors (m)			C/N$_0$ (dB-Hz)	Tracking satellites
		E	*N*	*U*		
Blind Eigen Vector	*2*	-2.3	-1.5	-0.9	43.8	8
	3	-149	-96	-56	41.4	9
	4	100	64	38	40.9	8
MPDR	*2*	-3.6	-2.3	-1.3	49.7	9
	3	-2.7	-1.7	-1.0	47.1	9
	4	--	--	--	--	--
E-MPDR	*2*	-3.6	-2.3	-1.4	49.8	9
	3	-6.6	-4.2	-2.5	48.7	9
	4	118	75	45	46.2	9
C-DL	*2*	0.7	0.4	0.3	47.3	9
	3	-6.5	-4.2	-2.4	39.9	8
	4	-19	-12	-7.0	40.2	9

Array gain patterns for the above four methods are shown in Figure 4-8 for Scenario 2. As previously mentioned a single set of filter weights is computed in the Blind Eigen Vector beamformer array gain pattern as shown in Figure 4-8(a). The inability of the blind method to provide sustained gain for all satellites (indicated with a tag ‘S’ in Figure 4-8) is evident. The MPDR, E-MPDR and C-DL methods use signal’s AoA; therefore illustrations are provided for only one satellite PRN (i.e. PRN8, marked in the figure as S8). The MPDR and E-MPDR exhibit similar beam patterns as shown in Figure 4-8(b) and Figure 4-8(c). However, there is an increased depth of the nulls in the interference direction in E-MPDR for a few satellites. Shallow nulls in the interference direction are

seen in C-DL (Figure 4-8(d)) and these can potentially cause a drop in C/N_0 values compared to other methods (as observed in Table 4-11).

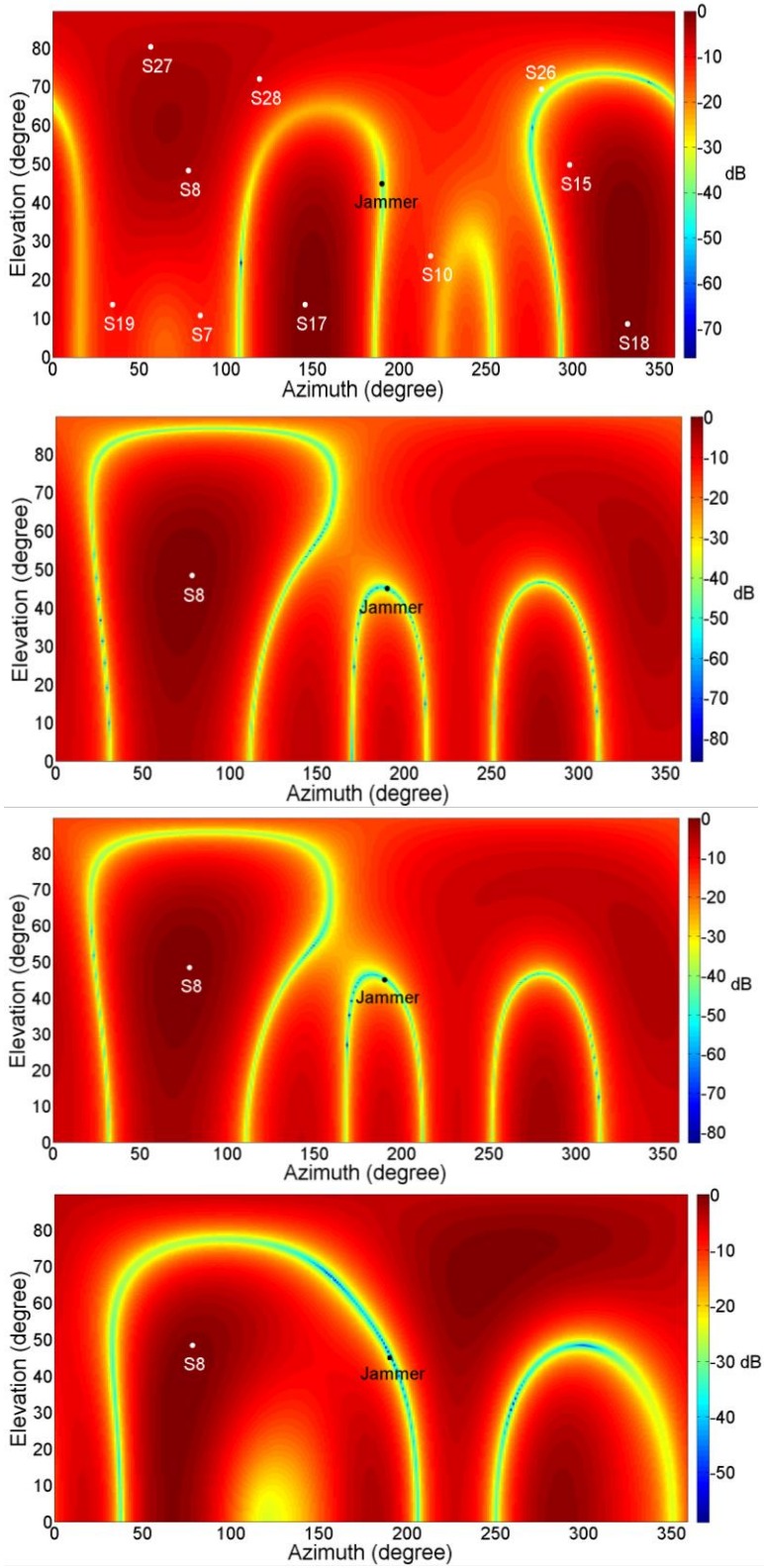

(a) *Blind Eigen Vector*

(b) *MPDR*

(c) *E-MPDR*

(d) *C-DL*

Figure 4-8: Normalized antenna array gain patterns at the interference frequency for different methods (PRN8 - Scenario 2)

4.5 Experimental Results and Analyses

The performance evaluation and comparison of the measurement distortions with different beamforming methods was done in the previous sections using simulated scenarios. Real data tests are now discussed.

4.5.1 Data collection setup and processing

Due to transmission regulations, interference was generated in software and added to digitized live GPS data samples collected using an antenna array. The data collection environment and test set up are shown in Figure 4-9. Intermediate frequency (IF) samples for GPS L1 C/A signals were collected using a six-element antenna array. Data was collected in a parking area with clear sky conditions for satellite visibility. The vehicle was moved in a circular trajectory to receive signals from various directions for the calibration process (Figure 4-9(a)). The antenna array was mounted on the vehicle top (Figure 4-9(b)) and the RF cables from the six antenna elements were connected to the phase coherent six-channel Fraunhofer/TeleOrbit RF front-end (Figure 4-9(c)). The received signals were then down-converted, digitized and stored for post processing (Figure 4-9(d)). A sampling frequency of 20 MHz was used. The reference position was obtained using a NovAtel SPAN^{TM} LCI system based differential positioning method and was accurate to a few centimetres in open-sky conditions.

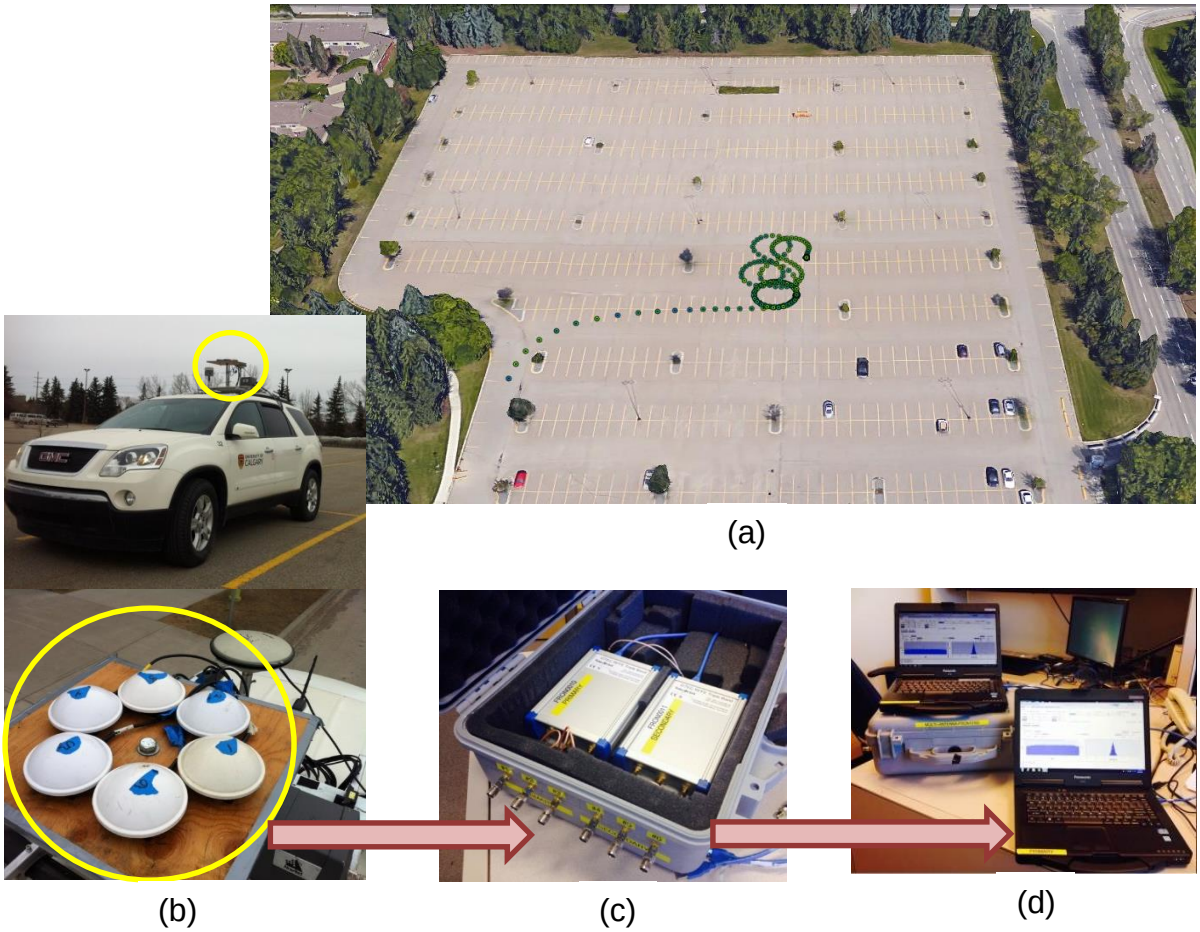

Figure 4-9: Data collection scenario and setup

The PRN codes and azimuth and elevation angles of the satellites visible during data collection are given in Figure 4-10; 10 GPS satellites were available.

PRN	Az (degree)	El (degree)	Sky plot
1	310	29	
4	284	52	
11	289	37	
14	140	83	
18	105	24	
19	239	18	
22	104	59	
24	41	19	
31	170	17	
32	284	41	

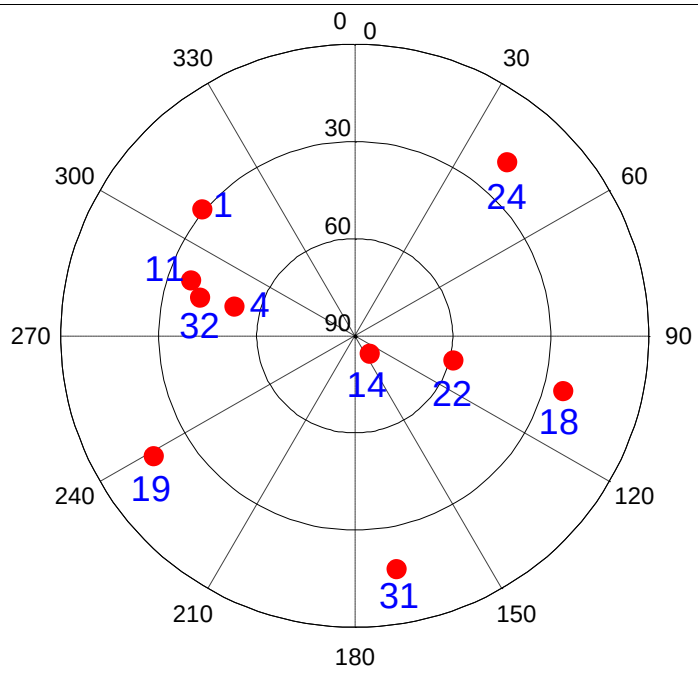

Figure 4-10: Satellite visibility during test – Real data

The antenna array used for interference mitigation consists of antenna elements placed close to each other. When antennas are placed in the near field of each other the amplitude and phase of the received signals at each element may vary. In addition, the amplitude and phase response at each element might be affected due to mutual coupling, differing cable lengths and antenna phase centre variations. This necessitates array calibration in many GNSS applications employing spatial processing, in order to steer nulls towards undesired signal directions while maintaining the main lobe of the beam pattern in the direction of the desired signal.

Antenna arrays are commonly calibrated using anechoic chambers by scanning all incident signals from different AoA values (Kim et al 2004). When antenna arrays are used in GPS, the GPS signals can themselves be used as radio frequency sources with

known AoAs. This eliminates the need for expensive anechoic chambers. An *on-site calibration* approach proposed in (Daneshmand et al 2014) was used. This calibration method is based on receiving GNSS signals during antenna platform motion. For the calibration process, satellite signals should be available from all azimuth and elevation angles. To achieve this, the antenna array is moved in a circular trajectory to cover all azimuth angles. The circular motion is repeated during several intervals with long enough separations to allow satellites to move significantly in the sky, covering all possible elevation angles. The precise calibration process is achieved in two-stage optimization; in the first stage constant uncertainties, e.g. uneven cable lengths, array configuration and platform orientation perturbations, and coupling between elements are estimated while in the second stage, factors depending on each antenna element gain and phase pattern of the signal's AoA are considered for refined calibration (imperfections of the antenna elements, radiation patterns, phase center variations and any other signal AoA dependent phenomena).

As discussed in Section 4.3.1, steering vectors model the phase offsets between each antenna element and the reference element. However, in general, as the beamforming methods cannot compensate the signal delays between the array elements in the pseudoranges, a small contribution to biases can be present in the results. Contributions from these biases should be noticed while comparing the real data results against the simulated results, as these biases are absent in the latter case.

4.5.2 Distortion analysis using position errors and C/N_0 value

When live data is collected, there can be additional contributors to the CCF distortion. The multipath signals arriving at the front-end might add up (constructively or destructively) and distort the CCF, in addition to the other sources described earlier. Here, only position errors and C/N_0 are analyzed for live scenarios and are given in Table 4-12. Simple and harsh scenarios are considered for live data results and the focus is to verify the results with those from the simulations discussed in the previous sections. Meanwhile, one can observe the contributions from additional measurement errors, e.g. errors due to atmospheric delays and multipath (if any).

Conclusions similar to those of the simulated data can be drawn. The magnitudes of position errors in Table 4-12 are higher than the errors in Table 4-11. These are likely due to the errors present in the signals before array processing and calibration errors. Improved SNR performance occurs with the E-MPDR method and the SNR performance of the C-DL method is inferior due to the possible usage of some array DoF for maintaining phase linearity; however, C-DL provides good position performance.

Table 4-12: GPS position domain results for different methods and interference scenarios (for live GPS signals) *

Beamforming method	*Scenario*	Position errors (m)			C/N_0 (dB-Hz)	Tracking satellites
		E	*N*	*U*		
Blind Eigen Vector	*2*	-1.6	1.6	-0.3	47.9	9
	4	621	4688	2021	40.9	7
MPDR	*2*	-1.6	0.6	2.7	51.5	10
	4	--	--	--	--	--
E-MPDR	*2*	-1.6	0.4	3.0	51.7	10
	4	42	-143	-160	43.8	10
C-DL	*2*	-1.9	1.1	4.2	48.6	10
	4	-45	-133	42	39.1	8

* *for 60 s of data in the static mode*

Consolidated analysis of results:

Based on the observations from previous sections for simulated and live data results, it is clear that STP distortions add substantial errors in pseudoranges, and this observation is of greater interest for high accuracy receivers. At the same time it is encouraging to observe the results for the *semi-distortionless* and *distortionless* methods. These methods reduce the error contributions compared to the *blind* method. The latter provided good results (at par with the *non-blind* methods) for mild interference conditions, but worst positioning performance for a higher number of interference sources. *Non-blind* methods i.e. *semi-distortionless* and *distortionless* methods, offered improved positioning performance at the cost of an increase in processing power requirement. The *Semi-*

distortionless method provided the best C/N_0 performance but the positioning performance was not as good as that of the *distortionless* method. On the contrary, the distortionless method provided very good estimated positions but poor C/N_0 performance. The *distortionless* method is constrained to produce less distortions; hence one cannot expect to get best C/N_0 performance at the same time. Therefore, an *optimal* design strategy should switch between these methods in an effective manner, based on the interference scenario.

The observations from Section 4.4.2 indicates that quality interference mitigation improves with an increase in the number of taps added in the temporal filter. However, measurement errors increases when number of taps increased beyond some point. These observations suggest a need to select an *optimal* number of taps in a particular design sufficient to mitigate interference and reduce errors at the same time.

4.6 Summary

A theoretical analysis of the distortions observed in the GPS measurements due to antenna array processing was provided and supported with results from simulated and live signals for different beamforming methods categorized as *blind*, *semi-distortionless* and *distortionless*. A distortion metric and a measure of overall bias that would help to quantify the distortions in space-time processing were introduced. The effects of the placement of the interference source relative to the correct signal direction were shown using overall measurement errors and a profile of the signal strength for different methods. The use of single PRN *noise free* signal simulations to study CCF distortions showed that STP contributes significantly to CCF distortion. In the presence of a higher

number of interference sources, mitigation performance improvement was observed when increasing the number of taps. The distortions and their contributions in the position errors were characterized for simulated signals and real data using a real antenna array. It can be concluded that STP borne distortions lead to erroneous pseudorange measurements and degrade GNSS position accuracy performance in challenging environments; however, these can be alleviated with proper filter design considerations.

CHAPTER 5: SPACE-TIME FILTER TO MITIGATE INTERFERENCE FROM TERRESTRIAL TRANSMITTERS

Several terrestrial communication systems use the same frequency spectrum as GNSS or bands close to it. Pseudolites constitute one such system that generally uses the GNSS spectrum for signal propagation. The signals from pseudolites in the operating region play a crucial role in augmenting satellite based user navigation. These signal transmitters are deployed at ground stations for the majority of their applications. In the near region, pseudolites are overpowered and cause impediments to normal receiver operation due to an increase in the noise floor. Interference and jammers form another source of GNSS disruption. Interference could result from intentional jammers or unintentional signal disturbances from in-band or out-of-band high power sources. A GNSS user can experience interference from near region pseudolites as well as from other interferers. These interference sources may have directional coexistence with pseudolites or GNSS satellites. Such disruptions might completely block signal acquisition and lead to processing failure.

The capability of antenna array space-time processing to counter the above mentioned scenario is demonstrated in this chapter. In addition to interference mitigation, pseudolite signal recovery in the near region and subsequent enhancements are shown. Results that demonstrate improvement in measurement geometry for various antenna array configurations and different processing modes are also shown.

5.1 Introduction to pseudolite system and operating zones

The position accuracy of receivers can be improved with the help of additional transmitters like pseudo-satellites, known as *pseudolites*. The deployment and usage of pseudolites creates a major implication in GNSS operation, namely the issue of *near-far* operation (Cobb 1997) as introduced in Section 1.4. This is caused by the higher dynamic range of the signal strength that a receiver experiences when it operates within the proximity of pseudolite signal transmitters (Wang 2002). There are three zones of operation for a pseudolite, namely *near region*, *far region* and *operating region*. For instance, the average signal power of signals coming from GPS L1 C/A satellites is -158.5 dBW. The pseudolite received power varies as 20 $\log_{10}(R)$, where R is the range between the pseudolite and the user's receiving antenna. The receiver will be in the *operating zone* whenever the pseudolite signal power is close to the nominal GPS signal power level and both will be received at the front-end. At a shorter range (i.e. in the *near region*), the effect from a pseudolite will be that of a wideband jammer on satellite signals. The *near region* is shown as the shaded area around pseudolites in Figure 5-1.

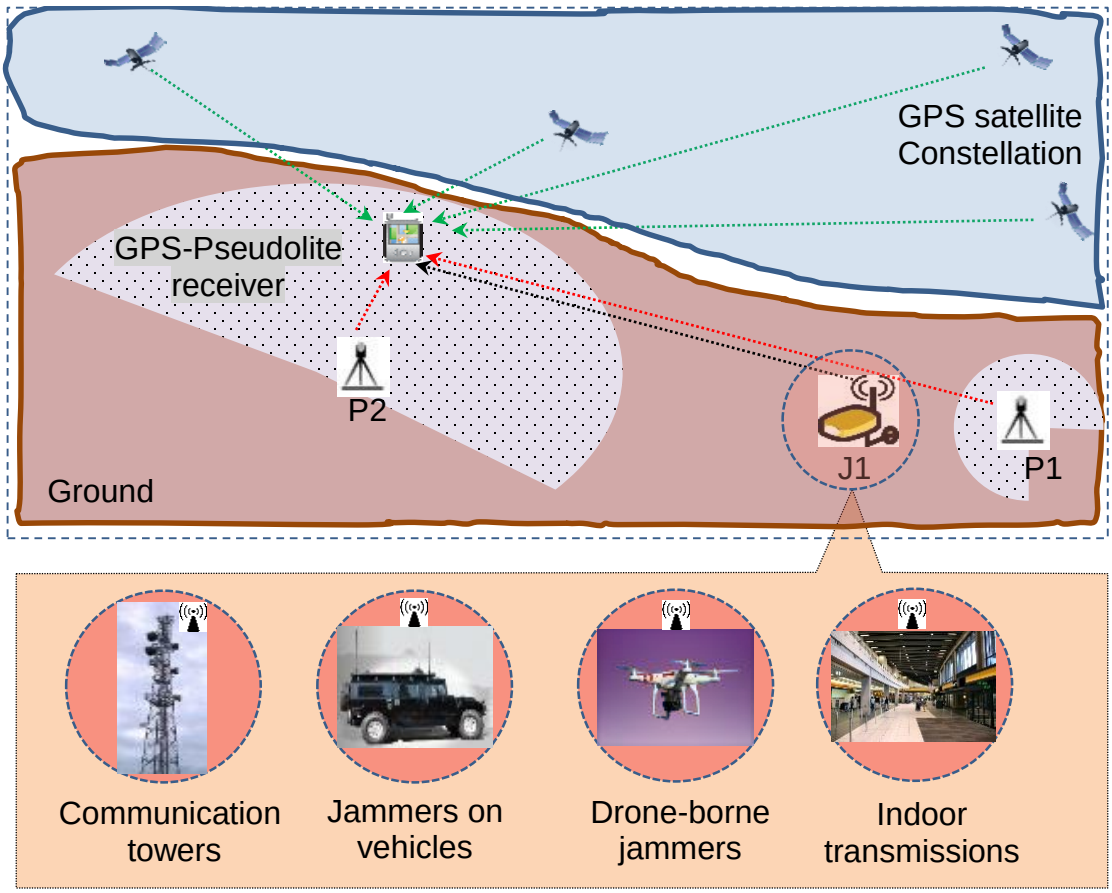

Figure 5-1: Illustration of pseudolite zones of operation with an additional interference source

In addition to *near field* disruptions, the user receivers can also be affected by intentional or unintentional high power transmissions. Some examples of outdoor/indoor signal transmissions that can potentially interfere with the desirable signals are as follows (also shown in Figure 5-1):

- transmission from communication towers
- intentional jammers mounted on automotive vehicles
- jammers mounted on drones or unmanned aerial vehicles (UAVs)
- transmission from high power signal sources and repeaters placed indoors.

To counter interference from the ground based transmitters, several interference excision methods have been proposed in the literature. In these methods, interference detection and mitigation are performed by analyzing temporal (e.g. digital pulse blanking), spectral (e.g. wavelet or Fourier transforms, notch filters, etc.) or spatial (e.g. beamforming antennas) properties of the incoming signals. Spatial processing methods typically use CRPA.

Antenna arrays have not been explored much as a countermeasure for interference caused by pseudolites and other terrestrial transmitters. Array processing is used for pseudolite interference mitigation by employing block adaptation in space-only processing (Juang & Chang 2005)**.** A continuous pseudolite station transmitting high level signals can be treated as a wideband interferer to GPS. Performing space-only processing might work effectively for dealing with high power pseudolites. However, the presence of CW interference (CWI, which has narrowband characteristics) makes the scenario more complex. Temporal filtering methods are effective in mitigating narrowband interference. Integrating the time domain and space domain methods enhances filtering performance. The ***STP*** is one such powerful approach to deal with the *near field* problem and interference mitigation. Since STP combines information from the spatial and temporal domains, it has the capability to mitigate both wideband interference and the narrowband interference present, even in the direction of satellites or pseudolites (Shuangxun et al 2006).

Array processing for the *near field* problem in pseudolite and the space-time processing for jammer mitigation with the possibility of directional coexistence with ranging signals (both GNSS and pseudolites) is discussed in the sequel of this chapter. In this research,

receiver is operating under the influence of two interference sources; one due to a high power pseudolite (in the *near region*) and another due to a CW interference coming from the direction of another pseudolite in its *operating region*.

As described in Section 1.4, pseudolites can be used for augmenting other navigation systems or for independent navigation. When used for independent navigation, they are generally placed indoors or on air vehicles (for navigation in higher altitude space). The number of pseudolites used and their placements depend on the application. In a typical application they transmit signals from ground based transmitting stations. A scenario that models ground based pseudolites is simulated.

Spatial processing methods form a correlation matrix using data from only antenna array elements whereas space time methods use information from both antennas and the TDLs. The main focus of the research presented in this chapter is to demonstrate the effectiveness of space time array processing methods to deal with high power pseudolites and counter jamming scenarios.

In this chapter, the advantages of using antenna array processing to address the *near region* issue in pseudolites and possible signal enhancements are demonstrated using simulations. Challenges involved in simulating pseudolites/interference and the use of a signal simulation testbed as an alternative are described. The discussions in the subsequent sections consist of comparison of performance of different methods using beam patterns, acquisition metric and the DOP obtained for different transmitter's (i.e. GPS/pseudolite) availability.

5.2 Signal model

The signal model in Equation (2-4) in Section 2.3 can be modified to incorporate pseudolite signals as

$$\underset{N\times 1}{\mathbf{x}} = \begin{bmatrix} x_1 \\ x_2 \\ \vdots \\ x_N \end{bmatrix} = \sum_{p=1}^{P} s_p \underset{N\times 1}{\mathbf{a}_p} + \sum_{l=1}^{L} i_l \underset{N\times 1}{\mathbf{b}_l} + \sum_{k=1}^{K} v_k \underset{N\times 1}{\mathbf{c}_k} + \underset{N\times 1}{\boldsymbol{\eta}}, \tag{5-1}$$

where the third term on the right hand side represents the pseudolite signals, $\mathbf{c}_k$ is the steering vector corresponding to pseudolites and *K* represents the number of pseudolites.

The beamformers used in this chapter are described in Chapter 2; the SPM beamformer method is described in Section 2.3.1.2 and the MPDR method in Section 2.3.1.3. Space-time filter's gain patterns (in dB) are calculated using Equation (2-17).

5.3 Scenario description

As discussed in Chapter 3, there are regulations regarding outdoor RF power transmission in the GNSS frequency bands. Considering these discussions, signals (i.e. IF data) required for the current research are generated using a GNSS antenna array simulation test bed as shown in Figure 5-2. The GPS signals and interference are simulated as explained in Section 3.2 and Section 4.2 and the block diagram shown in Figure 4-1 is slightly modified to incorporate pseudolite signal simulations and given in Figure 5-2. The parameters required for simulating the pseudolites are derived from their pre-assigned positions. Specifically in this research, signals from six GPS satellites, two

continuous pseudolites and one CW interference are simulated for two array configurations.

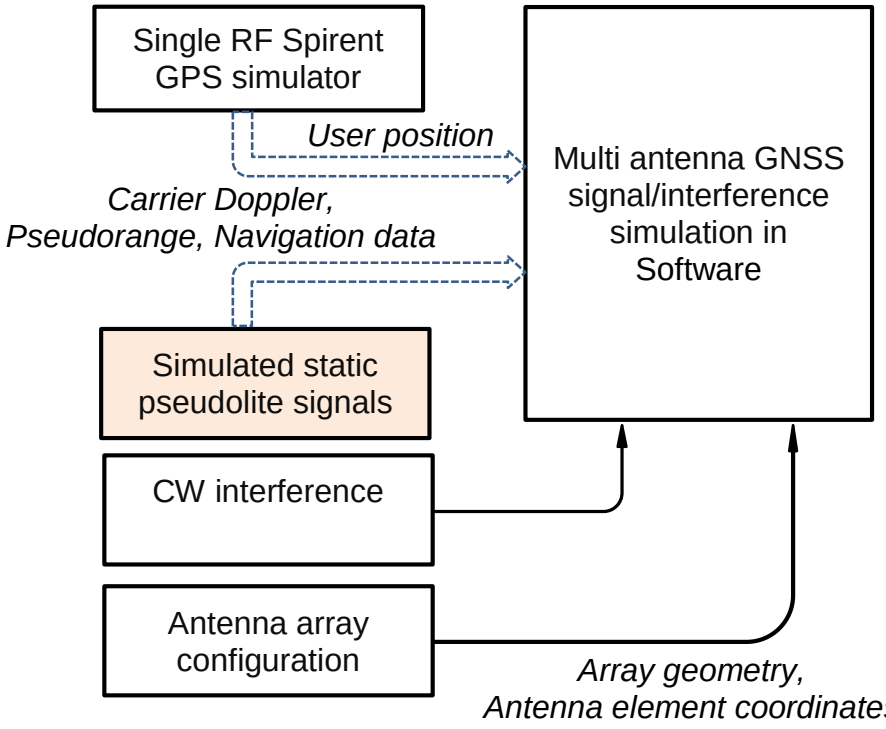

Figure 5-2: Mutli-antenna signal simulation in MatLab®

A scenario corresponding to a user operating on the ground is simulated. The receiver is assumed to have visibility of a sufficient number of satellites. As shown in Figure 5-1, pseudolite P1 is placed in such a way that the receiver is in the *operating region* of P1. Additionally, a strong CWI source (J1) is considered which shares exactly the same direction as P1 (as seen by the user). The receiver is being operated in the *near region* of another pseudolite (P2).

The receiver is close to the pseudolite having PRN 44 and the other pseudolite transmits the signal with PRN 38. A JNR of 20dB over a signal bandwidth of 10 MHz is considered

for in-band interference J1. Azimuth and elevation angles, PRNs and the signal power are given in Figure 5-3. The signal environment is modelled to be free from reflections and related multipath errors.

A uniform circular array of six isotropic elements with the radius equal to half a wavelength of GPS L1 signal and a rectangular array with elements being placed on the four corners of a typical smart phone (dimensions approximately 137 mm x 70 mm) (shown in Figure 5-4) are simulated. Potential effects due to array calibration uncertainties are ignored.

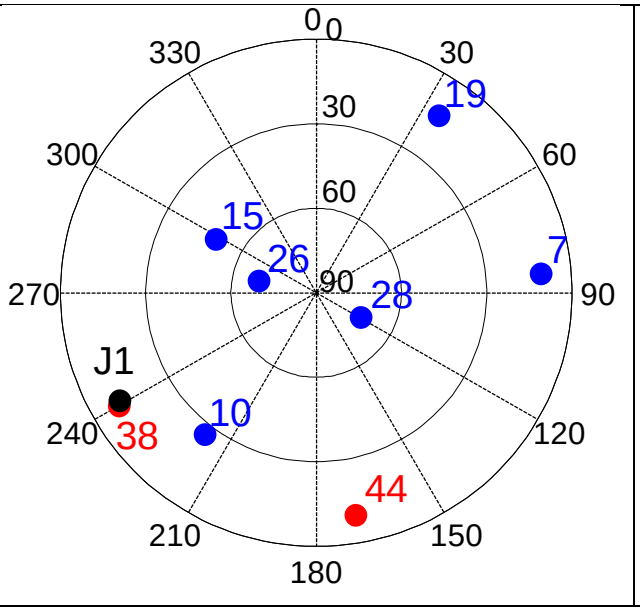

Type	PRN	Az (°)	El (°)	Power (dBW)
GPS	7	85	11	-159
GPS	10	218	26	-159
GPS	15	298	50	-159
GPS	19	34	14	-159
GPS	26	282	69	-159
GPS	28	119	72	-159
PSL	38	240	10	-159
PSL	44	170	10	-79
J1	--	241	11	-84

Figure 5-3: Skyplot and GPS/ pseudolites /interference signal parameters

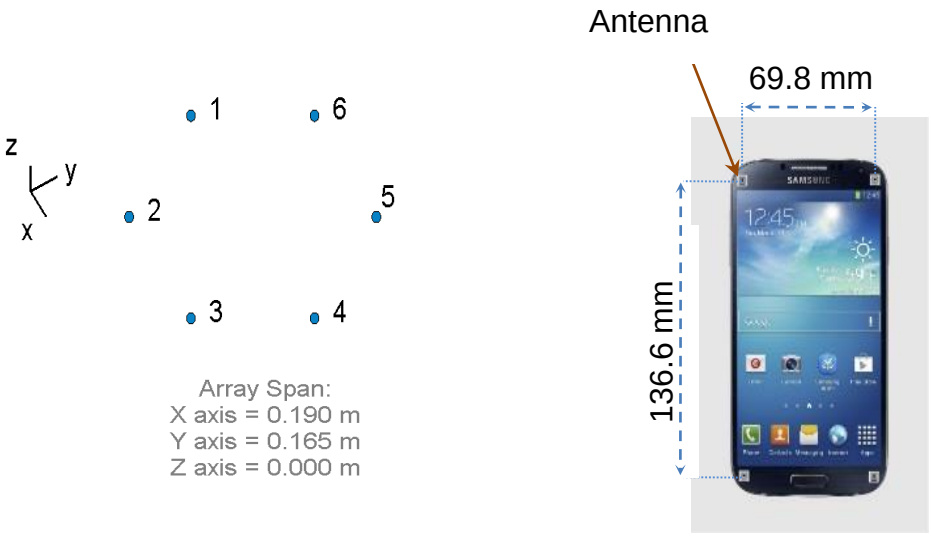

(a) Circular Array (b) Rectangular Array

Figure 5-4: Antenna array configurations: (a) 6-element circular (b) 4-element rectangular array with dimensions of a typical smartphone

5.4 Results and analyses

A multi-antenna receiver which is described in Section 3.4 is used to process array data. As pre-correlation array processing is employed, an additional block that performs beamforming is used before the acquisition stage of a standard receiver structure. Additionally, several changes have been incorporated into the standard software receiver proposed by Borre et al (2007), for pseudolite signal processing at different receiver stages. By using the multi-antenna receiver, the IF samples from the arrays were processed using space-only and space-time methods with the SPM and MPDR criteria. A tapped delay line with eight taps was used for space-time processing. A comparison of the results in different domains (spectrum, acquisition metric and DOP) is now given.

5.4.1 Space-time filter operation and spectrum

The frequency band under consideration is shown in Figure 5-5, before and after STP.

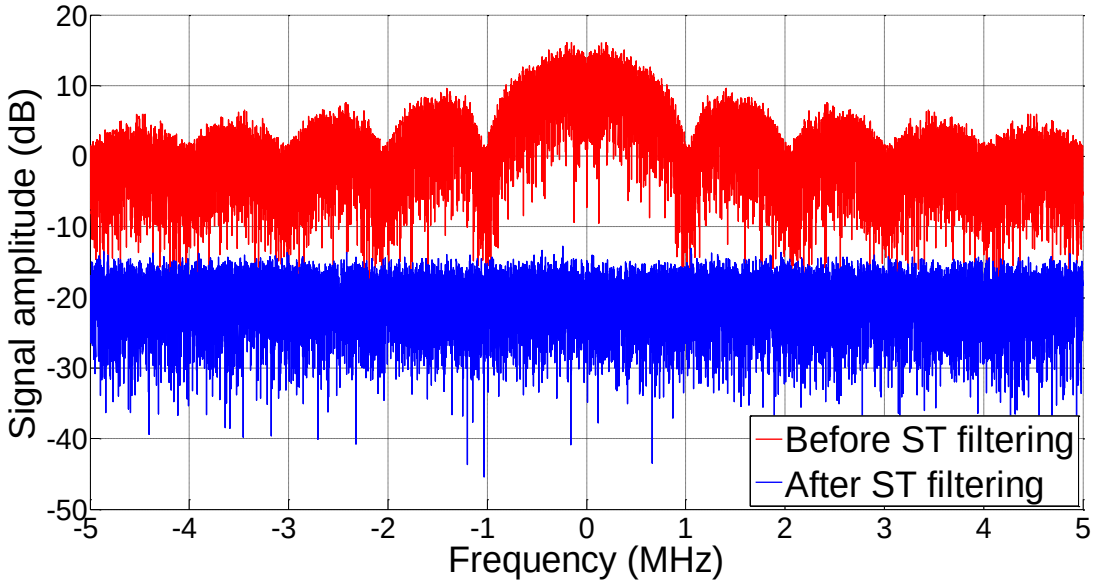

Figure 5-5: GNSS spectrum – before and after STP

In an interference free scenario, the GPS signal is buried in noise and one fails to observe the *sinc* like spectrum of the incoming signals. Due to the high power signal from the pseudolite, the wide band matched spectrum can be seen in the spectrum. The CWI at 200 kHz in the direction of P1 is not visible since it is masked within the pseudolite spectrum. After spatial processing or space time processing, the effects of the high power pseudolite and interference are reduced and the spectrum resembles that of the noise spectrum.

5.4.2 Interference mitigation and acquisition performance

The effectiveness of the methods being tested is evaluated using two metrics, namely the acquisition metric and the antenna array gain. The acquisition metric is the integrated correlator output obtained after Doppler removal and code wipe-off.

The results obtained for the different beamforming methods are presented and discussed. These are categorized in the following order:

- S-SPM : Spatial processing using SPM
- ST-SPM : Space time processing using SPM
- S-MPDR : Spatial processing using MPDR
- ST-MPDR : Space time processing using MPDR.

Antenna array gain beam patterns obtained for above methods are shown in Figure 5-6, Figure 5-8, Figure 5-9 and Figure 5-11, respectively. Successful acquisition is indicated as a *white* dot mark and acquisition failure is indicated as a *black* dot mark in the array gain patterns, and they are positioned at the respective azimuth and elevation angles of the PRNs. Successful acquisition of all GPS satellites was possible for all four previously listed methods with different interference mitigation performance. Additionally, the acquired signal strength and the pseudolite acquisition status differed based on the method used.

5.4.2.1 Using SPM

This is a type of blind beamformer as it does not use either the satellite AoA or that of interference. The results for spatial SPM and space time SPM are as follows:

S-SPM

Deep spectrum nulls were placed by the spatial filter in the direction of both P1 (interference due to CWI) and P2 (high power due to P2 itself) and they could not be acquired. Corresponding antenna gain pattern is given in Figure 5-6. As the signal's AoA details are not taken into account, SPM operates before the despreading process and directly on the IF samples. Therefore, a single set of filter weights is generated for all PRNs.

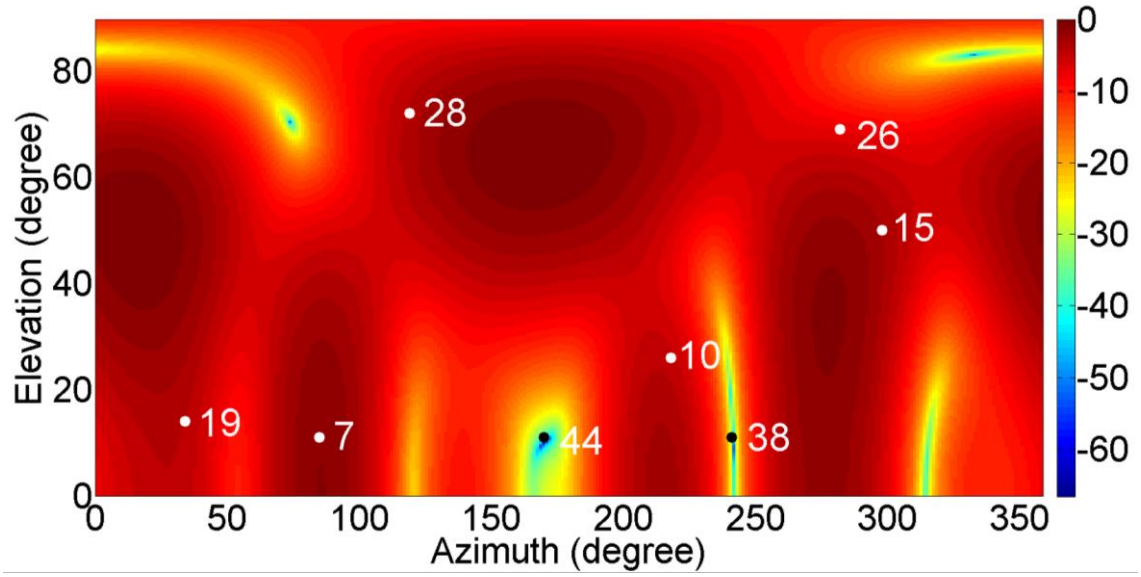

Figure 5-6: Normalized array gain pattern for S-SPM using a six element array (common gain pattern for all PRNs)

ST-SPM

By using ST-SPM, P1 acquisition and CWI excision were possible simultaneously. However, this is not always guaranteed and unintentional nulls could be present in any direction. The acquisition metrics for ST-SPM and S-SPM methods are compared in Figure 5-7 along with the metric for the *operating zone* (no interference).

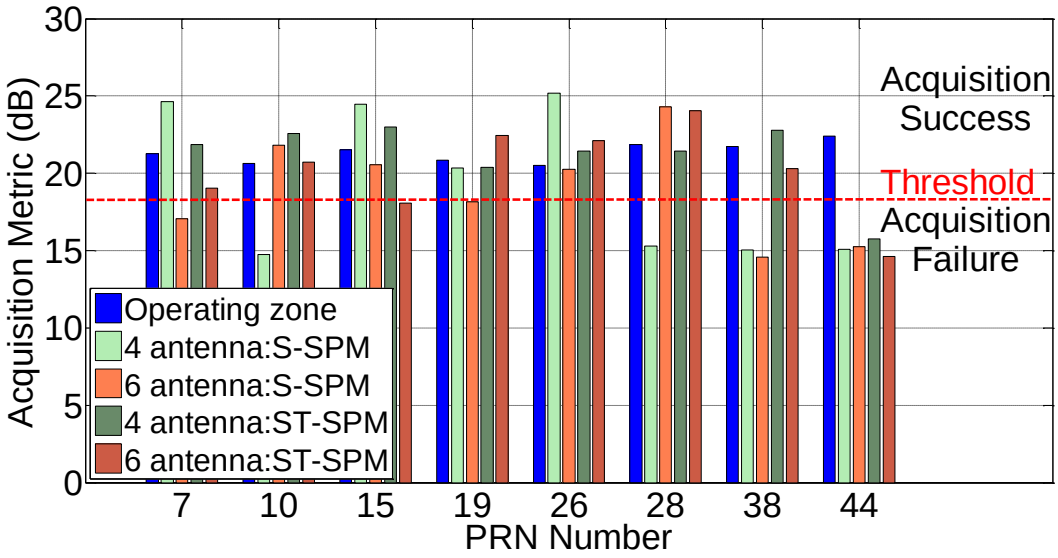

Figure 5-7: Demonstrating advantages of ST-SPM over S-SPM processing

Since the satellite AoA is not considered in the ST-SPM, unintentional nulls are present in the antenna beam pattern (Figure 5-8 (b)) and the acquisition metric varies for different satellites as a result. A null in the direction of PRN 44 confirms the excision of the *near region* pseudolite signal causing interference. Even though this method achieves acquisition of all GPS PRNs and pseudolite PRN 38, which is affected by CW interference, maximum gain at all PRNs is not guaranteed. Similar to S-SPM, a single set of filter weights is computed. Figure 5-8 (a) gives the array gain pattern at the CW interference frequency (corresponding to interference J1). Filtering only a portion of the spectrum allows successful acquisition of PRN 38. Using STP allows to distinguish between signals coming from the same direction.

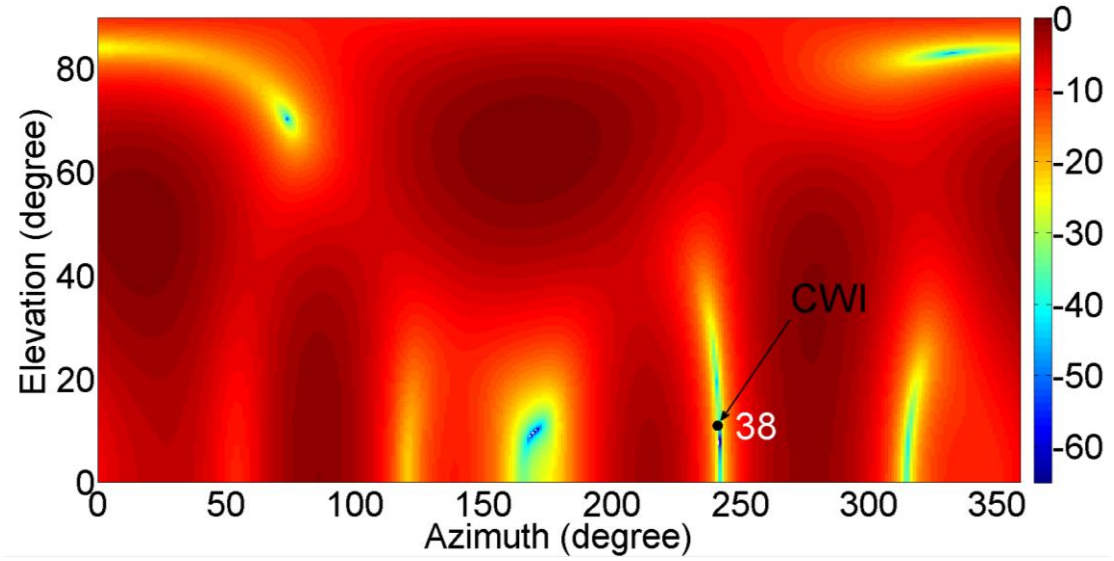

(a)

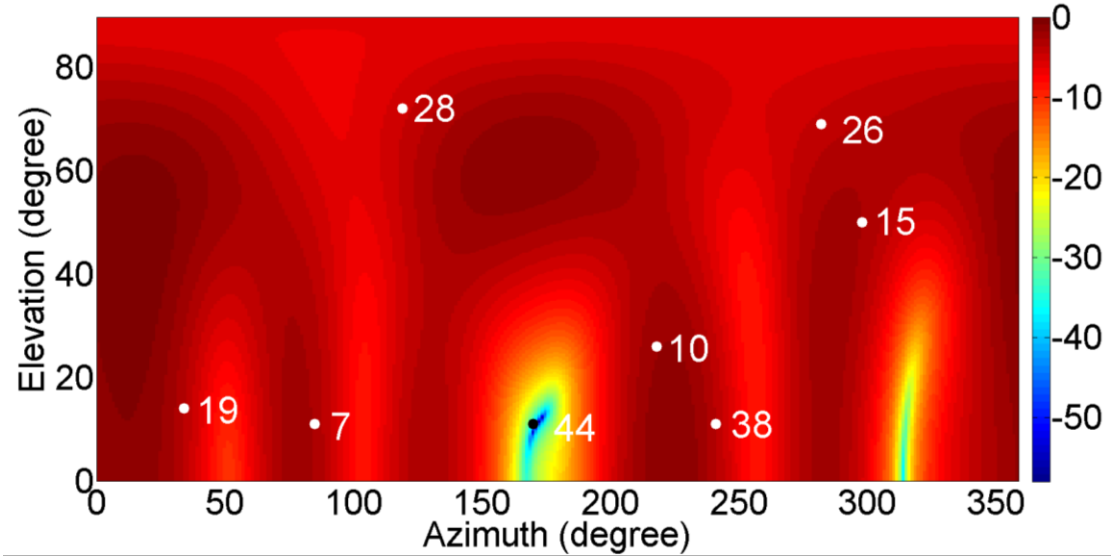

(b)

Figure 5-8: Normalized array gain patterns for ST-SPM using six element array (a) at the CW interference frequency (b) for all GNSS signals at the intermediate frequency

5.4.2.2 Using MPDR

The main advantage of the blind beamformers discussed in the previous sections is that they do not require directional details about the signals (PRNs) to find the filter weights to mitigate interference and therefore the computational complexity is reduced. The

downside of these methods is that they introduce unintentional nulls and fail to provide maximum gain to all PRNs.

The main advantage of pseudolites is that their positions are usually known in advance. This information can be exploited in beamforming to achieve signal enhancements. By using MPDR, beams can be directed in the desired direction of GNSS signals and pseudolites. Interference can then be mitigated and the GNSS and pseudolite signals can be acquired and tracked.

S-MPDR

The antenna gain patterns for the S-MPDR method are given in Figure 5-9 for pseudolites. As an independent beam is formed in the direction of PRN 44 (Figure 5-9 (b)) it can be acquired, even though the receiver is in its *near region*. Space-only processing fails to mitigate the interference lying in the direction of PRN 38 (Figure 5-9 (a)), leading to acquisition failure for this PRN.

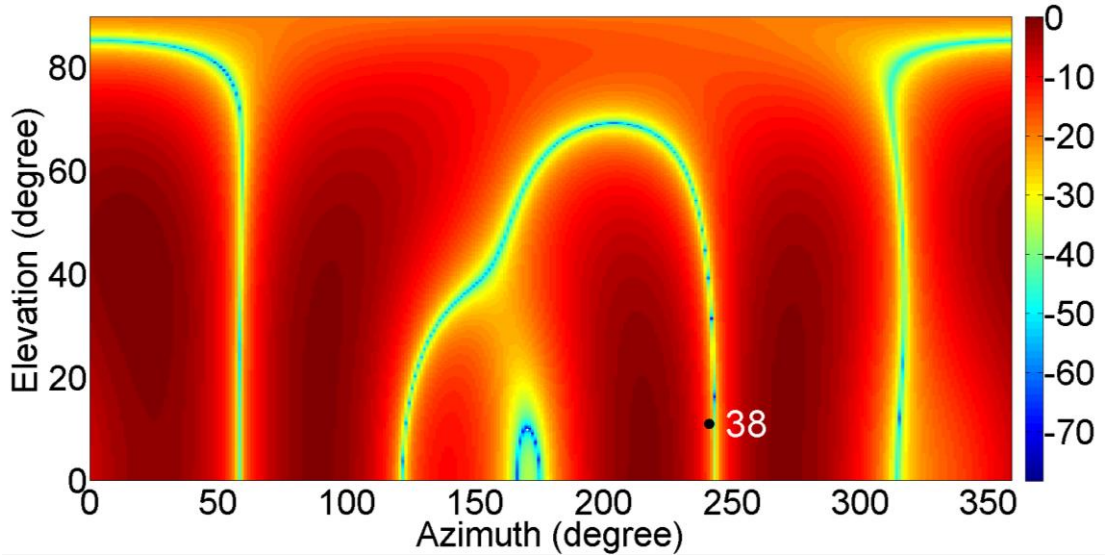

(a)

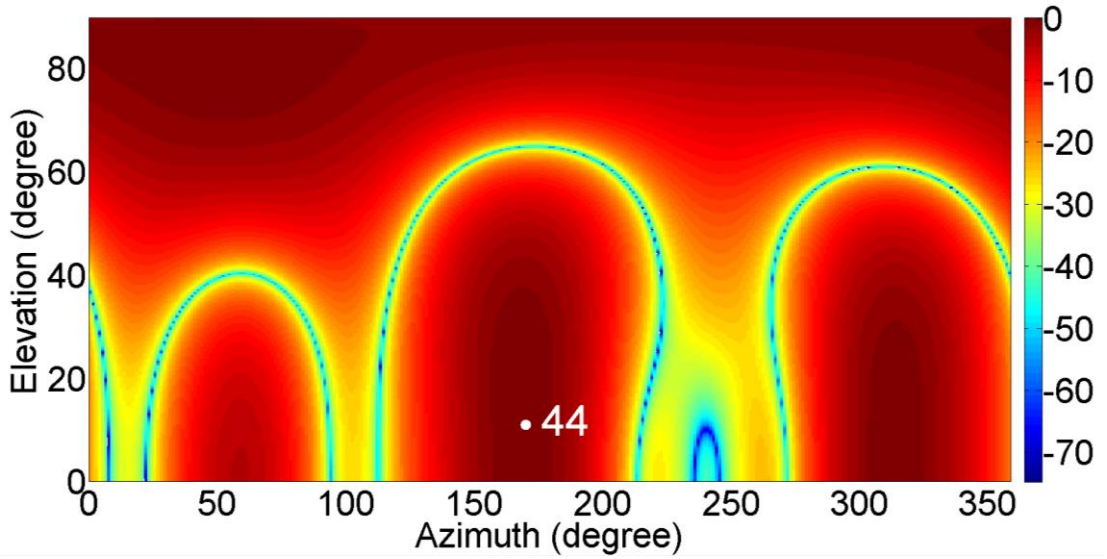

(b)

Figure 5-9: Normalized array gain patterns for S-MPDR using six element array (a) beam directed in the direction of PRN 38 (b) beam directed in the direction of PRN 44

ST-MPDR

The S-MPDR and ST-MPDR acquisition metrics are compared in Figure 5-10. With the S-MPDR criteria, the receiver was able to acquire all GPS PRNs and PRN 44. With ST-

MPDR all GPS and both pseudolite PRNs could be acquired. The antenna array gain patterns for all PRNs are given in Figure 5-11.

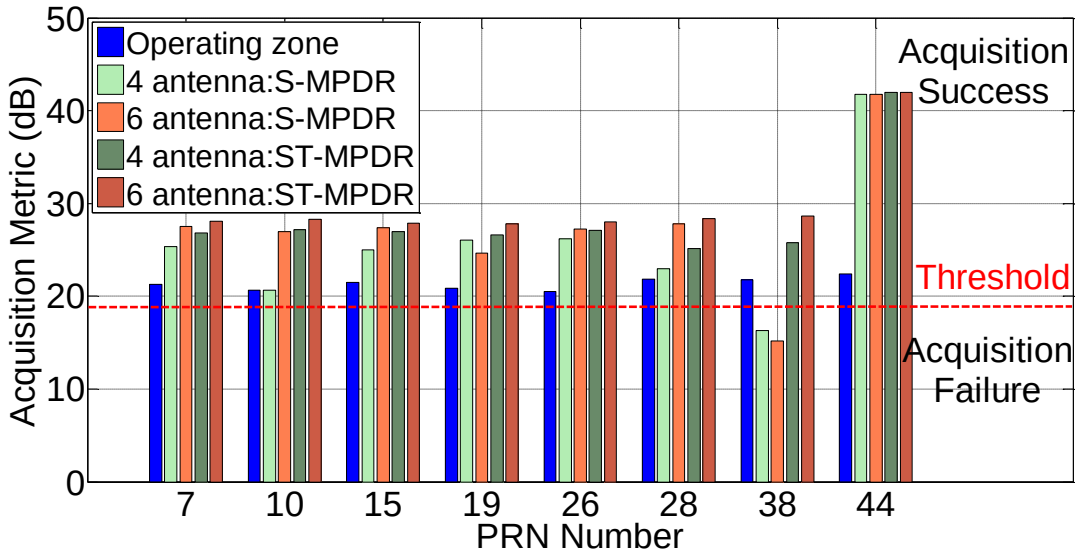

Figure 5-10: Demonstration of signal enhancements achieved using S-MPDR and ST-MPDR

A maximum gain (or minimum attenuation) can be seen for all GPS and pseudolite PRNs, in ST-MPDR. User is operating in the *near region* of PRN 44, however, acquires it as a result of the MPDR criteria, which was not possible with SPM methods. The acquired signal is validated by checking the correctness of the acquired carrier Doppler and the code offset.

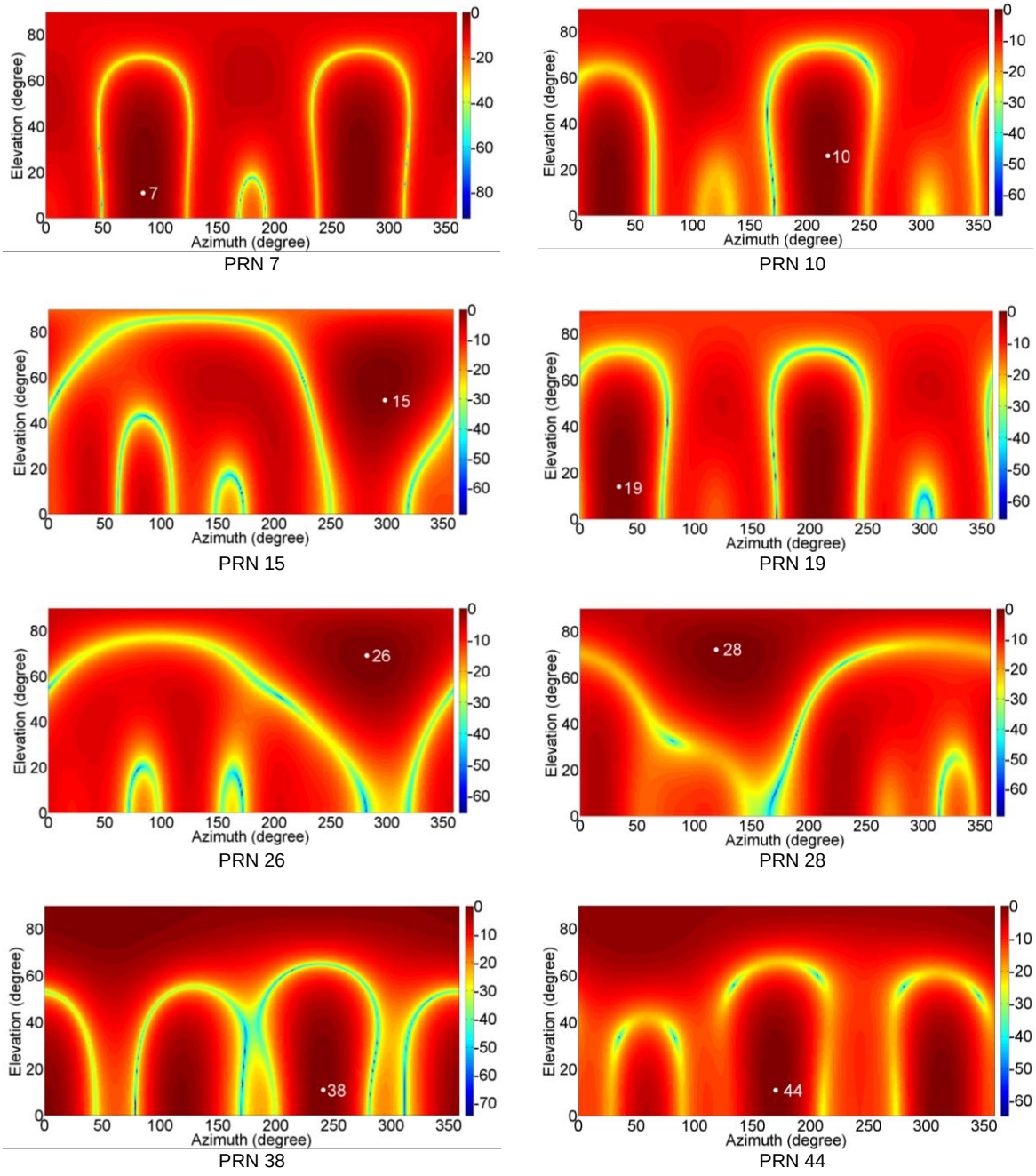

Figure 5-11: Normalized array gain patterns for the GPS and Pseudolite signals for the ST-MPDR beamformer using six-element array

The pseudolite signal (PRN 38) recovery from the direction of the CW interference was possible in ST-MPDR by adding the temporal processing along with the spatial processing.

In addition to success in acquisition of both pseudolites, improvement in GPS signals in terms of SNR also occur with ST-MPDR (comparing against the SPM methods).

A summary of acquired PRNs is given in Table 5-1. The results show that the ST-MPDR beamformer has the best performance for the scenario described in this chapter.

Table 5-1: Summary of acquisition status for different types of beamformers

Beamformer method	**PRNs acquired**		
	All GPS (PRNs 7, 10, 15, 19, 26, 28)	Pseudolite PRN 38	Pseudolite PRN 44
Spatial SPM	☑	☒	☒
Space time SPM	☑	☑	☒
Spatial MPDR	☑	☒	☑
Space time MPDR	☑	☑	☑

5.4.3 DOP evaluation

The position accuracy of a receiver is determined by the DOP and measurement accuracy. Improvement in both or any one of these leads to improved accuracy. Here, the DOP is computed for three cases, namely *(i) GPS only*, *(ii) GPS and a single pseudolite (PRN 38) combined* and *(iii) GPS and both pseudolites combined*.

Whenever measurements from different GNSS constellations or systems (in this research GPS and pseudolites) are combined, the inter-system timing bias must be considered. During state estimation an additional inter-system bias (between GPS and pseudolites) is found. If a single measurement is available from either GPS or pseudolite, it will be used to compute the inter-system bias; hence, the contribution from that single measurement will not be reflected in position estimates. To counter this issue of

synchronization, signal generation in one of the systems (e.g. pseudolite) can be triggered and synchronized with another system, for e.g. GPS (Ford et al 1996). In this case, since both systems are synchronized, no inter-system bias exists; this mode of system synchronization is used in the simulations discussed herein.

Due to the pseudolite arrangement and resulting observability of the position states (latitude, longitude, and height), an improvement in all DOP values was observed as shown in Figure 5-12.

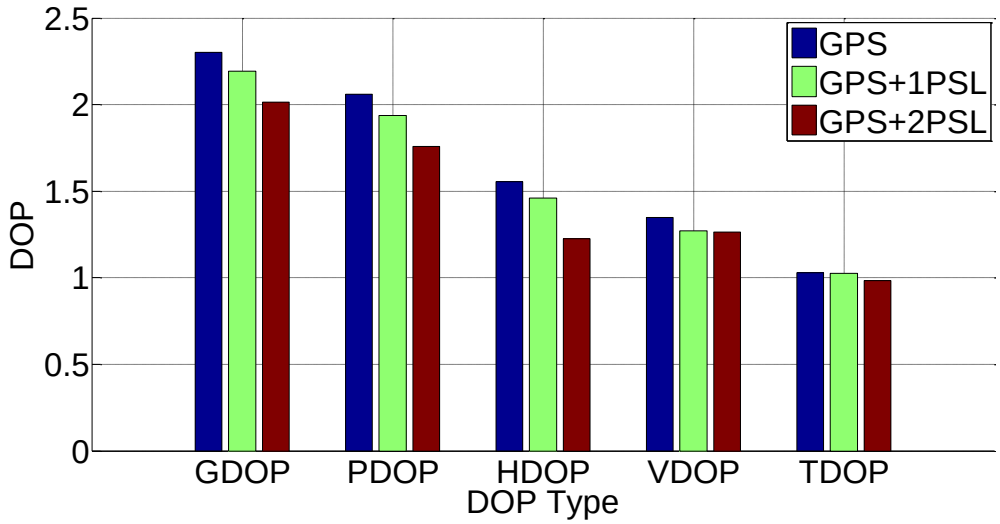

Operating mode	Type of DOP				
	GDOP	PDOP	HDOP	VDOP	TDOP
S-SPM *(GPS only)*	*2.302*	*2.060*	*1.556*	*1.350*	*1.029*
ST-SPM *(GPS+1PSL)*	*2.192*	*1.937*	*1.461*	*1.272*	*1.027*
ST-MPDR *(GPS+2PSL)*	*2.016*	*1.759*	*1.224*	*1.263*	*0.984*

Figure 5-12: Comparison of DOP values for S-SPM, ST-SPM and ST-MPDR

Since GPS and pseudolite measurements are synchronized, these measurements are not distinguished and combined GPS-pseudolite DOP values are computed, whenever pseudolite measurements are available. A single pseudolite could be added to the solution with the ST-SPM method and both pseudolites could be added with ST-MPDR. The MPDR criteria improves the performance in the desirable directions and temporal filtering can eliminate the CW contributions effectively.

Consolidated analysis of results:

As seen in the discussions of the previous sections, even a beamformer that does not use AoA of GPS satellites or pseudolites was able to mitigate a CW jammer and high power pseudolite. When non-participating receivers with GPS only capability have to operate in the *near* region of pseudolites, it is essential for the receiver to process only GPS signals and mask all other undesirable signals including high powered pseudolites. Due to the wideband interference nature of *near* pseudolites, as observed from experiments, a single antenna receiver failed to acquire GPS satellites. However, adding array processing with simple power minimization strategy enabled successful GPS only position estimation.

Since pseudolite positions are generally known in advance, the AoA of pseudolites are constructively used in array processing. Employing the MPDR method not only facilitated pseudolite acquisition but provided sustained gain to GPS satellites. Space-time processing provides narrowband filtering in the desired direction. Therefore, by using STP, the CW aligned in the direction of the pseudolite (in operating region) was mitigated

and pseudolite signals recovered at the same time. The ST-MPDR method combines the benefits of utilizing AoA with the spectral filtering capability of the ST filter to provide improved results.

In handheld or in smartphone applications, one can expect a continuous change in the orientation of the device. Supposing that an antenna array is embedded in such devices, even the antenna array's orientation changes with the device. The SPM method can directly be used even in such device maneuvering applications. However, this poses a challenge on beamforming methods that explore AoA of satellite signals like MPDR. This issue can be circumvented by using the IMU's on such handheld/smartphone devices (low cost IMUs are available in most of the present day devices). Finding the AoA of an interference source will continue to be a challenge with orientation changes; this information is anyway not used in finding beamformer/filter weights. This discussion emphasizes the practicability of applying proposed methods for real world scenarios.

5.5 Summary

Pseudolite interference mitigation capability using an antenna array was demonstrated through simulations. The effectiveness of the array processing methods for the interference impacted *non-participating* receivers was shown with a beamformer that does not use signal's AoA. Furthermore, results show the enhancements obtained by combining the use of signal's AoA and temporal filtering, for a *near zone* pseudolite. Considering recent advances in antenna design miniaturization, a higher number of antenna elements can be integrated in a small form factor, in which case antenna array

processing can be a very effective tool to mitigate interference due to terrestrial transmitters.

CHAPTER 6: CONCLUSIONS AND RECOMMENDATIONS

Based on the results and analyses described in previous chapters, this chapter provides the conclusions regarding the different aspects of STP considered in this research. Recommendations for possible future work in this context are then presented.

6.1 Conclusions

The main motive of this research was to characterize the distortions in antenna array STP and explore new applications of the STP methods for GNSS signals. Conclusions are presented in terms of three topics discussed in previous chapters. These are antenna array signal simulator for GNSS, characterization of measurement distortions due to STP and pseudolite interference mitigation and signal enhancements.

6.1.1 Array signal simulator

To cater to the needs of various activities undertaken in this research a multi antenna GNSS signal simulator was developed (as described in Chapter 3). The new method takes signal parameters from hardware simulators; therefore, some portion of signal simulation load is taken up by the hardware simulator. Since noise-free signal parameters can be recorded directly in the hardware simulator, high fidelity signal generation was possible using SimPLAN. With two approaches considered during simulations, the following points can be made:

- For some GNSS systems that transmit signals over a wider bandwidth (for e.g. AltBOC E5 signals entire transmitted bandwidth is greater than 90 MHz), narrowband assumption is not fully valid. Under such premises, the simulation

approach that uses individual antenna element signals should be used for faithful signal generation.

- Simulated signals are very resourceful in characterization of some processing methods, e.g. STP, predominantly when quantifying the performance metrics is inappropriate or impossible (in some cases) with the real data.

6.1.2 Characterization of STP distortions

Based on the assessment of measurement distortions in STP of GNSS signals (Chapter 4), the following conclusions can be made:

- Single PRN *noise-free* signal simulations to study CCF distortions shows that STP alone can contribute significantly to CCF distortions. These distortions result in erroneous measurements and degrade accuracy performance in challenging environments.
- In the presence of a higher number of interference sources, mitigation performance improves when increasing the number of taps. An increase in the position errors was observed when increasing the number of taps. This shows that there is a *sufficient* number of taps (which can be determined based on the success in acquisition and tracking) required for mitigating interference. However, increasing the number of taps beyond the *sufficient* number of taps will result in biased position estimates.
- A distortion metric DM was introduced to characterize the distortions due to GNSS antenna array STP.

- Based on the results obtained from the experiment involving changes in the interference source incident angle, the interference effects do not change by a large amount when the interference source and the satellite signal are spatially separated. For a single interference source, the MPDR method produced minimal distortions over a large space close to the interference with some variation in the signal strength, whereas the E-MPDR method provided an improved C/N_0 but higher distortion errors occur due to the temporal filter.
- Selection of a beamforming method depends on the interference scenario.
    - For a simple interference scenario, the number of acquired satellites, C/N_0 values and position accuracy were acceptable for all methods. The *blind* beamformer is a better choice for some low level interference scenarios, given its low complexity. In the *blind* method, since AoA are not used and the method does not involve modifications to the standard receiver operation, the method is independent of the receiver structure; therefore, an antenna array followed by the *blind* method can be used as a replacement for the antenna of any single antenna receiver.
    - The *blind* method is not a good choice for harsh interference scenarios or high accuracy applications because the number of acquired satellites and position accuracy are low. In harsh environments, the *semi-distortionless* (E-MPDR) or *distortionless* (C-DL) methods are better choices. They both have almost the same amount of complexity (the *distortionless* complexity is slightly higher).

- The *distortionless* method provides a higher accuracy whereas the *semi-distortionless* method results in a higher number of satellites acquired and C/N_0. As long as sufficient satellites are tracked with good signal strengths, the *distortionless* method is a better choice; if the number of satellites is reduced or C/N_0 decreases, then the *semi-distortionless* method is better. Therefore, an optimum receiver should switch between these two cases depending on the situation.

In summary, it can be concluded that STP borne distortions lead to erroneous pseudorange measurements and degrade GNSS position accuracy performance in challenging environments; however, these can be alleviated with proper design considerations.

6.1.3 Ground transmitter near zone interference mitigation

By employing antenna array methods for pseudolite *near zone* interference mitigation and analyzing the results obtained for the experiments (Chapter 5), the following conclusions can be made:

- Even with a simple form of beamforming i.e. by using Space only - SPM method, the majority of GPS satellites can be acquired. This demonstrates the effectiveness of the array processing methods for interference impacted *non-participating* receivers.
- For a scenario with directionally coexisting interference and desirable signals i.e. for GPS or pseudolite, the advantages of STP over space-only processing were demonstrated by comparing the acquisition status and antenna array gain

patterns. Additionally, by using the MPDR beamformer, signal enhancements to the GPS and pseudolite PRNs were provided.

- On comparing the acquisition performance of the methods considered in this research, it was concluded that the space time MPDR i.e. ST-MPDR beamformer performs best for the scenario described in Section 5.3. Furthermore, as a result of additional measurements from pseudolites, improvement in DOP was observed.

6.2 Recommendations for future work

Recommendations for future work are as follows:

- Even though the proposed simulation method can be used for static or dynamic user scenarios, in the scope of the current research, only static user scenarios were considered. Therefore, simulations are to be verified for dynamic user conditions. Similarly, SimPLAN can be extended to simulate moving interference scenarios.
- Since simulations were done for GPS signals, results from different simulation approaches mentioned in Chapter 3 did not differ greatly. However, the results from different approaches may differ by a large amount for higher bandwidth signals, for e.g. Galileo E5.
- While characterizing the STP distortions in Chapter 4, it is assumed that the interference environment is constant and does not vary over time. In case of time-varying interference scenarios, adaptive beamformers have to be used with STAP processing. In STAP one can expect similar distortions as in the

case of STP; in addition, due to adaptive nature of the STAP methods, distortions also may vary over time. However, further investigations of these distortions would be helpful for studying the navigation accuracy metrics, in the receivers that employ STAP in their processing.

- Comparing the distortion results for the simulated data and the live data, there are larger distortions in the live data. Simulation of array signals was taken up as an alternative to live signals, for quantifying the distortions. With live data, there are many contributors for measurement distortions; therefore, devising a method to quantify the distortions in detail for live signals would be very useful.
- In this thesis, distortion analyses were limited to code phase measurements. The STP distortion analysis of carrier phase based measurements would be of interest for high accuracy receivers.
- Pseudolite interference mitigation and signal enhancements were demonstrated for a single scenario and the data was simulated for four and six antenna elements. Further analysis is to be performed for other scenarios with a higher number of pseudolites and satellite signals while reducing the antenna elements.

REFERENCES

Abdizadeh, M. (2013) *GNSS Signal Acquisition in the presence of narrowband interference*, PhD Thesis, Department of Geomatics Engineering, University of Calgary, Canada, pp.74-75 (Available at http://plan.geomatics.ucalgary.ca/)

Allen, B. and M. Ghavami (2005) *Adaptive Array Systems Fundamentals and Applications*, John Wiley & Sons, Ltd, ISBN 0-470-86189-4

Amt, J. and J. Raquet (2007) "Flight Testing of a Pseudolite Navigation System on a UAV," in *Proceedings of the ION*, 22-24 January, San Diego CA, pp. 1147-1154, U.S. Institute of Navigation

Anantharamu, P. B., D. Borio, and G. Lachapelle (2011) "Space-Time Equalization Techniques for New GNSS Signals," in *the Proceedings of the 24th International Technical Meeting of the Satellite Division*, 20-23 September, Portland, OR, The US Institute of Navigation

Arribas, J., Fernández-Prades, and P. Closas (2013) "Antenna Array Based GNSS Signal Acquisition for Interference Mitigation," in *IEEE Transactions on Aerospace and Electronic Systems*, Vol. 49, January, pp. 223 - 243

Arribas, J., Fernández-Prades, and P. Closas (2011) "Array-based GNSS acquisition in the presence of colored noise," in *Proceedings of the IEEE International Conference on Acoustics, Speech and Signal Processing (ICASSP)*, 22-27 May, Prague, Czech Republic, pp. 2728 - 2731, IEEE

Balai, A. T., A. G. Dempster, and L. L. Presti (2009) "Characterization of the Effects of CW and Pulse CW Interference on the GPS Signal Quality," in *IEEE Transactions on Aerospace and Electronic Systems*, Vol. 45, October, pp. 1418 - 1431

Bao, J. and Y. Tsui (2000) *Fundamentals of Global Positioning System Receivers - A Software Approach*, John Wiley & Sons, Inc., ISBN 0-471-38154-3

Betz, J. W. (2001) "Effect of Partial-Band Interference on Receiver Estimation of C/N0: Theory," in *Proceedings of the ION NTM 2001*, 22-24 January, Long Beach, CA, pp. 817-828

Biggs, M. (2013) *Radio Frequency Interference*, presented at ICAO Regional Preparatory Workshop for WRC-15, US FAA Spectrum Engineering Services, 12 March, Lima, Peru (Available at http://www.icao.int/SAM/Documents/ITU-WRC-15/09%20CARSAM%20WRC-15%20Wkshp_USABiggs%20RFI.pdf)

Bo, Y. X. (2012) "An Improved GPS Receiver Anti-jammer Algorithm Based on Space-time Adaptive Processing," in *Proceedings of the International Conference on Computer Distributed Control and Intelligent Enviromental Monitoring*, 5-6 March, Hunan, pp. 106-109, IEEE Computer Society

B. Bonet, I. Alcantarilla, D. Flament, C. Rodríguez and N. Zarraoa (2009) "The Benefits of Multi-constellation GNSS: Reaching up Even to Single Constellation GNSS users," in Proceedings of *the 22nd International Technical Meeting of The Satellite Division of the Institute of Navigation (ION GNSS 2009)*, 22 - 25 September, Savannah, GA, pp. 1268 - 1280

Borio, D. and J. Fortuny (2010) *Impact of Pseudolite Signals on Non-Participating GPS Receivers*, JRC Scientific and Technical Reports, DOI-10.2788/5745, Department of JRC Scientific and Technical Reports, European Commission, Luxembourg, Publications Office of the European Union, 30 pages

Borio, D., C. O'Driscoll, and J. F. Guasch (2011) "Pulsed Pseudolite Signal Effects on Non-Participating GNSS Receivers," in *Proceedings of the International Conference on Indoor Positioning and Indoor Navigation*, 21-23 September , GUIMARAES, pp. 1-6, IEEE

Borio, D. (2008) *A Statistical Theory for GNSS Signal Acquisition*, PhD Thesis, Dipartimento di Elettronica, Politecnico di Torino, Italy (Available at http://plan.geomatics.ucalgary.ca/)

Borio, D. (2013) *Interference Detection and Mitigation*, presented at ESA International Summer School on GNSS, European Commission Joint Research Centre, ESA (Available at http://www.danieleborio.altervista.org/sumschool/EsaSc_Interference_BorioD_07Jun13.pdf) , 35 pages

Borre, K., D. M. Akos, N. Bertelsen, P. Rinder, and S. H. Jensen (2007) *A Software-Defined GPS and Galileo Receiver: A Single-Frequency Approach*, Springer Science Business Media LLC, Birkhäuser: Boston, USA, ISBN-10 0-8176-4390-7

Broumandan, A. (2013) *GNSS Receiver Design* ENGO 638, Course Notes, Department of Geomatics Engineering, University of Calgary, Canada

Chang, C.L. and J.C. Juang (2008) "Effect of Array Configurations on the Performance of GNSS Interference Suppression," in *International Journal of Control, Automation, and Systems*, Vol. 6, pp. 884-893

Chang, C. L. and B.H. Wu (2011) "Analysis of Performance and Implementation Complexity of Array Processing in Anti-Jamming GNSS Receivers," in *Scientific and Academic Publishing*, Vol. 1, pp. 79-84

Chuang, Y. C. and I. J. Gupta (2013) "Antenna induced biases in GNSS receiver measurements," in *Proceedings of the Institute of Navigation International Technical Meeting 2013, ITM 2013*, 28-30 January , San Diego, CA, pp. 164-171

Chuang, Y. C. and I. J. Gupta (2014) "Two Stage Beamformer for GNSS Receiver Antenna Arrays," in *Proceedings of the 27th International Technical Meeting of the ION Satellite Division, ION GNSS+ 2014*, 08-12 September, Tampa, FL, pp. 2277-2285, Institute of Navigation

Church, C., I. Gupta, and A. O'Brien (2007) "Adaptive Antenna Induced Biases in GNSS Receivers," in *Proceedings of the 63rd Annual Meeting of The Institute of Navigation*, 23-25 April, Cambridge, MA, pp. 204 - 212, The US Institute of Navigation

Citron, T. K. and T. Kailath (1984) "An Improved Eigenvector Beamformer," in *Proceedings of the IEEE International Conference on Acoustics, Speech, and Signal Processing, ICASSP '84*, San Diego CA, pp. 718-721, IEEE

Cobb, S. H. (1997) *GPS Pseudolites: Theory, Design, and Applications*, PhD Thesis, Department of Aeronautics and Astronautics, Stanford University, USA (Available at http://gps.stanford.edu/papers/Thesis/StewartCobbThesis97.pdf)

Compton, Jr., R.T. (1979) "The Power-Inversion Adaptive Array: Concept and Performance," in *IEEE Transactions on Aerospace and Electronic Systems*, Vol. AES-15, November, pp. 803-814

Cuntz, M., A. Konovaltsev, M. Sgammini, C. Hättich, G. Kappen, M. Meurer, A. Hornbostel, and A. Dreher (2011) "Field Test: Jamming the DLR Adaptive Antenna Receiver," in *Proceedings of the 24th International Technical Meeting of The Satellite Division of the Institute of Navigation (ION GNSS 2011)*, 20-23 September, Portland OR, pp. 384 - 392, ION

Curran, J. T., M. Navarro, M. Anghileri, P. Closas, and S. Pfletschinger (2016) "Coding Aspects of Secure GNSS Receivers," in *IEEE*, Vol. PP, March, pp. 1-17

Czabaranek, J. A. (2013) *Pseudolite Architecture and Performnace Aanalysis for the FAA's NextGen Airspace*, MSc Thesis, Department of the Airforce, AIR University (Available at http://oai.dtic.mil/oai/oai?verb=getRecord&metadataPrefix=html&identifier=ADA583613)

Dai, L., C. Rizos, and J. Wang (2001) "The Role of Pseudo-Satellite Signals in Precise GPS-Based Positioning," in *Journal of Geospatial Engineering*, Vol. 3, June, pp. 33-44

Daneshmand, S., A. J. Jahromi, A. Broumandan, and G. Lachapelle (2015a) "GNSS Space-Time Interference Mitigation : Advantages and Challenges," in *Proceedings of the International Symposium on GNSS (IS-GNSS 2015)*, 16-19 November, Kyoto, Japan, 11 pages

Daneshmand, S., A. J. Jahromi, A. Broumandan, and G. Lachapelle (2015b) "GNSS Space-Time Interference Mitigation and Attitude Determination in the Presence of Interference Signals," in *Sensors*, Vol. 15, May 2015

Daneshmand, S., N. Sokhandan, M. Z. Amirani, and G. Lachapelle (2014) "Precise Calibration of a GNSS Antenna Array for Adaptive Beamforming Applications," in *Sensors*, Vol. 14, pp. 9669-9691

Daneshmand, S. (2013) *GNSS Interference Mitigation Using Antenna Array Processing*, PhD Thesis, Department of Geomatics Engineering, University of Calgary, Canada (Available at http://plan.geomatics.ucalgary.ca)

de Bakker, P. F. (2007) *Effects of Radio Frequency Interference on GNSS Receiver Output*, Masters Thesis, Faculty of Aerospace Engineering, Delft University of Technology, Netherlands (Available at http://www.tudelft.nl/fileadmin/Faculteit/CiTG/Over_de_faculteit/Afdelingen/Afdeling_Geoscience_and_Remote_Sensing/MSc_theses/de_bakker07_msc.pdf)

De Lorenzo, S., F. Antreich, H. Denks, A. Hornbostel, C. Weber, and Enge (2007) "Testing of Adaptive Beamsteering for Interference Rejection in GNSS Receivers," in *Proceedings of the ENC GNSS*, 29 May-01 June, Genf, Schweiz

De Lorenzo, D. S., J. Gautier, J. Rife, P. Enge, and D. Akos (2005) "Adaptive Array Processing for GPS Interference Rejection," in *Proceedings of the The Institute of Navigation*, 13-16 September, Long Beach CA, pp. 618-627, US Institute of Navigation

De Lorenzo, D. S., S. C. Lo, P. K. Enge, and J. Rife (2011) "Calibrating adaptive antenna arrays for high-integrity GPS," in *GPS Solutions*, Vol. 16, pp. 221-230

Deshpande, S. M. (2004) *Study of Interference Effects on GPS Signal Acquisition*, MSc Thesis, Department of Geomatics Engineering, University of Calgary, Canada (Available at http://plan.geomatics.ucalgary.ca)

Divis, D. A. (2014) "FCC Courts GPS Community in Effort to Solve Spectrum Crunch," *Inside GNSS*, June, http://www.insidegnss.com/node/4068, Washington

Dong, L. (2003) *IF GPS Signal Simulator Development and Verification*, MSc Thesis, Department of Geomatics, University of Calgary, Canada (Available at http://plan.geomatics.ucalgary.ca/papers/03.20184.leidong.pdf)

Dovis, F. (2011) *Recent Trends in Interference Mitigation and Spoofing Detection*, presented at ICL-GNSS, 30 June, Tampere (Available at http://www.icl-gnss.org/2011/Dovis11.pdf)

Federal Communications Commission Official Website (2014) *Workshop on GPS Protection and Receiver Performance*, http://www.fcc.gov/events/workshop-gps-protection-and-receiver-performance, last accessed June 23, 2014

Fante, R. and J. J. Vaccaro (2000) "Wideband cancellation of interference in a GPS receive array," in *IEEE Transactions on Aerospace and Electronic Systems*, Vol. 36, Issue 2, pp. 549 - 564

Fante, R. L., R. M. Davis, and T. P. Guella (1996) "Wideband cancellation of multiple mainbeam jammers," in *IEEE Transactions on Antennas and Propagation*, Vol. 44, Issue 10, pp. 1402 - 1413

Fante, R. , M. Fitzgibbons, and K. McDonald (2004) "Effect of Adaptive Array Processing on GPS Signal Crosscorrelation," in *Proceedings of the International Technical Meeting of the Satellite Division of The Institute of Navigation*, 21-24 September, Long Beach, CA, pp. 579 - 583

Fernández-Prades, C., P. Closas, and J. Arribas (2011) "Eigenbeamforming for interference mitigation in GNSS receivers," in *Proceedings of the International Conference on Localization and GNSS*, 29-30 June, Tampere, pp. 93-97, IEEE

Fernández-Prades , C. and P. Closas (2009) "Synchronization of GNSS signals with unstructured antenna arrays by a multivariate minimization of the generalized variance," in *Proceedings of the 16th International Conference on Digital Signal Processing*, 05-07 July, Santorini-Hellas, pp. 1-8, IEEE

Ford, T., J. Neumann, N. Toso, W. Petersen, C. Anderson, P. Fenton, T. Holden, and K. Barltrop (1996) "HAPPI-A high accuracy pseudolite/GPS positioning integration," in *Proceedings of the Proceedings of US Institute of Navigation GPS-96*, 17-20 September, Kansas City MO, pp. 1719-1728, ION

Godara, L. C. (1995) "Application of the fast Fourier transform to broadband beamforming," in *The Journal of the Acoustical Society of America*, Vol. 98, February, pp. 230-240

GPS.gov - Official U.S. Government information about the Global Positioning System (GPS) and related topics (2015), *Information about GPS Jamming* http://transition.fcc.gov/eb/jammerenforcement/celjampos.pdf, last accessed August 30, 2015

Griffiths, J.W.R. (1983) "Adaptive array processing - A tutorial," in *IEE Communications, Radar and Signal Processing*, Vol. 130, February

Guerci, J. R. (2003) *Space-Time Adaptive Processing*, Artech House Publishers, Norwood, ISBN 1-58053-377-9

Hatke, G. F. (1998) "Adaptive array processing for wideband nulling in GPS systems," in *Proceedings of the Conferene on Signals, Systems and Computers*, 01-04 November, Pacific Grove, CA, pp. 1332 - 1336, IEEE

Haykin, S. (1996) *Adaptive Filter Theory*, Prentice-Hall, Inc., New Jersey, ISBN 0-13-322760-X

Hegarty, C. J., D. Bibyn, J. Grabowski, and A.J. V. Dierendonck (2011) "An Overview of the Effects of Out-of-band Interference on GNSS Receivers," in *Proceedings of the 24th International Technical Meeting of the Satellite Division*, 20-23 September, Portland OR, pp. 1941-1956, The Institute of Navigation

Heinrichs, G., E. Loehnert, and E. Wittmann (2010) "User RAIM integrity and interference mitigation test results with upgraded German Galileo test range GATE," in *Proceedings of the 5th ESA Workshop on Satellite Navigation Technologies and European Workshop on GNSS Signals and Signal Processing (NAVITEC)*,08-10 December, Noordwijk, pp. 1-7, IEEE

Hoey, M. D. and P. Benshoof (2005) *Civil GPS Systems and Potential Vulnerabilities*, ION GNSS 18th International Technical Meeting of the Satellite Division, 13-16 September, Long Beach CA, pp. 1291-1295, US Institute of Navigation

Hongwei , Z., L. Baowang, and F. Juan (2011) "Interference suppression in GNSS receiver using space-time adaptive processing," in *Proceedings of the 3rd International Conference on Communication Software and Networks (ICCSN)*, 27-29 May , Xi'an, pp. 381-385, IEEE

International Civil Aviation Organization (2012) *Aeronautical electromagnetic spectrum utilization*, Sixteenth meeting of The Communications/Navigation/Surveillance and Meteorology Sub-group, ICAO http://www.icao.int/APAC/Meetings/2012_CNS_MET_SG16, last accessed February 26, 2016.

Jiang, Z., C. Ma, and G. Lachapelle (2004) "Mitigation of narrow-band interference on software receivers based on spectrum analysis," in *Proceedings of the ION GNSS 2004*, 21-24 September , Long beach, CA, pp. 144-155, The Institute of Navigation

Juang, J. C. and C. L. Chang (2005) "Performance Analysis of GPS Pseudolite Interference Mitigation Using Adaptive Spatial Beamforming," in *Proceedings of the 61st Annual Meeting of The Institute of Navigation*, 27-29 June, Cambridge MA, pp. 1179-1187, The Institute of Navigation

Kalyanaraman, S. K. (2009) *High Accuracy GPS Phase Tracking Under Signal Distortion*, PhD Thesis, Russ College of Engineering and Technology, Ohio University, USA (Available at https://etd.ohiolink.edu/rws_etd/document/get/ohiou1251221460/inline)

Kaplan, E. D. and C. J. Hegarty (2006) *Understanding GPS - Principles and Applications*, Artech House, Inc, Norwood, USA

Kay, S. M. (2009) *Fundamentals of Statistical Signal Processing Estimaion Theory*, Prentice Hall, New Jersey, ISBN 0-13-345711-7

Kim, U. S., D. D. Lorenzo, J. Gautier, P. Enge, and J. A. Orr (2004) "Phase Effects Analysis of Patch Antenna CRPAs for JPALS," in *Proceedings of the ION GNSS 17th International Technical Meeting of the Satellite Division*, 21-24 September , Long Beach, CA, The Institute of Navigation, pp. 1531-1538

Konovaltsev, A., F. Antreich, and A. Hornbostel (2007) "Performance Assessment of Antenna Array Algorithms for Multipath and Interference Mitigation," in *Proceedings of the 2nd Workshop on GNSS Signals & Signal Processing - GNSS SIGNALS'2007*, 24-25 April, Noordwijk, Netherlands, ESA-ESTEC

Konovaltsev, A., D. De Lorenzo, A. Hornbostel, and P. Enge (2008) "Mitigation of Continuous and Pulsed Radio Interference with GNSS Antenna Arrays," in *Proceedings of the International Technical Meeting of the Satellite Division of The Institute of Navigation*, 16-19 September, Savannah, GA, pp. 2786 - 2795

Kuusniemi, H., E. Airos, M. Z.H. Bhuiyan, and T. Kröger (2012) "Effects of GNSS Jammers on Consumer Grade Satellite Navigation Receivers," in *Proceedings of the European Navigation Conference (ENC) 2012*, 25-27 April, Gdansk, Poland, 13 pages

Landry, R. J. and A. Renard (1997) "Analysis of Potential Interference Sources And Assessment of Present Solutions For GPS/GNSS Receivers," in *Proceedings of the 4th International Conference on Integrated Navigation Systems*, 26-28 May, St. Petersburg, 13 pages

Li, M., A. G. Dempter, A. T. Balaei, C. Rizos, and F. Wang (2011) "Switchable Beam Steering/Null Steering Algorithm for CW Interference Mitigation in GPS C/A Code Receivers," in *IEEE Transactions on Aerospace and Electronic Systems*, Vol. 47, pp. 1564-1579

Lijun , W., Z. Huichang, and Y. Xiaoniu (2007) "Adaptive Array Antenna for GPS Interference Mitigation and its Performance Analysis," in *Proceedings of the International Conference on Microwave and MillimeterWave Technology*, 18-21 April, Builin, pp. 1-4, IEEE

Lu, S. and J. Sun (2010) "A Novel Adaptive Interference Mitigation Approach Based on Space Time Processing for Global Navigation System Receiver Arrays," in *Proceedings*

of the International Conference on Signal Processing ICSP 2010, 24-28 October, Beijing, pp. 369-372, IEEE

Lu, D., Q. Feng, and R. Wu (2006) "Survey on Interference Mitigation via Adaptive Array Processing in GPS," in *Proceedings of the Progress In Electromagnetics Research Symposium*, 26-29 March, Cambridge, pp. 357-362

Lu, D., R. Wu, Z. Su, and W. Huang (2007) "A space-frequency anti-jamming algorithm for GPS," in *Proceedings of the Antennas and Propagation Society International Symposium*, 9-15 June, Honolulu HI, pp. 4216 - 4219, IEEE

Madhani, P. H., P. Axelrad, K. Krumvieda, and J. Thomas (2003) "Application of successive interference cancellation to the GPS pseudolite near-far problem," in *IEEE Transactions on Aerospace and Electronic Systems*, Vol. 39, pp. 481-488

Marathe, T., S. Daneshmand, and G. Lachapelle (2015a) "Pseudolite Interference Mitigation and Signal Enhancements Using an Antenna Array," in *Proceedings of the International Conference on Indoor Positioning and Indoor Navigation (IPIN)*, 13-16 October, Banff, AB, IEEE

Marathe, T., S. Daneshmand, and G. Lachapelle (2015b) "Characterizing Signal Distortion Due to Space-time Processing of Interference Impacted GNSS Signals," in *Proceedings of the ION GNSS+ 2015*, 14-18 September, Tampa, FL, The Institute of Navigation

Martin, S., H. Kuhlen, and T. Abt (2007) "Interference and Regulatory Aspects of GNSS Pseudolites," in *Journal of Global Positioning Systems*, Vol. 6, Issue 2, pp. 98-107

Misra, P. and P. Enge (2001) *Global Positioning System - Signals, Measurements, and Performance*, Ganga-Jamuna Press, Lincoln, USA

Mitch, R. H., R. C. Dougherty, M. L. Psiaki, S. P. Powell, B. W. O'Hanlon, J. A. Bhatti, and T. E. Humphreys (2012) "Know Your Enemy - Signal Characteristics of Civil GPS Jammers," *GPS World*, vol. 24, January, Richard Langley, Cleveland, OH, pp. 64-71

Moelker, D.J., E. v.d. Pol, and Y. Bar-Ness (1996) "Adaptive Antenna arrays for Interfernce Cancellation in GPS and Glonass Receivers," in *Proceedings of the Position Location and Navigation Symposium, 1996*, 22-26 April, Atlanta, GA, pp. 191 - 198, IEEE

Monzingo, R. A., R. L. Haupt, and T. W. Miller (2011) *Introduction to Adaptive Arrays,* SciTech Publishing, Inc, Raleigh, pp. 499-501, ISBN 978-1-891121-57-9

Moore, T. D. (2002) *Analytic Study of Space-TIme and Space-Frequency Adaptive Processing for Radio Frequency Interference Suppression*, PhD thesis, Department of Electrical Engineering, The Ohio Sate University, USA (Available at https://etd.ohiolink.edu/!etd.send_file?accession=osu1037380239&disposition=inline)

Motella, B., M. Pini, and L. L. Presti (2012) "GNSS Interference Detector Based on Chi-square Goodness-of-fit Test," in *Proceedings of the 6th ESA Workshop on Satellite Navigation Technologies and European Workshop on GNSS Signals and Signal Processing, (NAVITEC)*, 5-7 December, Noordwijk, pp. 1-6, IEEE

Motella, B., S. Savasta, D. Margaria, and F. Dovis (2011) "Method for Assessing the Interference Impact on GNSS Receivers," in *IEEE Transactions on Aerospace and Electronic Systems*, Vol. 47, pp. 1416 - 1432

Myrick, W. L. and J. S. Goldstein (1999) "Anti-jam Space-time Preprocessor for GPS Based on Multistage Nested Wiener Filter," in *Proceedings of Military Communications Conference*, 31 October - 03 November, Atlantic City NJ, pp. 675-681, IEEE

Myrick, W. L., G. J. Scott, and M. D. Zoltowski (2001) "Low complexity anti-jam space-time processing for GPS," in *Proceedings of the IEEE International Conference on Acoustics, Speech, and Signal Processing (ICASSP '01)*, 07-11 May, Salt Lake City, UT, pp. 2233 - 2236, IEEE

Myrick, W. L., M. D. Zoltowski, and J. S. Goldstein (2000) "Exploiting conjugate symmetry in power minimization based pre-processing for GPS: reduced complexity and smoothness," in *Proceedings of the International Conference on Acoustics, Speech, and Signal Processing*, 05-09 June, Istanbul, pp. 2833 - 2836, IEEE

Navipedia (2011), *GNSS Applications* http://www.navipedia.net/index.php/GNSS_Applications

Novatel (2015), http://www.novatel.com/, last accessed September 2015

O'Brien, J. and I. J. Gupta (2011) "Mitigation of adaptive antenna induced bias errors in GNSS receivers," in *IEEE Transactions on Aerospace and Electronic Systems*, Vol. 47, January, pp. 524-538

O'Driscoll, C., D. Borio, and J. Fortuny (2011) *Scoping Study on Pseudolites*, JRC Scientific and Technical Reports, DOI-10.2788/10293, European Commission, Luxembourg: Publications Office of the European Union, 31 pages

Paonni, M., J. G. Jang, B. Eissfeller, S. Wallner, J.A. A. Rodriguez, J. Samson, and F. A. Fernadez (2010) "Innovative interference mitigation approaches: Analytical analysis, implementation and validation," in *Proceedings of the 5th ESA Workshop on Satellite Navigation Technologies and European Workshop on GNSS Signals and Signal Processing*, 08-10 December, Noordwijk, pp. 1-8, IEEE

Parkinson, B. W. and J. J. Spilker Jr. (1996) *Global Positioning System: Theory and Applications Volume I*, American Institute of Aeronautics and Atronautics, Inc, Washington, USA, ISBN 1-56347-106-X

Y. Peng, Z. Deng, G. Fan and P. Chen (2012) "Time Domain Filtering Based Compensation Technique for Space-Time Adaptive Processing," in *Proceedings of China Satellite Navigation Conference (CSNC) 2012*, vol. 161, Berlin Heidelberg, Springer, pp. 559-569

Petovello, M. G., C. O'Driscoll, G. Lachapelle, D. Borio, and H. Murtaza (2008) "Architecture and Benefits of an Advanced GNSS Software Receiver," *in Journal of Global Positioning System,* Vol. 7, pp. 156-168

Pinto, H. D., J. E. Valdez, L. M.B. Winternitz, M. A. Hassouneh, and S. R. Price (2012) "Development And Test of A Digitally Steered Antenna Array for The Navigator GPS Receiver," in *Proceedings of the 27th Space Simulation Conference*, 5-8 November,

Annapolis, MD, American Inst. of Aeronautics and Astronautics; Reston, VA, United States

Powell, S. R. and P. M. Chau (1991) "A Technique for Realizing Linear Phase IIR Filters," *in IEEE Transactions on Signal Processing,* Vol. 39, Issue 11, pp. 2425-2435, IEEE

Puska, H., H. Saarnisaari, and J. Iinatti (2005) "Comparison of antenna array algorithms in DS/SS code acquisition with jamming," *in Proceedings of the Military Communications Conference (MILCOM)*, 17-20 October, Atlantic City, NJ, pp. 2074 - 2080 Vol 4, IEEE

Rohde & Schwarz GmbH & Co. KG (2014) "Satellite Navigation Digital Standards for R&S® SMBV - Operating Manual," Mühldorfstr, Munich, 333 pages

Septentrio (2012) *GNSS Interference Detection*, White Paper, published as Report No SSNWP 06/2012/01, Department of Satellite Navigation

Shuangxun, L., C. Zhu, H. Kan, and X. Hongyin (2006) "A Compensating Approach for Signal Distortion Introduced by STAP," in *Proceedings of the International Conference on Communication Technology, ICCT '06*, 27-30 November, Guilin, pp. 1-4, IEEE

Sklar, J. R. (2003) "Interference Mitigation Approaches for the Global Positioning System," in *Lincoln Laboratory Journal*, Vol. 14, pp. 167-180

So, H., T. Lee, S. Jeon, C. Kim, C. Kee, T. Kim, and S. Lee (2010) "Implementation of a Vector-based Tracking Loop Receiver in a Pseudolite Navigation System," *in Sensors,* Vol. 10, June, pp. 6324-6346

Soon, B.K.H., E.K. Poh, J. Barnes, J. Zhang, H.K. Lee, and C. Rizos (2003) "Flight Test Results of Precision Approach and Landing Augmented by Airport Pseudolites," *in Proceedings of the 16th International Technical Meeting of the Satellite Division of The Institute of Navigation*, 09-12 September, Portland, OR, pp. 2318 - 2325, US Institute of Navigation

Spirent Communications plc (2012) "Simgen Software User Manual," Paignton, 548 pages

Stansell, J. T.A. (Spring 1986) "RTCM SC-104 Recommended Pseudolite Signal Specification," *in Navigation: Journal of The Institute of Navigation*, Vol. 33(1), Issue 1, pp. 42-59

Thiel, A. and M. Ammann (2009) *Anti-Jamming techniques in u-blox GPS receivers*, White paper, u-Blox AG (Available at https://www.u-blox.com/images/downloads/Product_Docs/u-blox%20anti-jamming_whitepaper_(GPS-X-09008).pdf)

Torrieri, D. and K. Bakhru (2008) "Adaptive-Array Algorithm for Interference Suppression Prior to Acquisition of Direct-Sequence Signal," in *IEEE Transactions on Wireless Communications*, Vol. 7, September, pp. 3341 - 3346

Trinkle, M. and D. Gray (2001) "GPS Interference Mitigation; Overview and Experimental Results," *in Proceedings of the 5th International Symposium on Satellite Navigation Technology & Applications*, Canberra, Australia, pp. 1-14, MENAY Pty Ltd

Tsujii, T., M. Harigae, and K. Okano (2004) "A New Positioning/Navigation System based on Pseudolite Installed on High Altitude Platforms Systems (HAPS)," i*n Proceedings of the 24th International Congress of the Aeronautical Sciences (ICAS 2004)*, 03 September, 10 pages

Van Trees, H. L. (2002) *Optimum Array Processing - Part IV of Detection, Estimation, and Modulation Theory*, John Wiley & Sons, Inc., New York PA, pp. 556-574, ISBN 0-471-09390-4

Van Veen, B. D. and K. M. Buckley (1988) "Beamforming: A Versatile Approach to Spatial Filtering," in *IEEE ASSP Magazine*, Vol. 5, April, pp. 4-24

Wang, J. (2002) "Pseudolite Applications in Positioning and Navigation: Progress and Problems," *in Journal of Global Positioning Systems*, Vol. 1, Issue 1, July, pp. 48-56

Yuhe, S. (2014) "An Anti-jam Adaptive Algorithm for GPS," *in International Journal of Emerging Technology and Advanced Engineering*, Vol. 4, pp. 1-8

Zhao, W.Y., L.F. Xu, and R.B. Wu (2006) "A Simulation Tool for Space-time Adaptive Processing in GPS," in *Proceedings of the Progress in Electromagnetics Research Symposium*, 26-29 March, Cambridge, USA

Zheng, Y. (2008) *Adaptive Antenna Array Processing for GPS Receivers*, MSc Thesis, School of Electrical & Electronics Engineering, The University of Adelaide, Australia (Available at https://digital.library.adelaide.edu.au/dspace/bitstream/2440/49670/8/02whole.pdf)

Zhou, , J. Zhou, Wang, C. Lu, and G.E. Sobelman (2010) "Novel and flexible Complex Coefficient Linear phase IIR filters for communications," *in Proceedings of the IEEE Asia Pacific Conference on Circuits and Systems*, 06-09 December, Kuala Lumpur, pp. 434 - 437, IEEE